UNIVERSITÉ DU QUÉBEC À MONTRÉAL

DÉVELOPPEMENT DE REVÊTEMENTS HYDROPHOBES ET SUPERHYDROPHOBES STABLES POUR SURFACES VITRÉES DESTINÉES AUX PANNEAUX SOLAIRES ET AUTRES APPLICATIONS OPTIQUES

THÈSE

PRÉSENTÉ(E)

COMME EXIGENCE PARTIELLE

DU DOCTORAT EN CHIMIE

PAR

NESRINE KHITAS

NOVEMBRE 2025

UNIVERSITÉ DU QUÉBEC À MONTRÉAL

DEVELOPMENT OF STABLE HYDROPHOBIC AND SUPERHYDROPHOBIC COATINGS FOR GLASS SURFACES INTENDED FOR SOLAR PANELS AND OTHER OPTICAL APPLICATIONS

THESIS

PRESENTED

AS PARTIAL REQUIREMENT

OF THE DOCTORATE IN CHEMISTRY

BY

NESRINE KHITAS

NOVEMBER 2025

ACKNOWLEDGEMENTS

Guided by the belief that "Difficult roads often lead to beautiful destinations"[1], I found the strength to persevere through the challenges of this PhD journey, holding on to the conviction that each step brought me closer to success. Despite the difficulties, what mattered most was to keep moving forward, no matter how small or slow the steps were. This journey has been truly life-changing and would not have been possible without the support and contributions of many people, to whom I express my deepest gratitude.

First and foremost, I wish to express my warmest gratitude for the unconditional love and support provided by my family, friends, and all those whose presence and generosity have meant more to me than words can ever express. To my supportive partner, my dear husband, who has always been there for me through the best and the worst moments, thank you. For your unconditional love and encouragement throughout this journey, for cheering me up in my moments of frustration, for motivating me to keep going, and above all, for believing in me. Thank you for your patience. I am truly grateful to have you in my life. I am greatly thankful to my mother, my brothers, my sister, my brother-in-law, and sisters-in-law, my dearest aunt Lamia, Samy, Yasmine, Dorhane, and Assala, for their belief in me, the encouragement, and the unwavering support they provided me on every step along the way. My special thanks go to Elsa for her professional support and guidance during challenging times.

I would like to extend my sincere gratitude to my supervisor, Prof. Ali Nazemi, for giving me the opportunity to join his research group. His invaluable support, constructive feedback, and unwavering encouragement enabled me to develop valuable skills and knowledge. I would also like to extend my gratitude to the entire team of our collaborator, *Edgehog Technologies Inc.* (Calvin, Siamak, Fabien, Nasim, Bojan, Claudine, Ishrat, Minh-Tam, Bao, Michael, Kyle, and François), for their insightful discussions, collaborative spirit, and the supportive environment they provided during my time with them. Working with such a dynamic team in their open space was truly an inspiring and enriching experience. I also thank Mitacs Globalink for their financial support, which made the completion of this thesis possible.

[1] Zig Ziglar

I would like to thank Prof. Dror Warschawski and Prof. Sylvain Canesi for their early support and guidance. I extend my sincere appreciation to the committee members, Prof. Gelareh Momen, Prof. Abdelkrim Azzouz, and Prof. Guillaume Goubert, for their valuable time and insightful comments throughout the review process of this thesis.

I am grateful to Prof. Luc Stafford from UdeM for providing access to the goniometer to Pierre, Laura, Nelsie-Anne, and Mariam for their valuable training and support. Special thanks to Julien from Géotop, to Nicole and Philippe from $(CM)^2$ at Polytechnique Montréal, to NanoQAM's research professionals (Gwenael, Galyna, Mohsen, and Alexandre), as well as to the Department of Chemistry's administration and technical staff (Pascale, Mylène, Marie-Claude, Luc, Chantal, Jacqueline, Isabelle, and Asma) for all their support. I would also like to thank Prof. Mohamed Siaj for encouraging collaboration and Maziar for generously dedicating his time and specialized knowledge to promote the advancement of our collaborative project. To all my colleagues (Arunava, Nadjib, Diep, Marilyne, Loveline, Hossein, Hichem, Noémie, Lucas, and Thomas) and all the dedicated people, I had the privilege of meeting at UQAM. Thank you for making my journey so enjoyable and filled with unforgettable memories.

Nesrine

Montreal, May 2025

DEDICACE

For all the challenges, sacrifices, and dreams still unfolding,

I dedicate this thesis to my late father and grandfather.

To my dearest mother, for her ongoing support and unconditional love.

To my precious brothers and sister, to my sisters- and brothers-in-law, and to my dearest nieces and nephew.

To my beloved grandmothers.

To all my family and in-laws, for their constant support and encouragement.

Last but not least, to my soulmate, my husband.

TABLE OF CONTENTS

LIST OF FIGURES

LIST OF SCHEMES

LIST OF TABLES

LIST OF ABREVIATIONS

2D	Two-dimentional
3D	Three-dimentional
AFM	Atomic Force Microsopy
ATCS	Allyltrichlorosilane
ATR-FTIR	Attenuated Total Reflectance-Fourier-Transform-Infrared Specroscopy
CA	Static Water Contact Angle
CAH	Contact Angle Hysteresis (or hysteresis)
$(CM)^2$	Le Centre de Caractérisation Microscopique des Matériaux
GRIN	Graded-Index Structures
MTCS	Methyltrichlorosilane
OTS	*n*-octadecyltrichlorosilane or octadecyltrichlorosilane
PDMS	Polydimethylsiloxane
PFOTS	trichloro(1H,1H,2H,2H-perfluorooctyl)silane or perfluorooctyltrichlorosilane
PiFM	Photo-induced Force Microscope
PTFE	Polytetrafluoroethylene (or Teflon)
RMS	Root Mean Square
SA	Sliding Angle
SAM	Self Assembled Monolayer
sccm	Standard Cubic Centimeter
SEM (or MEB)	Scanning Electron Microscopy
UV-Vis	Ultraviolet-Visible

WCA	Water contact angle
MTCS	Trimethylchlorosilane
SiO_2	Silicon dioxide

LIST OF EQUATIONS

RÉSUMÉ

La modification des surfaces joue un rôle important dans l'amélioration des performances des matériaux et l'élargissement de leurs applications, en les adaptant à des exigences spécifiques. Récemment, les revêtements hydrophobes et superhydrophobes inspirés de la nature ont suscité un intérêt particulier en raison de leur capacité à relever des défis tels que la pollution environnementale, la dégradation des surfaces et la perte d'efficacité dans de nombreux secteurs, notamment l'optoélectronique, l'automobile et les infrastructures extérieures. En collaboration avec *Edgehog Advanced Technologies Inc*, nous avons exploré l'utilisation d'organosilanes commerciaux pour la modification du verre, en raison de leur simplicité, polyvalence et capacité à former des liaisons stables. Ces agents de silanisation permettent de modifier la topographie, de réduire l'énergie de surface, de conférer des fonctionnalités spécifiques et d'effectuer des réactions de post-modification sans altérer le revêtement préexistant.

Ce travail s'articule autour de trois approches, chacune se concentrant sur des aspects clés de la modification et de la caractérisation de surface. La première approche étudie l'utilisation de silanes alkylés et perfluoroalkylés déposés par tremge sur du verre régulier et nanotexturé. Nous avons évalué la mouillabilité, la topographie, les propriétés optiques et la stabilité des revêtements dans des conditions environnementales simulées (pluie et exposition à l'extérieur). Les résultats ont montré que les chaînes perfluoroalkyles courtes augmentaient l'hydrophobie et réduisaient la réflectance, tandis que les chaînes alkyles longues produisaient des revêtements plus lisses avec moins d'agrégats polymérisés. La combinaison de la texturation et de la rugosité de surface a augmenté de manière significative l'angle de contact avec l'eau, démontrant le potentiel de ces revêtements en tant que couches protectrices contre les conditions extérieures telles que l'accumulation de poussière et l'irradiation UV.

Dans la deuxième approche, nous avons utilisé des alcényltrichlorosilanes à chaîne courte pour modifier les surfaces de verre dans le but d'améliorer leur mouillabilité, propriétés optiques et leur stabilité. Nous avons employé une stratégie de modification de surface en deux étapes : un revêtement par immersion suivi d'une fonctionnalisation avec un alcanethiol *via* une réaction click thiol-ène radicalaire. Nous avons étudié l’impact d’une variation d'un seul atome de carbone dans

les agents de silanisation sur les propriétés de surface, ainsi que l'influence de la fonctionnalisation sur la stabilité des surfaces superhydrophobes. Des techniques de caractérisation avancées, notamment des mesures d'angle de contact avec l'eau, la microscopie électronique à balayage (MEB), la microscopie à force atomique (AFM), la spectroscopie UV-Vis, la spectroscopie infrarouge à transformée de Fourier avec réflexion totale atténuée (ATR-FTIR) et la microscopie à force photo-induite (PiFM), ont été utilisées pour analyser la mouillabilité, la morphologie, la structure, la composition optique et chimique des revêtements. Le PiFM, en particulier, a fourni de nouvelles informations sur l'uniformité de la fonctionnalisation et l'efficacité de la réaction click thiol-ène, offrant ainsi de nouvelles perspectives pour le développement de revêtements superhydrophobes durables.

La troisième approche introduit une méthode innovante pour fonctionnaliser les surfaces de verre en utilisant des alcynes activés dans des conditions douces. Cette méthode permet l'incorporation directe de diverses molécules, offrant une plateforme polyvalente pour créer des surfaces fonctionnelles aux propriétés ajustées. Contrairement aux méthodes conventionnelles, qui nécessitent souvent des conditions agressives ou rencontrent des difficultés pour obtenir une fonctionnalisation uniforme et stable, cette approche offre une voie plus efficace et flexible pour la modification de surface. L'approche que nous proposons offre une efficacité supérieure et une polyvalence adaptée à des applications permettant une détection sensible et sélective.

Mots clés : Surfaces hydrophobes; revêtements anti-réflexion; mouillabilité; revêtement pour le verre; transparence; revêtements auto-nettoyant; panneaux solaires.

ABSTRACT

Surface modification plays an important role in enhancing materials performance and expanding their potential applications, enabling them to be tailored to meet specific requirements. Recently, nature-inspired hydrophobic and superhydrophobic coatings have received particular attention due to their ability to address challenges such as environmental pollution, surface degradation, and loss of efficiency in many industries, including optoelectronics, automotive, and outdoor structures. In collaboration with Edgehog Advanced Technologies Inc., we explored the use of commercially available organosilanes for glass surface modification for their simplicity, versatility, and ability to form stable bonds. These silanizing agents enable us to modify surface topography, reduce surface energy, impart specific functionalities to glass surfaces, and carry out post-modification reactions without altering the pre-existing coating.

This work is structured around three approaches, each focusing on key aspects of surface modification and characterizations. The first approach investigates the use of alkyl and perfluoroalkyl silanes deposited onto regular and nanotextured glass *via* dip-coating. We evaluated the wettability, topography, optical properties, and stability of the coatings under simulated environmental conditions, including rainfall simulation and outdoor exposure. Results demonstrated that short perfluoroalkyl chains enhanced hydrophobicity and reduced reflectance, while long alkyl chains produced smoother coatings with fewer polymerized aggregates. The combination of texturing and surface roughness significantly increased the water contact angle, demonstrating the potential of these coatings as protective layers against outdoor conditions such as dust accumulation and UV irradiation.

In the second approach, we used short chain alkenyltrichlorosilanes to modify glass surfaces with the aim to enhance wettability, optical properties, and stability. We employed a two-step surface modification strategy: dip-coating followed by functionalization with an alkanethiol *via* a radical-initiated thiol-ene click reaction. We investigated how a single-carbon variation in silanizing agents affects surface properties and how functionalization improves the stability of superhydrophobic surfaces. Advanced characterization techniques, including water contact angle measurements, scanning electron microscopy (SEM), atomic force microscopy (AFM), UV-Vis spectroscopy,

attenuated total reflectance-Fourier transform infrared spectroscopy (ATR-FTIR) and photo-induced force microscopy (PiFM), were employed to analyze the wettability, morphology, structure, optical and chemical composition of the coatings. PiFM, in particular, provided novel insights into the uniformity of functionalization and the efficiency of the thiol-ene click reaction, offering new perspectives for the development of durable superhydrophobic coatings.

The third approach introduces an innovative approach to functionalize glass surfaces using activated alkynes under mild conditions. This method enables the direct incorporation of various molecules, offering a versatile platform for creating functionalized surfaces with tailored properties. Unlike conventional methods, which often require harsh conditions or face challenges in obtaining uniform and stable functionalization, this approach offers a more efficient and flexible route to surface modification. Our proposed approach offers superior efficiency and versatility for applications enabling sensitive and selective detection.

Keywords : Hydrophobic surfaces; anti-reflection coatings; wettability; glass coatings; transparency; self-cleaning coatings; solar panels.

CHAPTER 1
INTRODUCTION

1.1 From Natural Waterproof Surfaces to Biomimetic Materials

In nature, various biological systems exhibit remarkable interactions with surrounding fluids, particularly water, through specialized multifunctional surfaces, as illustrated in Figure 1.1. These interactions result in a wide range of phenomena, such as the self-cleaning abilities of lotus leaves, the water-running capabilities of basilisk lizards (Tucker-Schwartz and co-workers), the slipperiness of Nepenthes pitcher plants (Bohn & Federle, 2004), and the antireflective properties of moth eyes (Han et al., 2020). Additional examples of nature's ingenuity include the anisotropic surface wettability of butterfly wings (Sun, Fang, et al., 2009) and the capability of water striders to stand and move on water (Hu & Bush, 2005). These examples demonstrate diverse strategies employed by natural surfaces to manage liquid interactions, ranging from extreme water repellency to specialized adhesion and slipperiness. Such systems not only ensure survival and adaptation to harsh environments but also inspire the development of biomimetic technologies, driving advancements in material science and engineering (Bhushan, 2009).

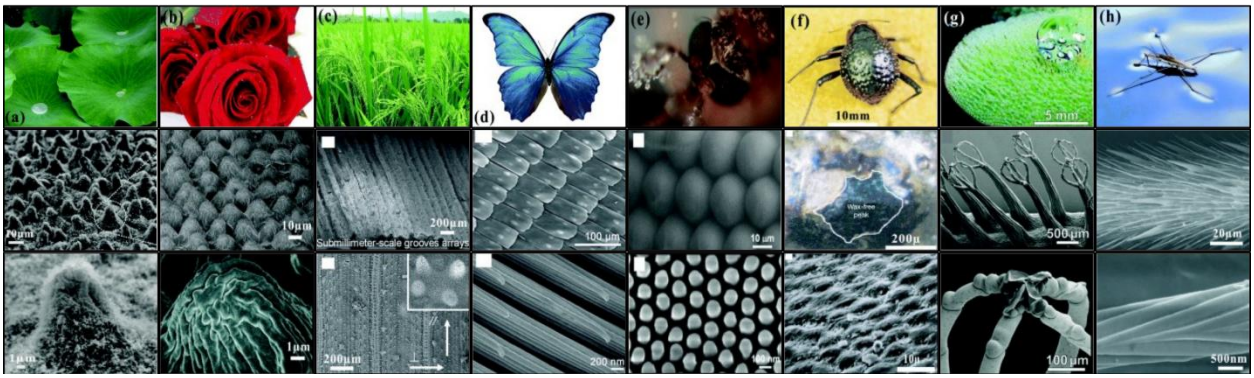

Figure 1.1 Photographs and corresponding multiscale structures (SEM images) of multiple biological surfaces exhibiting unique liquid interactions. (a) lotus leaf enabling superhydrophobicity and self-cleaning. (b) red rose petal exhibiting superhydrophobicity with high water adhesion. (c) rice leaf enabling anisotropic superhydrophobicity. (d) butterfly wing displaying directional liquid adhesion, superhydrophobicity and self-cleaning properties. (e) mosquito eye demonstrating superhydrophobic, antifogging, and antireflection properties. (f) desert beetle showing a unique combination of hydrophilic and hydrophobic patterns for efficient fog harvesting. (g) salvinia plant exhibiting superhydrophicity and underwater air retention. (h) water strider leg demonstrating remarkable superhydrophobic properties. Adapted from (Yong et al., 2017).

The natural waterproof behavior of certain plants, particularly the lotus leaf (Nelumbo nucifera), has attracted significant attention due to their ability to remain clean despite exposure to environmental contamination. Neinhuis and Barthlott (1997a) studied the surface topography of nearly 200 plant species and identified key features responsible for this phenomenon. These surfaces mostly exhibit common characteristics: (a) a hydrophobic wax coating, often in the form of an epicuticular film or crystalloids, which results in a Young contact angle greater than 90°; (b) micro-scale textures, such as bumps, typically around 10 μm in size; and (c) a secondary layer of nanostructures, often in the form of tiny hairs, measuring about 1 μm in size and placed on the microstructures (Otten & Herminghaus, 2004). The combination of hierarchical roughness and the low-surface-energy wax layer traps air beneath water droplets. This minimizes adhesion and enables the self-cleaning effect known as the lotus effect (Barthlott & Ehler, 1977; Barthlott & Neinhuis, 1997; Gao & McCarthy, 2006a; Neinhuis & Barthlott, 1997a; Quéré, 2005) .

Since these discoveries, the unique wetting characteristics of biological surfaces have inspired many researchers to develop synthetic analogs (Feng et al., 2008; Szczepanski et al., 2017; Wang, Xu, et al., 2022; Webb et al., 2011; Zhai et al., 2006). These biomimetic materials aim to replicate the morphological and interfacial properties of biological surfaces, with applications in multiple areas ranging from self-cleaning coatings to advanced fluid manipulation systems (Gao & McCarthy, 2006a; Zhu et al., 2021). Understanding the fundamental principles of wettability is essential for designing such materials with tailored liquid interactions. The following section discusses these principles in more detail.

1.2 Fundamentals on Wettability

Wettability is a fundamental surface property that defines the interaction between liquids and solid surfaces, playing a crucial role in various biological, chemical, and physical processes (Huhtamäki et al., 2018). When a liquid droplet interacts with a solid surface, it may either retain a hemispherical or a nearly spherical shape or spread out entirely, representing two distinct wetting behaviors. These behaviors are described as antiwetting, where the droplet minimizes contact with the surface, and superwetting, where the liquid completely spreads across the surface (Belhadjamor et al., 2018; Darband et al., 2020).

At the molecular level, wettability is determined by the balance of surface and interfacial free energies. The liquid's surface tension (γ_L, N m^{-1} or mJ m^{-2}) represents the reversible work required to create a unit area of new surface. The solid's surface free energy (γ_S, N m^{-1} or mJ m^{-2}) reflects the excess energy of atoms or molecules at the solid–vapor interface, arising from unbalanced intermolecular forces. Wettability results from the competition between these energies and the interfacial tension (γ_{SL}) at the liquid–solid interface, which dictates how a liquid spreads on a solid surface. High-energy surfaces (such as metals and glass) exhibit strong adhesion with liquids, resulting in low contact angles and high wettability. Low-energy surfaces (such as polymers or fluorinated materials) display weak adhesion with liquids and high contact angles, characteristic of hydrophobic or superhydrophobic behavior. Thus, controlling the surface free energy of solids provides a practical approach of tuning wettability for targeted functional applications (Hassanizadeh, 2024; Navascues, 1979; Zhu et al., 2023).

Thomas Young (1805) proposed an initial theoretical model to describe wettability on an ideal smooth and flat surface. This model is mathematically defined by Young's equation as follows:

$$cos\ \theta = \frac{\gamma_{SV} - \gamma_{SL}}{\gamma_{LV}} \qquad \text{Equation (1.1)}$$

Where, as shown in Figure 1.2, the contact angle (θ) is defined at the three-phase interface of the solid, liquid, and vapor phases. The terms γ_{SL}, γ_{LV}, and γ_{SV} represent the interfacial surface tensions of solid-liquid, liquid-vapor, and solid-vapor interfaces, respectively.

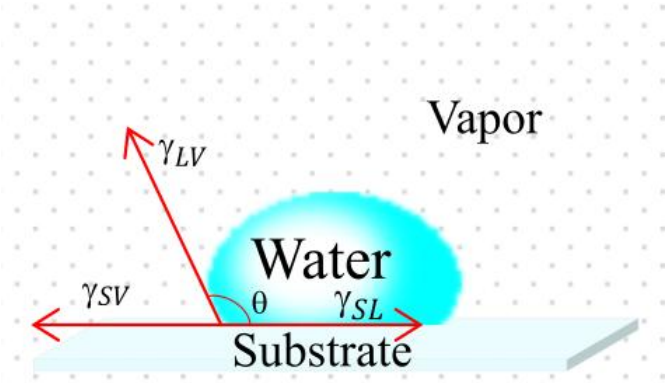

Figure 1.2 Schematic illustration of the correlation between the contact angle and interfacial tensions at a three-phase interface.

The interfacial behavior of a liquid droplet in contact with a solid substrate involves a balance of surface tensions at the three-phase contact line (Li et al. 2017). If γ_{SV} is larger than γ_{SL}, the droplet exhibits a spreading behavior across the surface, resulting in a contact angle less than 90°. However, when γ_{SL} is larger than γ_{SV} the liquid reduces its interaction with the surface by contracting into a more spherical shape, which leads to a contact angle exceeding 90°. A contact angle of 0° represents complete wetting, while 180° indicates complete non-wetting. However, these extremes are rarely observed in practice. As illustrated in Figure 1.3, surface wettability is conventionally categorized as follows: superhydrophilic ($\theta < 10°$), hydrophilic ($10 \leq \theta < 90°$), hydrophobic ($90° \leq \theta < 150°$), and superhydrophobic ($150° \leq \theta \leq 180°$) (Das et al., 2018).

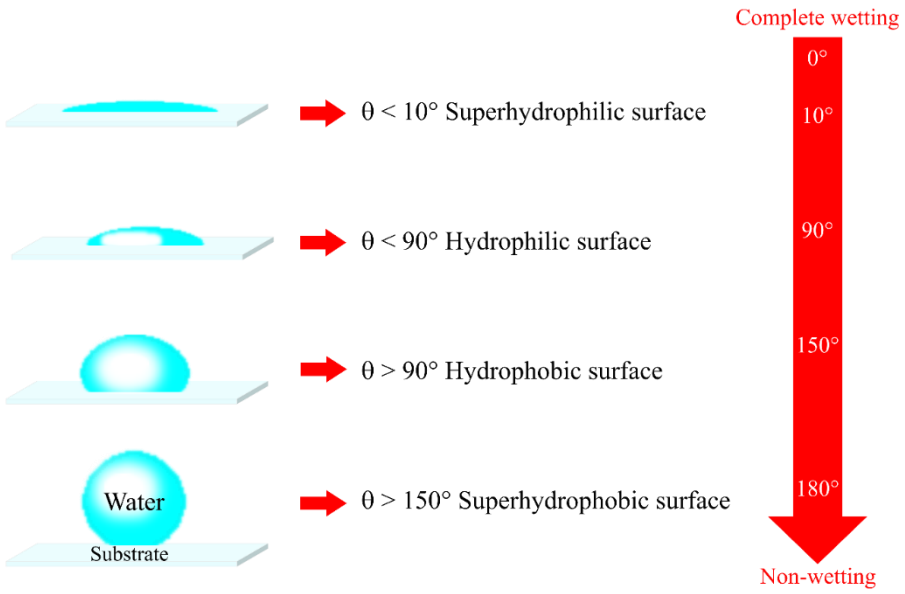

Figure 1.3 Schematic illustrations of surface wettability as defined by the water contact angle (θ). The wettability categories include superhydrophilic surface ($0 \leq \theta < 10°$), where the surface exhibits complete wetting; hydrophilic surface ($10 \leq \theta < 90°$), showing partial wetting; hydrophobic surface ($90° \leq \theta < 150°$), where water forms droplets on the surface, and superhydrophobic surface ($150° \leq \theta \leq 180°$), characterized by progressively decreasing wettability. At 180°, the surface achieves complete non-wetting. Adapted with permission from (Das et al., 2018). Copyright 2018 American Chemical Society.

1.3 Influence of Surface Roughness on Wettability

The wettability of a liquid on a solid substrate is governed by its interaction with the surface, with surface roughness playing an important role in controlling wettability (Belhadjamor et al., 2018). While Young's equation provides a foundational model for understanding wettability on an ideal, smooth, and flat surface, real-world surfaces are rarely perfectly smooth or flat. Wenzel (1936) assumed that a droplet placed on a rough surface spreads until it reaches equilibrium, involving more actual surface area than on a smooth surface. This amplifies the effect of surface energy, enhancing the material's intrinsic wetting properties. As a result, hydrophilic surfaces exhibit enhanced wettability, while hydrophobic surfaces demonstrate increased repellency. In 1936, Wenzel introduced an empirical correlation between surface roughness and apparent contact angle (Equation (1.2)).

$$\theta_W = r \cos \theta_Y \ with \ (r \geq 1) \qquad \text{Equation (1.2)}$$

Where θ_W corresponds to the apparent contact angle observed on rough surfaces according to Wenzel, while θ_Y represents the equilibrium contact angle predicted by Young for smooth surfaces. Surface roughness is characterized by the ratio (r) of the actual liquid-solid interfacial area to the projected geometric area (Equation (1.3)).

$$r = \frac{actual\ surface\ area\ in\ contact\ with\ the\ liquid}{geometric\ surface\ area} \qquad \text{Equation (1.3)}$$

As illustrated in Figure 1.4, the Wenzel model demonstrates that the liquid completely fills the valleys of the rough surface, leading to a homogeneous wetting. Because the actual surface area in contact with the liquid is larger than the flat geometric area, the roughness factor is always greater than 1. Consequently, larger values of r enhance hydrophilicity when $\theta_Y < 90$, whereas they enhance hydrophobicity when $\theta_Y > 90$.

While the Wenzel model effectively describes homogeneous wetting on rough surfaces, it is limited to thermodynamically stable states and surfaces with uniform chemical composition. Consequently, it is not suitable for dynamic wetting conditions or for surfaces with chemical heterogeneity (Sigmund & Hsu, 2015). Additionally, the Wenzel model does not adequately describe superhydrophobic behavior, where contact angles exceed 150° and heterogeneous wetting occurs due to trapped air pockets at the interface (McHale et al., 2004; Shome et al., 2022). Cassie and Baxter (1944b) proposed an alternative model to describe wetting on porous surfaces where the liquid does not fully penetrate the surface features (Figure 1.4). The Cassie-Baxter's equation, which describes this behavior, is given by:

$$cos\ \theta_{CB} = f_{SL}(cos\ \theta_Y + 1) - 1 \qquad \text{Equation (1.4)}$$

Where f corresponds to the fraction of the solid surface area in direct contact with the liquid relative to the total real surface area of the porous material. The θ_{CB} and θ_Y are the Cassie-Baxter's apparent contact angle and the contact angle derived from Young's equation, respectively. In 1948, this equation was further refined by Cassie into a more general form (Equation (1.5)). This was primarily developed to describe the wetting behavior of surfaces with heterogeneous chemical compositions.

$$cos\ \theta_C = f_1\ cos\ \theta_1 + f_2\ cos\ \theta_2\ \ with\ (f_1\ +\ f_2\ =\ 1)$$ Equation (1.5)

Where θ_C is Cassie's apparent contact angle, f_1 and f_2 are the fractions of the surface areas occupied by two components forming the heterogeneous surface ($f_1 + f_2 = 1$). θ_1 and θ_2 are the intrinsic contact angles of the liquid on these components, respectively. If both components have an equilibrium contact angle > 90°, the apparent contact angle θ_C also exceeds 90°, resulting in a hydrophobic surface. Conversely, if both components have an equilibrium contact angle < 90°, the θ_C will also be less than 90°, resulting in a hydrophilic surface. However, when one component has a contact angle higher than 90° and the other lower than 90°, the surface wettability is therefore determined by the relative surface fractions f_1 and f_2 (Cassie, 1948b).

Furthermore, liquid droplet behavior on surfaces with specific morphology, such as the lotus leaf, can be described more precisely by incorporating the roughness factor (r) into Cassie's equation as follows:

$$cos\ \theta_{CB}^{W} = r\ f_{SL}\ cos\ \theta_C - f_{LV}$$ Equation (1.6)

Where, f_{SL} and f_{LV} represent the area fractions of the solid-liquid and liquid-vapor, respectively, where $f_{SL} + f_{LV} = 1$ (Banerjee, 2008).

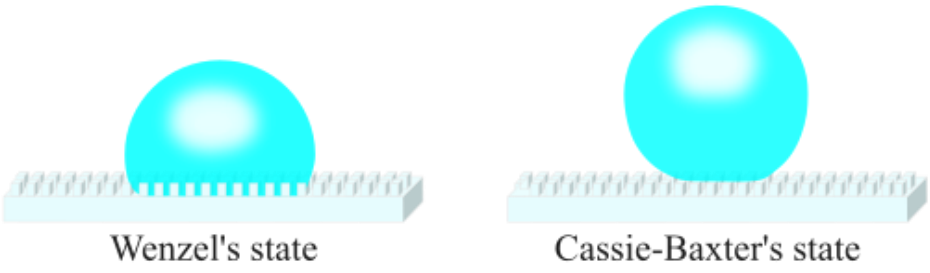

Figure 1.4 Schematic illustration of the homogeneous wetting regime (Wenzel's state), where the liquid completely fills the valleys of the rough surface, and the heterogeneous wetting regime (Cassie-Baxter's state), where the liquid rests on a dual-phase interface of solid and trapped air.

1.4 Wettability Characterization

Understanding how wettability is experimentally characterized is essential for quantifying liquid-solid interactions and distinguishing between the Wenzel and Cassie-Baxter wetting states (Law,

2022). This characterization involves several key parameters described below, including static water contact angle (WCA), contact angle hysteresis (CAH), and sliding angle (SA).

1.4.1 Static Water Contact Angle (WCA)

Static contact angle (θ), a key parameter in determining wettability, is defined as the angle formed at the three-phase interface of water, solid, and air. Experimentally, it is measured using an optical tensiometer, also known as a goniometer. This instrument (Figure 1.5) captures droplet images and analyzes the angle formed between the tangent of the droplet's surface and the solid surface (Huhtamäki et al., 2018). However, the static contact angle alone is insufficient for surfaces with high roughness, chemical heterogeneity, or dynamic wetting behavior. For superhydrophobic surfaces, in particular, additional parameters such as contact angle hysteresis and sliding angle must be considered (Miwa et al., 2000).

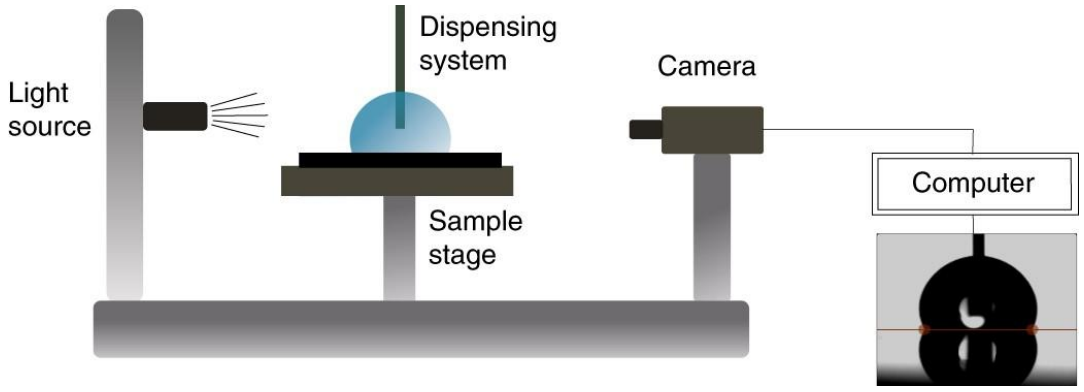

Figure 1.5 Schematic of an optical tensiometer consisting of an illumination source, a motorized sample stage, and a dispenser. Reproduced from (Huhtamäki et al., 2018) with permission from Springer Nature, copyright 2018.

1.4.2 Contact Angle Hysteresis (CAH)

Contact angle hysteresis is defined as the difference between the advancing (θ_{Adv}) and receding (θ_{Rec}) contact angles, arising due to surface roughness, chemical heterogeneity, and liquid adhesion (Nadkarni & Garoff, 1994). These angles are measured using either the needle-in method or the tilt-stage method (Figure 1.6). In the needle-in method, the droplet volume is systematically increased and decreased on the substrate surface, resulting in two distinct contact angle values. In the tilt-stage method, the droplet is deposited on a tilt-stage, and the CAH is determined right before the droplet starts to move. Superhydrophobic surfaces exhibit hysteresis as low as 10°, while

hydrophobic and hydrophilic surfaces show significantly larger values (Brzoska et al., 1994; Nadkarni & Garoff, 1994; Zhang et al., 2008). Such measurements are critical for characterizing superhydrophobic surfaces, providing insights into coating heterogeneity, surface roughness, and water droplet mobility.

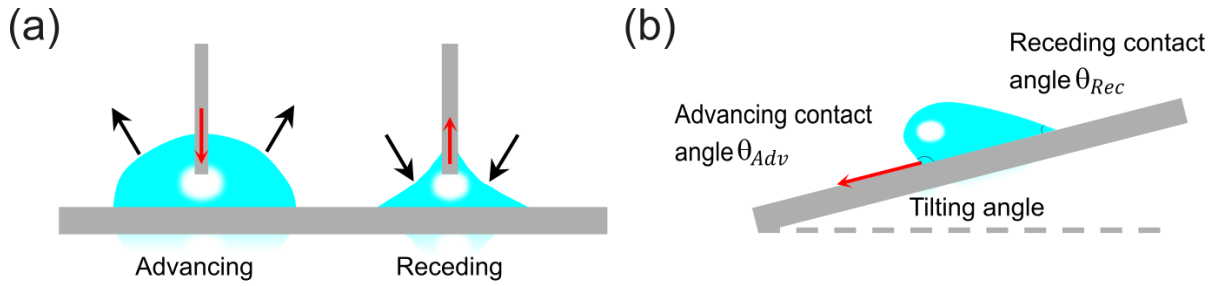

Figure 1.6 Measurement of contact angle hysteresis ($\theta_{Adv} - \theta_{Rec}$) using (**a**) the needle-in method and (**b**) the tilt-stage method.

The wetting state plays a crucial role in determining CAH behavior. In the Wenzel state, water droplets fill the valleys of the rough surface, creating strong pinning and making the surface sticky with high CAH. In contrast, in the Cassie-Baxter state, droplets rest on a dual-phase interface of solid and trapped air, resulting in reduced adhesion, making the surface slippery with low CAH (David et al., 2003; McHale et al., 2004; Patankar, 2003, 2004; Wang et al., 2010). However, irreversible transitions between the Cassie-Baxter and Wenzel states can occur, often leading to the loss of anti-adhesion properties typically characteristic of superhydrophobic surfaces (Lafuma & Quéré, 2003).

Some natural surfaces, such as rose petals, exhibit high water contact angles and, at the same time, very strong adhesion with water (Szczepanski et al., 2017). This phenomenon was explained by Feng et al. (2008) through the Cassie impregnating state, where the liquid partially fills surface textures while the plateaus remain dry, as depicted in Figure 1.7. The hierarchical micro- and nanostructures on the rose petals' surface were replicated on a polymer surface, confirming the relevance of the proposed Cassie impregnating state.

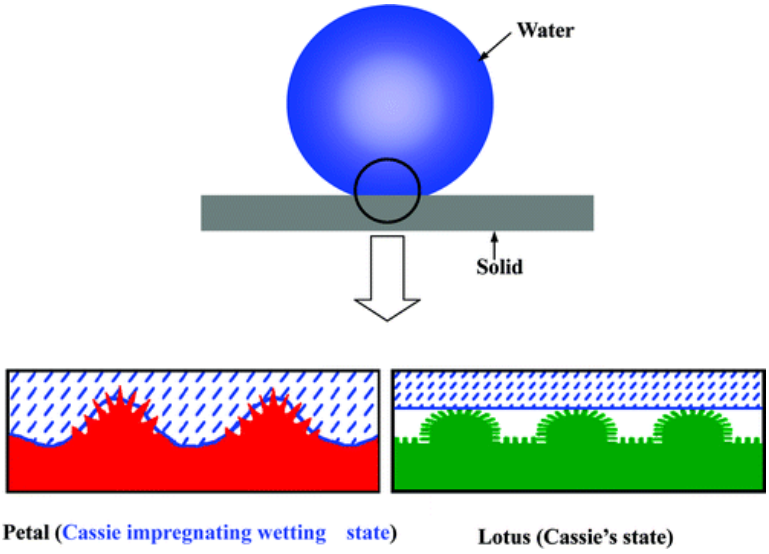

Figure 1.7 Schematic illustration of water droplet wetting behavior on a rose petal, exhibiting the Cassie impregnating wetting state, and a lotus leaf, exhibiting the Cassie state. Reprinted with permission from (Feng et al., 2008). Copyright 2008 American Chemical Society.

A subsequent study by Raza et al. (2012) demonstrated that hierarchical micro- and nanoscale roughness enables precise control of superhydrophobic surfaces, enabling the transition from high-pinning (CAH~48° and SA>90°) to non-pinning states (CAH~7° and SA~3°) (Figure 1.8). Their study highlighted that while surface roughness dominates chemical modification in achieving superhydrophobicity, the multi-scale structure controls the low adhesion behavior. Thus, optimizing such multi-scale roughness can achieve minimal CAH values, often less than 10°, characteristic of the Cassie-Baxter state. Wu et al. (2013) further investigated the correlation between CAH, sliding angle, and pinning force in superhydrophobic surfaces. Their study revealed that the interfacial adhesion forces exhibit no direct correlation with CAH. Instead, adhesive behavior was found to be primarily controlled by surface morphology, particularly the solid-liquid contact fraction and surface geometric features. These results highlight the critical role of hierarchical roughness in designing superhydrophobic surfaces with tunable wetting properties.

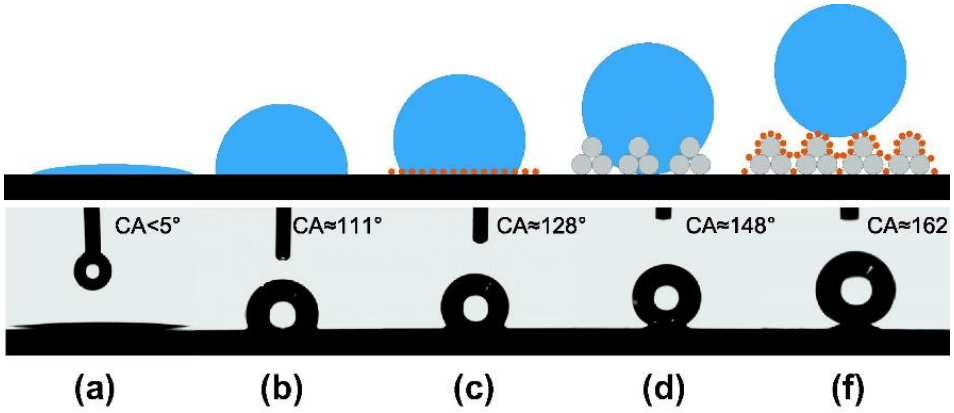

Figure 1.8 Impact of chemical composition and surface roughness on wettability. (a) water droplet on an untreated flat silicon substrate. (b) moderately hydrophobic surface after PFOTS treatment. (c) highly hydrophobic surface with gold nanoparticles deposition and chemical modification. (d) near-superhydrophobic surface using silica microsphere arrays with 1H,1H,2H,2H-perfluorooctyltriethoxysilane. (f) superhydrophobic hierarchically rough surface with gold nanoparticles and silica spheres after chemical modification. Reprinted from (Raza et al., 2012), Copyright 2012, with permission from Elsevier.

1.4.3 Sliding Angle (SA)

While CAH quantifies the change in contact angle as a droplet expands or contracts on a surface, the sliding angle refers to the minimum tilt angle required to overcome adhesion and initiate droplet motion. Thus, SA provides complementary insights into surface adhesion and self-cleaning efficiency, as illustrated in Figure 1.9 (Feng et al., 2008; Miwa et al., 2000). On hydrophobic surfaces (Figure 1.9a), SA typically exceeds 10°, with higher values reflecting stronger adhesion due to surface chemical composition and a relatively smooth topography. Consequently, droplets slide rather than roll off, which leads to inefficient contaminant removal. In contrast, superhydrophobic surfaces (Figure 1.9b) exhibit SA values below 10°, where droplets readily roll off due to minimal adhesion, enabling effective self-cleaning. However, SA is less quantitative than CAH, as it can be influenced by droplet volume (Yong et al., 2014). Additionally, it does not directly correspond to advancing and receding angles but rather to their difference (Zhang et al., 2008).

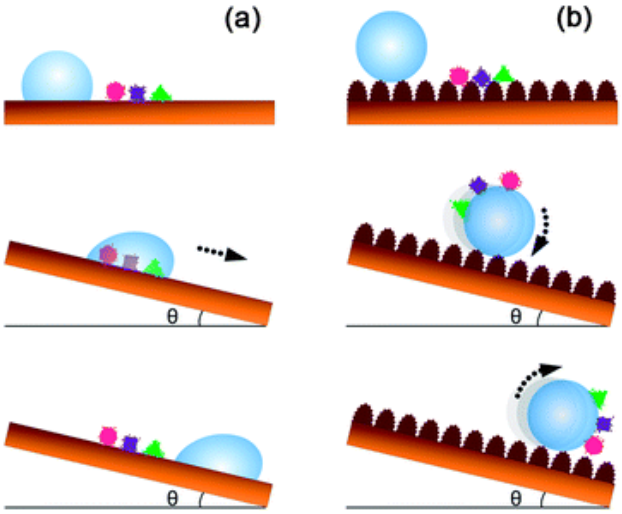

Figure 1.9 Illustration of self-cleaning performance on hydrophobic versus superhydrophobic surfaces. (**a**) on a smooth surface, the water droplet slides without effectively removing surface contaminants. (**b**) on a superhydrophobic surface, the droplet remains spherical and rolls off easily, carrying away surface contaminants. Used with permission of the Royal Society of Chemistry, from (Zhang et al., 2012); permission conveyed through Copyright Clearance Center, Inc.

1.5 Influence of Surface Chemistry on Wettability

Although roughness can enhance wetting properties, the surface chemistry fundamentally determines the interaction between a liquid and the surface (Good, 1992; Sun, Feng, et al., 2005). While many studies have focused on roughness modification to tailor wettability (Hideo et al., 1998; Kubiak et al., 2011; Uelzen & Müller, 2003), others have explored tuning surface free energy through chemical treatments (Nuzzo et al., 1990; Song et al., 2019). These chemical approaches typically involve using high- or low-surface-energy materials to introduce polar or nonpolar functional groups to the surface (Borras & González-Elipe, 2010; Jothi Prakash & Prasanth, 2021).

Silanes are widely used chemicals for surface modification (Artus et al., 2006a; Gao & McCarthy, 2006b; Wong & Yu, 2013b), as they form stable covalent Si–O–Si bonds with oxide surfaces while introducing low-surface-energy terminal groups, such as $-CH_3$ and $-CF_3$. These terminal groups exhibit weak intermolecular interactions, thereby reduce surface free energy and result in low wettability and high contact angles, characteristics typical of low-surface-energy surfaces (Choi et al., 2016; Huang et al., 2019; Li et al., 2015a; Pujari et al., 2014b; Yu et al., 2020). Moreover, perfluorinated coatings, known for their extremely low surface energy (~6-18 mN m^{-1}), are particularly effective in achieving hydrophobicity and oleophobicity, enabling applications in anti-

biofouling, drag-reduction, and self-cleaning surfaces (Cheng et al., 2013; Cichomski et al., 2020; Fadeev & McCarthy, 1999; Knepper & Lange, 2011; Kujawa et al., 2016; Stefanie et al., 2004; Zhang, Wang, et al., 2014). Other techniques for modifying surface chemistry include gas- and liquid-phase oxidation (Seo & Park, 2009), plasma (Caschera et al., 2014), and UV/ozone treatment (Hamdi & Poulis, 2021).

While surface energy is a fundamental factor influencing a material's intrinsic wettability (Liu et al., 2013; Su et al., 2016b), surface roughness plays a pivotal role in achieving exceptional anti-wetting characteristics. Recent studies have shown that re-entrant structures can inherently enhance superhydrophobicity regardless of surface energy (Joly & Biben, 2009; Silvestrini & Brito, 2017; Song et al., 2019). Moreover, the interaction between surface energy and roughness significantly governs the overall wettability, enabling enhanced superhydrophobic properties (Coffinier et al., 2013; Dallinger et al., 2023; Su et al., 2019). Therefore, combining surface chemistry and topography allows designing materials with tailored wetting properties for diverse applications.

1.6 Fabrication of Hydrophobic and Superhydrophobic Surfaces

Inspired by natural non-wettable surfaces, researchers have developed multiple methods to fabricate hydrophobic and superhydrophobic surfaces (Nambafu et al., 2022; Wang, Xu, et al., 2022). These methods typically combine surface roughness with low surface energy, achieved through physical and chemical modifications in parallel. Polytetrafluoroethylene (PTFE), paraffin wax, and alkyl- or perfluoro-alkylsilanes typically exhibit water contact angles between 90° and 120° on smooth surfaces. They are commonly used to prepare hydrophobic surfaces (Xu et al., 2020). Early experiments by Ollivier (1907) investigated how variations in topography and surface chemical composition influence wetting behavior and capillarity of polished metal surfaces. They demonstrated that applying wax coating (paraffine or tallow) and fine powders (such as soot, lycopodium, or arsenic trioxide) could significantly enhance water repellency. While hydrophobic surfaces primarily rely on materials with low surface energy, achieving superhydrophobicity additionally requires the presence of micro- or nanoscale surface roughness. In some cases, microscale roughness combined with low surface energy is sufficient to achieve superhydrophobicity (contact angles >150°) (Bhushan & Chae Jung, 2007; Raza et al., 2012). However, hierarchical roughness is often preferred for enhanced performance, including reduced

contact angle hysteresis, improved self-cleaning properties, and superior mechanical durability (Bittoun & Marmur, 2012; Michael & Bhushan, 2007).

Current fabrication methods are generally classified as either top-down or bottom-up approaches (Figure 1.10). These strategies enable precise control over surface wettability for a wide range of applications, including self-cleaning surfaces used in optoelectronics and automotive, oil-water separation membranes used in wastewater treatment, anti-icing and de-icing coatings used in power lines and aircraft surfaces, microfluidics and lab-on chip devices. Top-down approaches involve physical modifications (molding, laser ablation, etching, and lithography) followed by chemical treatments. In contrast, bottom-up approaches rely on building roughness structures through processes such as chemical vapor deposition (CVD), sol-gel synthesis, and self-assembly, providing scalable and cost-effective solutions (Zhu et al., 2021).

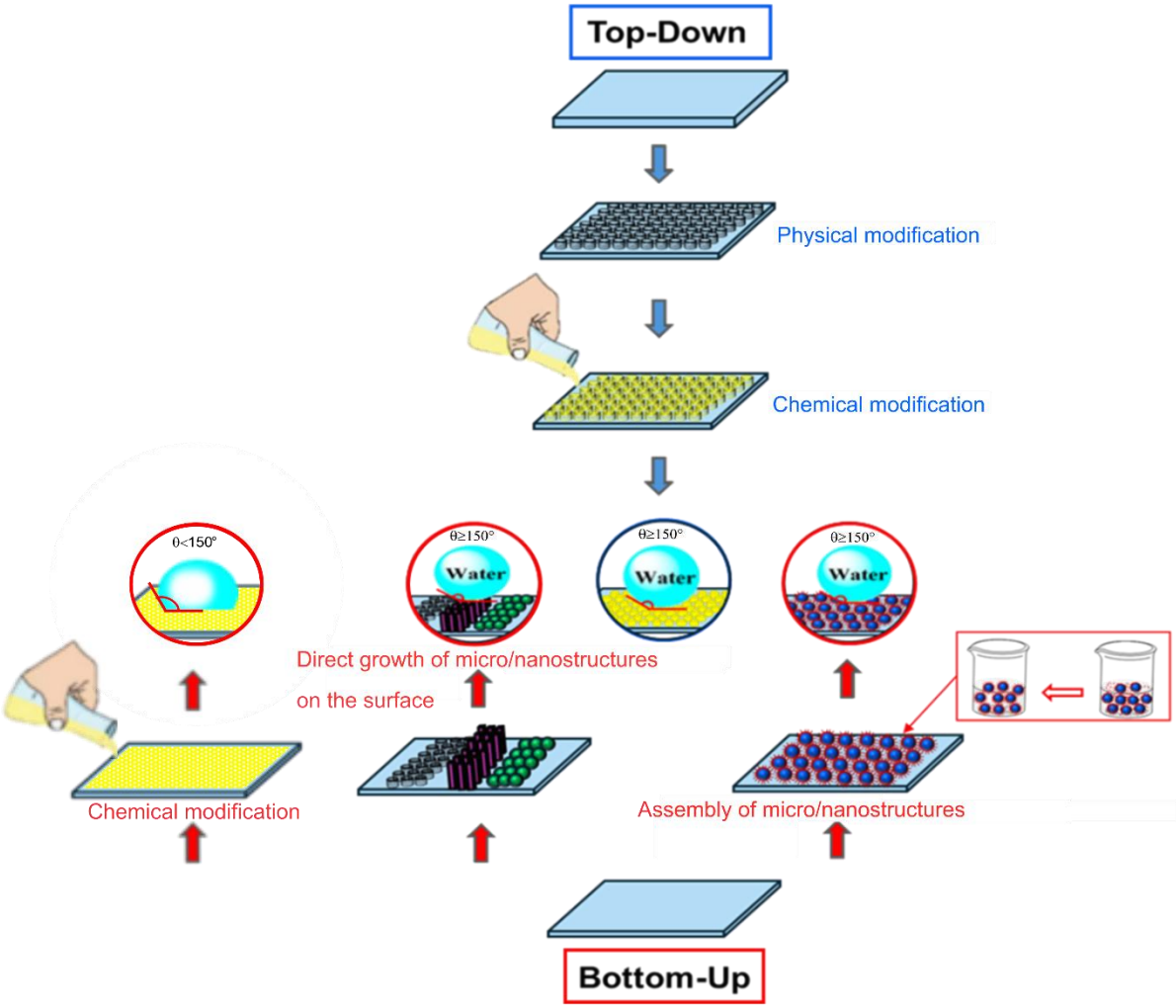

Figure 1.10 Schematic representation of the top-down and bottom-up approaches for fabricating hydrophobic and superhydrophobic surfaces. The top-down approach involves physical modification techniques followed by chemical treatments. The bottom-up approach relies on micro- or nanostructures that are either grown directly or assembled onto the surface with tailored roughness and reduced surface energy.

1.6.1 Top-Down Approaches

Molding replication is recognized as one of the simplest and cost-effective techniques for mimicking hierarchical micro- and nanostructures. As a method inspired by natural non-wettable surfaces such as lotus leaves, it is not limited to these biological models. Synthetic templates, such as those fabricated through laser processing, lithography or etching, can also be replicated to produce superhydrophobic surfaces (Chen et al., 2025). In a typical process, the pattern is first microstructured on a substrate, creating a negative mold, using silicon or aluminum oxide as a

template, and the complex patterns are then replicated onto a synthetic substrate using polymers such as polydimethylsiloxane (PDMS), polystyrene, or polypropylene.

Fürstner et al. (2005) demonstrated the effectiveness of this method by replicating the lotus leaf hierarchical structure using a two-component silicone mold. The process involved applying the silicone compound to the leaf surface, curing it to create a flexible mold, and then casting polyether into it. Due to the polymer's inherent hydrophobicity, no additional surface treatment was required. However, the replication process was unable to reproduce the delicate 200 nm wax crystals of the lotus leaf. Despite this limitation, the replica demonstrated exceptional superhydrophobicity and excellent self-cleaning properties when exposed to water droplet fog or kinetic-driven energy water droplets. This indicated that the microstructure of the papillae alone was sufficient to achieve optimal water repellency.

Similarly, Sun, Luo, et al. (2005) replicated the hierarchical structures of the lotus leaf onto PDMS using a nanocasting technique (Figure 1.11). The process involved casting a mixture of liquid PDMS and its catalyst onto a fresh lotus leaf. Upon curing and subsequent detachment, this process yielded a model PDMS surface exhibiting the inverse topography of the natural leaf. This first mold exhibited moderate hydrophobicity with 110°. Further coating the mold with trimethylchlorosilane (MTCS) as a non-adhesive layer was performed. A second casting with PDMS produced a positive replica, closely duplicating the original lotus leaf surface. This second mold achieved superior hydrophobicity (~160°). This method replicated the hierarchical structures of the lotus leaf, as confirmed by SEM analysis.

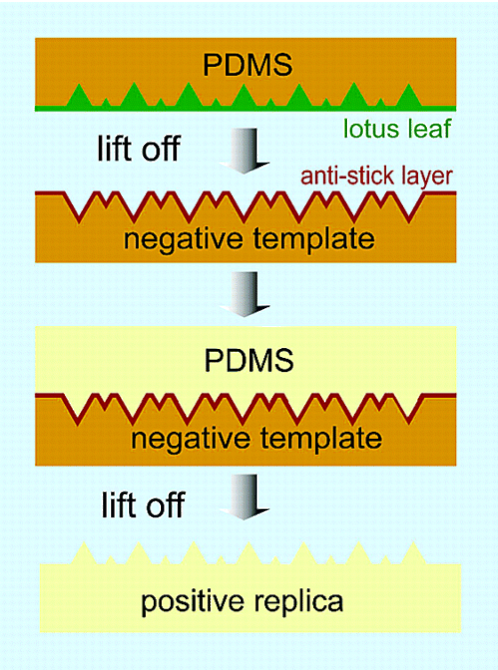

Figure 1.11 Schematic illustration of the fabrication process for a bio-inspired superhydrophobic surface using lotus leaf as a replication template. Reprinted with permission from (Sun, Luo, et al., 2005). Copyright 2005 American Chemical Society.

In addition to flexible molds made from silicone and PDMS, rigid molds are commonly employed in creating superhydrophobic surfaces. Han et al. (2019) developed a flexible biomimetic film that combines self-cleaning and antireflective properties. The researchers employed a sol-gel process to fabricate a polymethylmethacrylate replica of cicada wing nanostructures (Figure 1.12). This approach holds significant potential for implementation in optical systems requiring multifunctional performance.

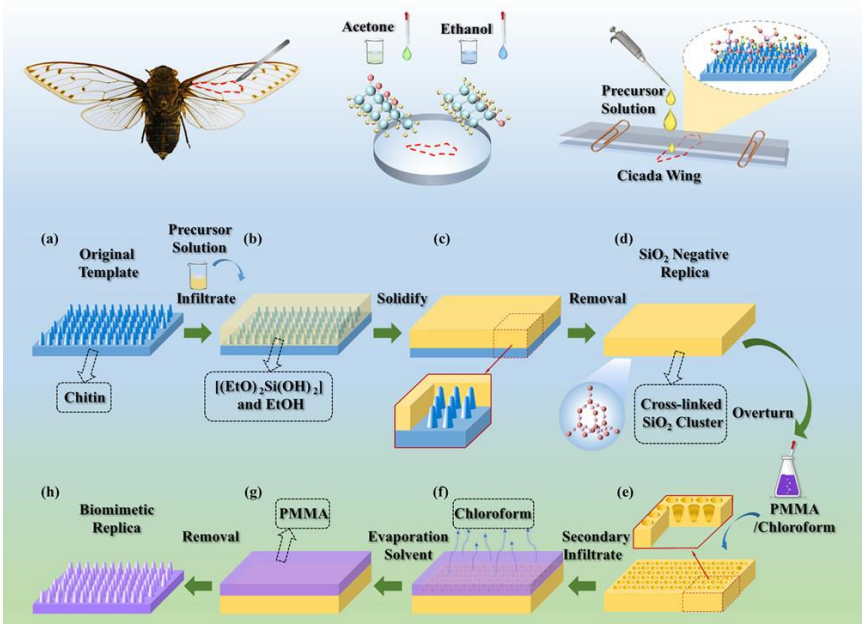

Figure 1.12 Illustration of the fabrication of a hierarchical biomimetic superhydrophobic film using PMMA mold. Reprinted with permission from (Han et al., 2019). Copyright 2019 American Chemical Society.

Lithography and nanoimprint techniques have also been employed in micro- and nanostructure processing due to their large-scale and high-resolution advantages. Wu et al. (2016) reported an effective method to replicate the complex vein patterns of multiple plant leaves accurately. The process involved creating a negative mold of the leaf's vein structure by soft lithography and casting PDMS onto the mold to transfer the complex patterns. This approach replicated the leaf surface's hierarchical micro- and nanoscale features and enabled the creation of enclosed microfluidic networks within the PDMS substrate. The replicated surfaces exhibited superhydrophobicity combined with low surface adhesion. The integrated microfluidic networks demonstrated potential for applications in microscale analytical devices and biomimetic designs.

Superomniphobic surfaces, exhibiting universal liquid repellency against both high- and low-surface-tension liquids, have recently gained significant attention (Pan et al., 2013). Liu et al. (2024) developed a novel fabrication strategy for flexible re-entrant liquid-super-repellent surfaces with robust superomniphobicity. Their approach employed a cost-effective single-exposure ultraviolet proximity lithography technique to produce microstructures with finely controlled single and double re-entrant features. The researchers used nanoclay-modified poly(N-isopropylacrylamide) and fluorinated silica particles in the molding process to enhance durability and pressure resistance.

The resulting three-layer hierarchical surface demonstrated excellent omniphobic self-cleaning properties with adequate optical transparency.

Nature-inspired surfaces exhibiting superamphiphobic characteristics have also been widely investigated. Atthi et al. (2021) developed a scalable approach for producing microstructured surfaces with simultaneous superhydrophobic and oleophobic functionalities. They employed roll-to-plate nanoimprint lithography, an advanced technique to replicate micro pillars and circular ring patterns on polycarbonate and polyethylene terephthalate substrates. This method proved more effective than conventional methods for large-area fabrication, showing potential for anti-biofouling applications.

Laser ablation is another promising technique for fabricating superhydrophobic surfaces, demonstrating controllable and eco-friendly effectiveness across different materials (Ahmad et al., 2018). Jagdheesh et al. (2011) demonstrated the effectiveness of ultrashort-pulse laser machining in creating dual-scale roughness on metallic substrates. Following laser texturing, the surfaces were functionalized with perfluorinated octyltrichlorosilane, resulting in a robust superhydrophobicity. The study revealed that the laser-induced dual-scale structures significantly enhanced water repellency, achieving static contact angles greater than 150°.

1.6.2 Bottom-Up Approaches

While extensive progress has been made, top-down approaches face challenges in fabricating superhydrophobic surfaces, such as directional manufacturing limitations, poor scalability, and incompatibility with complex geometries. These limitations have led to the development of bottom-up approaches, which offer high flexibility, scalability, and compatibility with various materials and geometries. Bottom-up approaches involve the direct growth of micro/nanostructure on a surface, or the assembly of micro/nanostructures followed by their integration onto the surface.

Gao and McCarthy (2006b) reported a simple approach using a silicon wafer substrate and phase separation process to prepare a transparent superhydrophobic surface. Their method involved immersing a silicon wafer in a toluene solution of methyltrichlorosilane, followed by rapid solvent extraction using ethanol. The fabricated silicone surface demonstrated extreme hydrophobicity, with both advancing and receding contact angles of approximately 180°. The formation of a 3D

methylsilicone network structure was confirmed through SEM analysis (Figure 1.13), which revealed fibers with a diameter of about 40 nm.

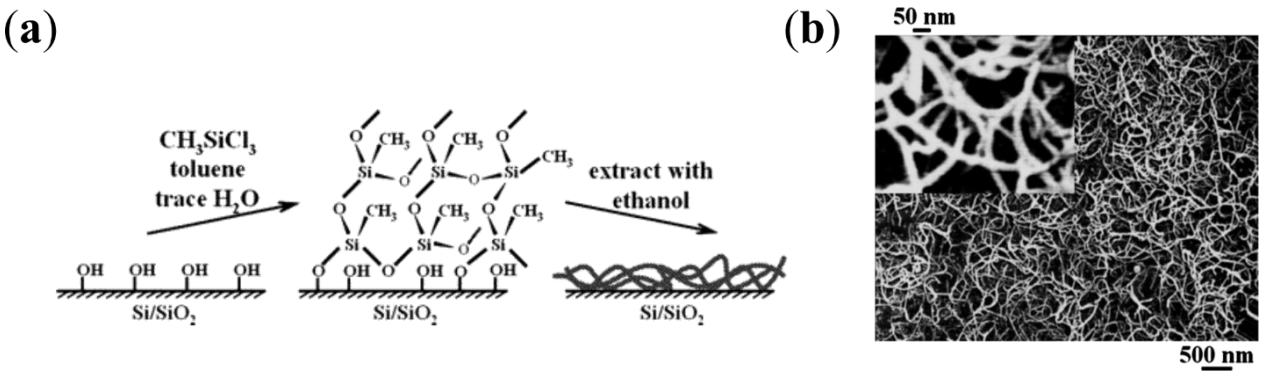

Figure 1.13 Fabrication of a superhydrophobic surface (a) 3D methylsilicone network formation (b) SEM images of the network's nanostructure. Reprinted with permission from (Gao & McCarthy, 2006b). Copyright 2006 American Chemical Society.

While dip-coating offers cost effectiveness and simplicity, aerosol deposition enables localized deposition without complete immersion, allowing uniform coverage on complex and enclosed substrates. Wong et al. (2017) developed an omnidirectional flame aerosol deposition technique to create highly transparent (up to 99.97%), superhydrophobic and oleophobic surfaces using SiO_2 nanoparticles. Their approach enables the fabrication of inverted cone nanotextures with unique re-entrant angles, resembling the branched structure of broccoli (Figure 1.14). By varying deposition times between 15 s and 120 s, the researchers were able to finely control the thickness of the resulting nanotextures. They tailored the crown diameter and significantly reduced the inter-pitch distance (from tens to sub-10-nanometer scales). This precise control enabled the surface to effectively repel picoliter-sized droplets. Subsequent functionalization with trichloro(1H,1H,2H,2H-perfluorooctyl)silane (PFOTS) imparted superamphiphobicity, enabling the surface to repel liquids with surface tensions as low as 25 mN m^{-1}. This approach overcomes previous limitations in imparting multifunctional coatings across flat, curved, and even enclosed surfaces such as tubes and hypodermic needles.

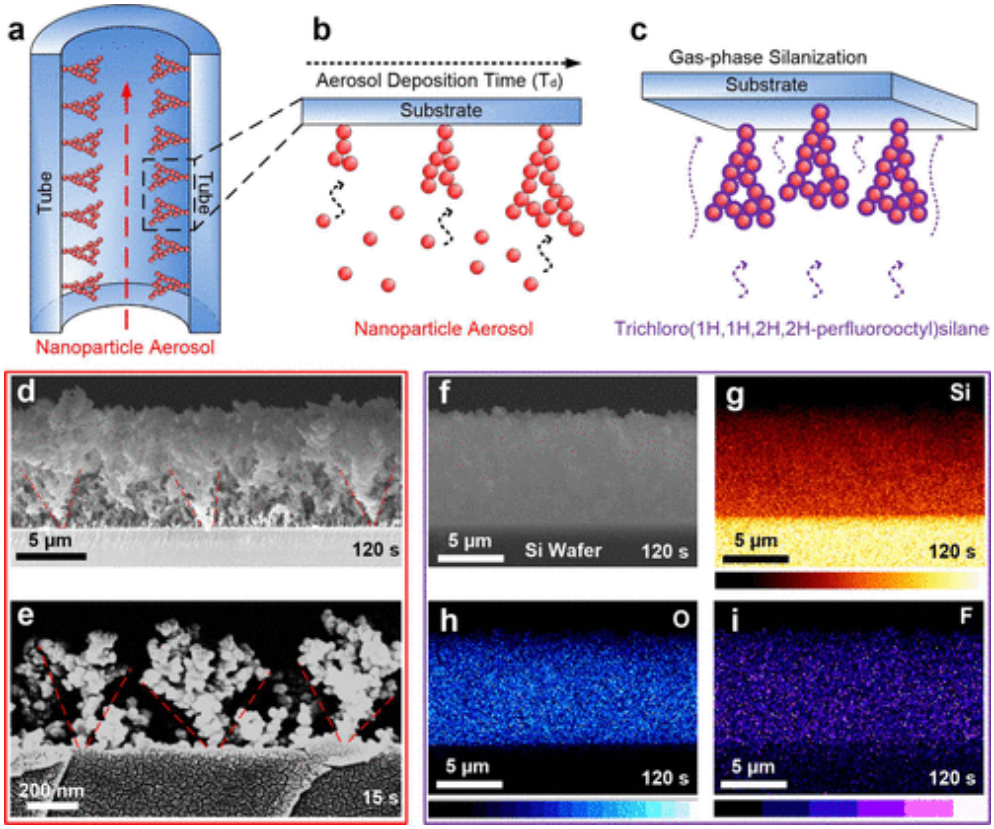

Figure 1.14 Omnidirectional nanoparticle assembly. (a,b) aerosol deposition and subsequent (c) vapor-phase silanization. Morphological evolution shown *via* cross-sectional SEM images at (d) 120 s and (e) 15 s deposition. (f–i) EDX elemental maps confirming fluorosilanization with (i) fluorine atoms shown in purple. Reprinted with permission from (Wong et al., 2017). Copyright 2017 American Chemical Society.

Huang and Yu (2021) developed a stable superhydrophobic and oleophobic coating *via* spray-coating approach (Figure 1.15). They dispersed nano- and micron-sized SiO_2 particles in different mass ratios into fluorinated epoxy. The optimized coating was achieved using equal quantities of nano- and micro-sized silica particles, resulting in a re-entrant structure that enhanced liquid repellency. This coating provided high contact angles of 158.6° for water, 152.4° for glycerol, 153.4° for ethylene glycol, and 140.7° for diiodomethane. Additionally, the coating demonstrated excellent mechanical and chemical durability, along with self-cleaning behavior, resistance to corrosion, and anti-icing properties performance, making it a promising candidate for multiple practical applications.

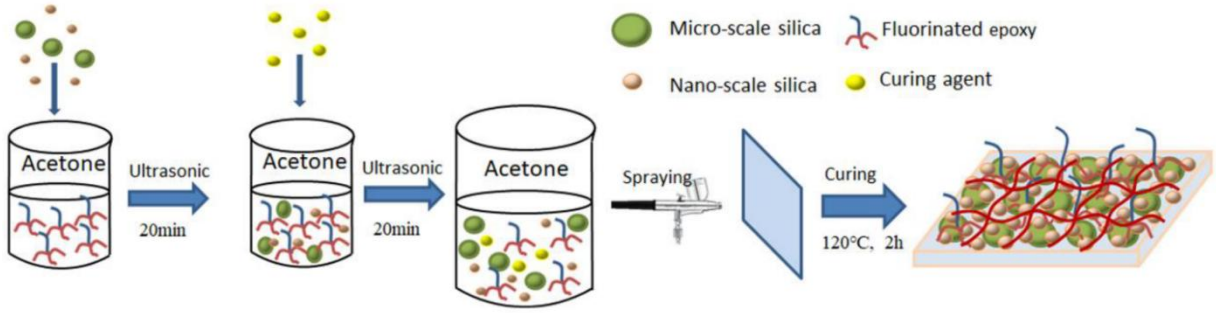

Figure 1.15 Scheme of the preparation of a superhydrophobic and repellent coating by spray coating approach. Reproduced with permission from (Huang & Yu, 2021); published by MDPI, 2021.

Wu et al. (2020) developed a cost-effective method to fabricate a candle soot-silica-PDMS-based photothermal icephobic surface (Figure 1.16). The surface featured hierarchical nano/microstructures combined with photothermal activity and mechanical durability. It achieved superhydrophobicity through the low-surface-energy of PDMS brushes. Under simulated solar exposure, the surface temperature increased by 53 °C, preventing ice formation even at ambient temperatures as low as -50 °C. Additionally, accumulated ice and frost melted within 300 s. The superhydrophobic coating allowed melted water to slide off, keeping the surface clean and dry. Notably, oxygen plasma-treated surfaces showed instant superhydrophobic recovery upon sunlight exposure due to the rearrangement of the PDMS brushes. This approach provides an eco-sustainable and energy-efficient approach to anti-icing applications using cost-effective materials and simple fabrication techniques.

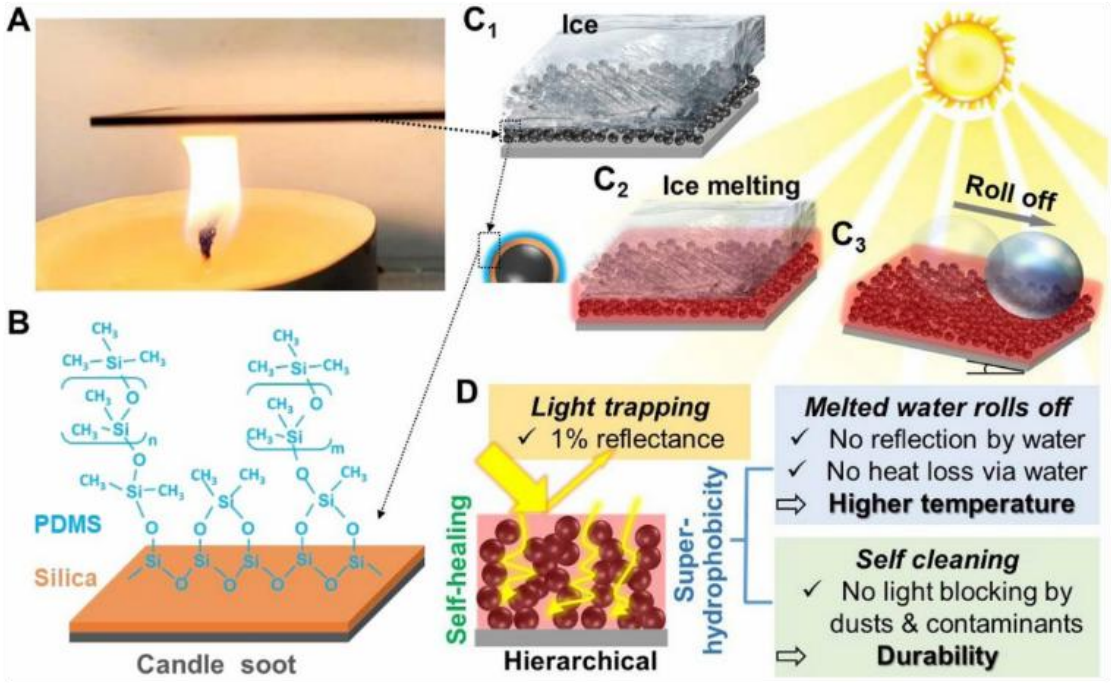

Figure 1.16 Fabrication process and mechanism of a photothermal icephobic surface. (**A**) flame deposition of candle soot on glass substrate; (B) hierarchical multicomponent structure (candle soot-SiO_2 shell-grafted PDMS brushes); (**C**) de-icing mechanism: (**C_1**) ice accumulation, (**C_2**) photothermal melting, and (**C_3**) droplet rolling off the surface on a tilted surface. (**D**) dual functionality: sunlight absorption and superhydrophobicity. Reproduced from (Wu et al., 2020).

1.7 Organosilanes Self-Assembly

Among various bottom-up approaches, self-assembly has emerged as a simple and versatile method for surface modification. It enables chemical modification and nanoscale roughness, which are critical features for superhydrophobic surfaces. Self-assembled monolayers (SAMs) are ordered structures that form through the spontaneous adsorption of active precursor molecules onto solid substrates, providing an efficient route to functionalized surfaces (Prashar, 2012). While the concept of monolayer formation was first introduced by Bigelow et al. (1946), research on SAMs remained unexplored until Sagiv (1980a) demonstrated the covalent grafting of *n*-octadecyltrichlorosilane (OTS) in the early 1980s. Since then, the field has seen extensive development (Ulman, 1996), particularly in understanding the assembly of organosilanes on multiple substrates such as silicon, glass, mica, and gold (Carson & Granick, 1989a; Fadeev & McCarthy, 2000; Huang et al., 2017b; Jumrus et al., 2020a; Kessel & Granick, 1991; Kondo et al.,

2013; Nanda et al., 2017b; Pesek & Matyska, 1997a; Wasserman et al., 1989; Zhang, Li, et al., 2014a).

Organosilanes with the general formula $RSiX_3$, $RSi(CH_3)X_2$ or $RSi(CH_3)_2X$ (where X=Cl, OCH_3, or OC_2H_5) react with hydroxylated oxide surfaces under either vapor- or liquid-phase reactions (Pallandre et al., 2006). Alkyltrichlorosilanes are the most widely studied due to their ability to form densely packed self-assembled monolayers (Ulman, 1996; Wasserman et al., 1989). The self-assembly mechanism involves four steps in the presence of trace amounts of water: physisorption, hydrolysis, covalent grafting to the substrate, and in-plane reticulation (Figure 1.17). After physisorption of the organosilane on the water layer, it hydrolyzes, yielding hydroxysilanes ($RSi(OH)_3$). Subsequently, these hydroxysilanes adsorb onto the oxide surface *via* hydrogen bonds, while maintaining lateral mobility. This yields molecular aggregates driven by intermolecular interactions, including van der Waals forces, dipole-dipole interactions, and hydrogen bonding (Brzoska et al., 1994; Pujari et al., 2014b; Ulman, 1996). Therefore, the adsorbed water layer is essential for the hydrolysis of silane headgroups and lateral molecular mobility, ensuring the formation of well-ordered monolayers (Pallandre et al., 2006). Finally, covalent bonding occurs *via* condensation between the silanol groups of the adsorbed silanes and the surface hydroxyl groups, as well as with neighboring silanol groups, yielding siloxane bonds, enabling the formation of a densely packed monolayer. Uncontrolled conditions may additionally promote intermolecular crosslinking, yielding 3D polysiloxane networks (Brzoska et al., 1994; Pujari et al., 2014b; Sagiv, 1980a; Ulman, 1996).

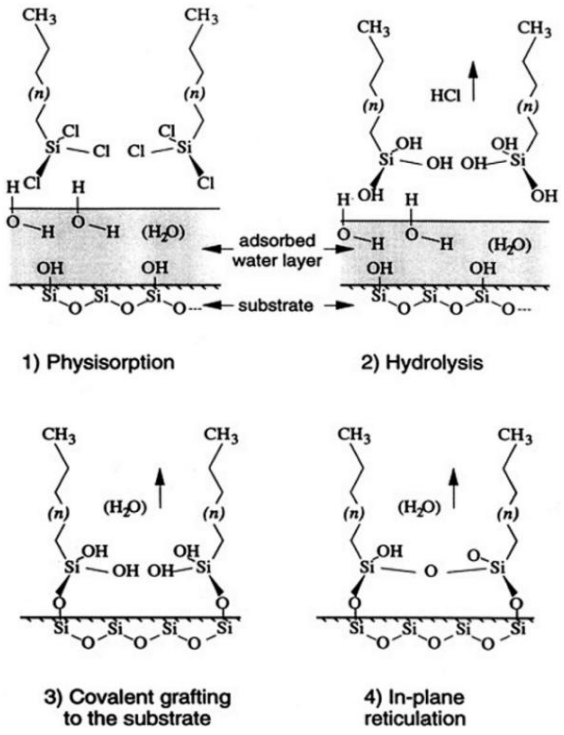

Figure 1.17 General mechanism for the silanization reaction. Reprinted with permission from (Brzoska et al., 1994). Copyright 1994 American Chemical Society.

More recently, Fadeev and McCarthy (2000) demonstrated that mono- di- and trifunctional silanes react with oxide surfaces through multiple pathways beyond conventional monolayer self-assembly depending on the reaction conditions. In addition to covalent grafting, other mechanisms, including lateral and vertical polymerization, leading to the formation of polysiloxane networks on the surface, are also possible, as illustrated in Figure 1.18. They highlighted the importance of reaction conditions (solvent, temperature, and catalyst) and alkyl chain length (C1-C18) in determining the final structure of the covalently attached layers. In vapor phase deposition, short- and intermediate-chain trichlorosilanes predominantly formed polysiloxane grafted layers through a proposed 3D polycondensation mechanism (Figure 1.18). However, longer alkyl chains enabled ordered self-assembly driven by intermolecular interactions. In liquid phase reactions, particularly using an amine catalysis at high temperatures, covalent grafting of alkyltrichlorosilanes occurred. This suggested lower bonding density and greater alkyl chain disorder than conventional self-assembled monolayers.

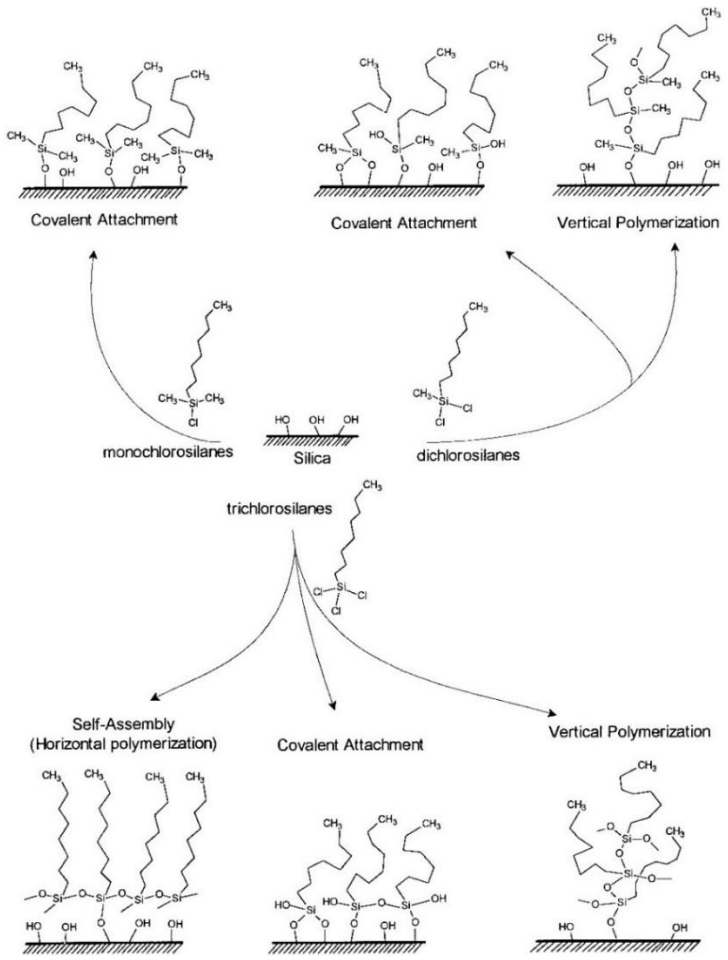

Figure 1.18 Schematic representation of alkylchlorosilanes' possible bonding to silicon dioxide surfaces. Reprinted with permission from (Fadeev & McCarthy, 2000). Copyright 2000 American Chemical Society.

The reproducibility of uniform organosilane self-assembled structures relies on careful optimization of reaction conditions, including humidity, temperature, solvent, reaction time, and silane concentration (Ariga, 2012; Brzoska et al., 1994; Khoo & Tseng, 2008; Watson, Nie, et al., 2015). Among these factors, the amount of water present during silanization plays a decisive role, as the initial hydrolysis of trichlorosilanes governs the film's final quality and morphology (Pujari et al., 2014b). Monolayer formations (covalent grafting and self-assembly) or vertical polymerization into multilayer or bulk polymerization are mainly governed by the concentration of surface hydroxyl groups and the adsorbed water layer (Rollings & Veinot, 2008; Zimmermann, 2008). In solution-phase silanization, the concentration of water in the solvent and the degree of surface hydration strongly influence silane reactivity and monolayer formation. Tripp and Hair (1992) investigated the reactivity of alkyltrichlorosilanes on silica surfaces under varying water

concentrations of adsorbed water. They demonstrated that alkyltrichlorosilanes require more than a monolayer of adsorbed water to achieve optimal monolayer deposition. Additionally, McGovern et al. (1994) demonstrated that even trace amounts of water were shown to be essential for initiating hydrolysis and subsequent condensation of trichlorosilanes. They reported that a low water concentration of approximately 0.15 mg per 100 mL of solvent is optimal for forming well-defined monolayers. Although, such low water concentration may slow down the adsorption kinetics, sometimes resulting in incomplete coverage. Angst and Simmons (1991) observed that hydrated silicon wafers facilitate a densely packed OTS monolayers, whereas dehydrated substrates yield incomplete coverage. In contrast, excessive water promotes uncontrolled polycondensation, leading to 3D siloxane networks and rough heterogeneous films (Fadeev & McCarthy, 2000).

The amount of water in the system during oxide surface modification with trichlorosilanes is critical in determining the resulting nanostructure morphology. In contrast, more complex nanostructures can emerge when the water content increases. Zhang, Wang, et al. (2014) developed a *Nepenthes* pitcher-inspired coating composed of perfluorinated silicone nanofilaments infused with Krytox using toluene with a water content of 12 mg per 100 mL of solvent. The resulting nanofilaments exhibited diameters ranging from 50 to 90 nm. Similarly, Zhang and Seeger (2011) employed water concentrations ranging from 5.6 to 19.4 mg per 100 mL of toluene. They produced transparent superhydrophobic coatings on glass *via* dip-coating and subsequent chemical modification. The proposed approach yielded perfluorinated silicone nanofilaments of similar diameter (50 to 90 nm). However, neither study specified the method of water addition to the toluene, or the technique used to measure water concentration.

Vapor-phase silanization offers an alternative approach with enhanced control of relative humidity and film morphology. Artus et al. (2006a) demonstrated that reactions between equimolar amounts of MTCS and water vapor (corresponding to 37% relative humidity) yield polysiloxane nanofilament-structured surfaces with diameters of 20 to 50 nm. In solution-phase approaches, excessive humidity induces phase separation and the formation of spherical particles, leading to reduced hydrophobicity. In contrast, lower humidity or insufficient reaction time yields smoother films with diminished surface roughness. Gao and McCarthy (2006b) showed that brief exposure to controlled relative humidity (30–65%) during sample immersion generates a well-defined 3D methylsilicone network, consisting of vertically aligned cylindrical fibers approximately 40 nm in

diameter. Jin et al. (2011b) fabricated a 3D perfluorinated silicone network on glass substrates using a phase separation method adapted from Gao and McCarthy (2006b). The superhydrophobic coating was prepared using a 3:2 (v/v) mixture of water-saturated toluene and anhydrous toluene. Water-saturated toluene was obtained as the upper phase after mixing deionized water with anhydrous toluene and allowing the mixture to equilibrate for 2 hours under ambient temperature and pressure conditions. This process yielded nanofilaments with an average diameter of 90 nm. Li et al. (2015a) prepared porous nanofilament structures with approximately 30 to 50 nm diameter in toluene containing 200 mg of water per 100 mL The mixture was sonicated at 70 °C for one hour to ensure complete water dissolution into toluene.

Khoo and Tseng (2008) investigated the growth of MTCS nanostructures by varying reagent concentration (7-500 mM), reaction time (2-120 min), and relative humidity (30%, 60%, and 90% RH). They found that as concentration increased, the nanostructures progressed from separate short fibers to an interconnected fibrous network and then disintegrated into rougher isolated fibers. The fiber diameters ranged from 18 to 90 nm, with some exhibiting superhydrophobicity (contact angle ~168° and hysteresis ~6°), while others showed high water contact angles with significant hysteresis (~160° and ~80°, respectively). Reaction time also influenced morphology, as fibers at 14 mM and 60% RH gradually formed quasi-continuous networks. Humidity variations induced distinct morphologies, where 14 mM under 30% and 90% RH produced sponge-like structures, whereas 50 mM at 90% RH yielded large spherical nanoparticles. While all surfaces demonstrated superhydrophobicity, sponge-like structures outperformed those produced at 50 mM and 60% RH, likely due to fiber alignment reducing water contact area. Under optimized conditions (14 mM, 60% RH, 2 h), surfaces maintained high wettability (160.2±2.3°) with minimal hysteresis (5.4 ±1.1°). These results showed 80% reproducibility across this study.

Further insights into silane self-assembly have been gained through molecular modeling and spectroscopy. The structure and electronic properties of alkylsilane SAMs, including OTS and perfluorodecyltrichlorosilane (PFDTS), have been studied using molecular dynamics simulations, providing insights into molecular packing and density (Katasho et al., 2015; Roscioni et al., 2016). Experimental studies using atomic force microscopy (AFM) and Fourier-transform infrared spectroscopy (FTIR) revealed that monolayer formation begins with island growth, progressing to

a smooth surface at full coverage, with disordered molecular islands forming above monolayer coverage (Banga et al., 1995). These findings highlight the importance of precursor structure, deposition condition, and substrate properties in controlling SAM organization and functional properties.

Recent advances in silanization tegchniques have expanded their applications in surface engineering. Jumrus et al. (2020a) fabricated superhydrophobic glass surfaces using a simple method of combining low-temperature annealing, wet etching, and MTCS coating. This process transformed hydrophilic glass into superhydrophobic surfaces with CA~154° and a SA~3°. The annealing-assisted etching induced micro/nano roughness, while the MTCS coating formed polysiloxane nanofilaments, enhancing surface hydrophobicity. The annealing-assisted etching process was found to play a crucial role in modifying surface roughness at the nanoscale through residual stress relaxation and hardness reduction. In addition, this technique induced a morphological transition from microscale spherical structures to nanoscale filamentary structures, as depicted in Figure 1.19. Similarly, Wong and Yu (2013b) achieved superhydrophobicity on glass slides using MTCS, which formed a 3D silicone network, enabling water droplets to rest in the Cassie–Baxter state. In contrast, OTS created densely packed, methyl-terminated monolayers, resulting in hydrophobic surfaces. Both methods preserved the optical clarity of glass, making them suitable for applications requiring transparency and self-cleaning properties. Advancements in organosilane self-assembly continue to expand their potential, making them highly suitable for biosensing, droplet manipulation, and drag reduction (Khoo & Tseng, 2008; Wong & Yu, 2013b).

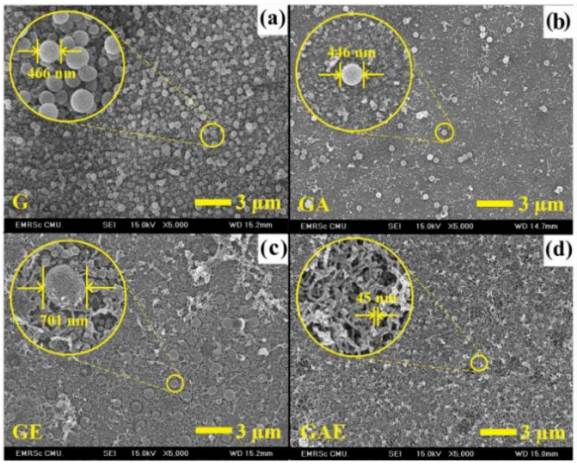

Figure 1.19 Surface morphology evolution of (a) bare glass, (b) annealed glass at 100 °C for 1 h under atmospheric pressure, (c) hydrofluoric acid etched glass, and (d) annealed and etched glass after being coated with MTCS. Reprinted from (Jumrus et al., 2020a), Copyright 2020, with permission from Elsevier.

Overall, the morphology, uniformity, and wetting properties of organosilane-based coatings are governed by a complex interplay of parameters, with water concentration and humidity playing a critical role in controlling hydrolysis and condensations reactions. Low water concentrations promote the formation of uniform monolayers, whereas higher concentrations promote polymerization and growth of nanostructured features. Reagent concentration, reaction duration, and temperature further influence film roughness and surface energy, thereby affecting hydrophobicity and reproducibility. While solution-phase silanization enables tunable nanostructure formation, vapor-phase and controlled-humidity approaches offer more precision. Understanding these interdependent effects is essential for designing reproducible, high-performance organosilane coatings for functional surface applications.

1.8 Transparency and Antireflection for Optimal Optical Performance

Biomimetic techniques inspired by lotus leaves and moth eyes have led to the development of transparent superhydrophobic surfaces with multifunctional properties, including self-cleaning, anti-icing, and anti-reflection (Ensikat et al., 2011; Han et al., 2020; Wilson & Hutley, 1982). By combining the water-repellent properties of lotus leaves with the nanopillar structure of moth eyes, researchers have created films that exhibit superhydrophobicity, high transparency, and antireflective properties (Itoh, 2019). Recent advancements include the use of solid paraffin wax coatings on nanopillar structures, resulting in icephobic, self-healing, antireflective, and highly

transparent surfaces. These bio-inspired surfaces address the limitations of conventional superhydrophobic coatings and slippery liquid-infused porous surfaces (SLIPS) by offering improved mechanical robustness and eliminating issues related to lubricant volatilization (Han et al., 2020).

Despite these advances, applying superhydrophobic surfaces in optoelectronics and other fields requiring light interaction and transparency remains challenging (Lyu et al., 2021; Shang & Zhou, 2016). Their inherent surface roughness often induces significant light scattering and reduces optical clarity (Gupta et al., 2016). Additionally, the refractive index discontinuity at the surface of optically transparent materials, such as glass, causes small reflections of approximately 4% to 6.5% on each air-substrate interface (Wang & Shu, 2013). Such reflections lead to significant energy losses in applications such as photovoltaic panels. To address this, considerable efforts have been made to develop antireflective coatings that minimize reflection losses (El-Khozondar et al., 2021). An ideal antireflective structure would achieve 0% reflection across the entire solar spectral range and at all incidence angles, potentially eliminating the need for mechanical tracking devices to align solar panels (Zhou et al., 2007). However, achieving this ideal performance remains challenging due to limitations in available materials. As an alternative, researchers aim to minimize reflectance by introducing destructive interference between light reflected at the air-coating and coating-substrate interfaces. For optimal performance, the coating thickness (d) should satisfy:

$$d = \frac{\lambda}{4 \times n_{eff}} \qquad \text{Equation (1.7)}$$

where n_{eff} is the effective refractive index of the coating at the design wavelength (λ).

Ideally, n_{eff} should match the geometric mean of the refractive indices of the air ($n_{air} \approx 1$) and the substrate ($n_{glass} \approx 1.5$) expressed as:

$$n_{eff} = \sqrt{(n_{air} \times n_{glass})} \qquad \text{Equation (1.8)}$$

These conditions are optimized for normal incidence, and performance decreases at oblique angles or broadband wavelengths (Brewster, 1992; Galy et al., 2020; Motamedi et al., 2018a). To address

these limitations, advanced designs have been developed to maintain low reflectance over a broader range of angles and wavelengths (Spinelli et al., 2012).

Researchers have explored three major solutions to achieve a low refractive index. The first involves single- or multilayer quarter-wavelength films (Li, Yang, et al., 2017), which rely on destructive interference between reflected waves by precisely tuning both the refractive index and thickness for each deposited layer. However, this approach faces challenges, such as the limited materials selection with desired refractive indices and the difficulty of achieving precise thickness control. The second, consists of graded-index (GRIN) structures (Wang et al., 2019) exhibits a gradual decrease in refractive index from the substrate-coating to the coating-air interface. While GRIN structures can achieve extremely low reflection across a wide range of incident angles, their practical implementation is hindered by the complexity of controlling refractive index profiles. The third implies antireflection coating surfaces (Chi et al., 2020), such as subwavelength-scale textured surfaces, porous films, and biomimetic nanostructures (inspired by the moth-eye or cicada wing). These structures create an effective medium with a gradual refractive index transition across the broad spectral and angular ranges. When combined with a low-index coating, they can achieve near-zero reflection over a broad spectral range (Padhan et al., 2025; Raut et al., 2011; Shanmugam et al., 2020; Zhou et al., 2007).

Recent studies demonstrated that even minor improvements in transmittance or reflectance can significantly enhance performance. For example, a 5% increase in solar transmittance can improve the energy collection efficiency of photovoltaic panels by up to 10% (Allsopp et al., 2020). Guo et al. (2024) reported a 0.69% increase in light transmittance for a fluoropolymer-coated glass panel compared to an uncoated one, along with a 1.4% reduction in light absorption. These improvements led to a 1.11% increase in efficiency for the coated panel, while the uncoated panel's efficiency decreased by 3.8%. Such findings highlight the importance of optimizing optical properties for applications such as self-cleaning surfaces for photovoltaic panels, urban infrastructure, sensor systems, and aerospace components.

Among recent advances, nanostructure-based strategies have emerged as a promising approach for multifunctional coatings, with growing interest in the fabrication of well-organized multilayer systems. Bravo et al. (2007) developed a layer-by-layer assembly technique using silica

nanoparticles to create transparent, superhydrophobic, and antireflective coatings on glass slides and silicon wafers (Figure 1.20a). Their approach involved the sequential deposition of three functional layers: an adhesion layer, a body layer, and a top layer, where each block is composed of a polyelectrolyte pair/SiO_2 of different particle sizes. By adjusting the number of body layers, the researchers optimized surface roughness to enhance superhydrophobicity while minimizing light scattering (<10%). Further functionalization with PFOTS *via* chemical vapor deposition (CVD) enhanced the film's water repellency. The multilayer structure exhibited a low refractive index ($n \sim 1.23$), confirming its nanoporous nature, with optimal performance achieved using 20 body layers and 3 top layers of the smallest nanoparticles (20 nm or 7 nm). This configuration resulted in a high-water contact angle (>150°) and a low contact angle hysteresis (5-7°). Consequently, this precise control over nanoparticle aggregation enabled the "lotus effect" without compromising optical transparency.

Mazumder et al. (2014) further developed hierarchical nanostructured coatings with combined superamphiphobicity and excellent optical performance (Figure 1.20b). They fabricated a dual-nanostructured surface composed of primary nanopillars (~ 100-200 nm in height and ~ 100 nm in width) decorated by branching nanoparticles (~ 10–30 nm). The coatings achieved ultralow reflectance (<0.5%), high average transmission (93.8% across 400-700 nm), and low haze (~ 1%) after treatment with fluorosilane. The branching nanostructures, grown preferentially on nanopillars (20-25% surface coverage), enhanced porosity but were mechanically fragile. To address this, the researchers employed solid nanonodules (25-50 nm clusters) that maintained 95% average transmission while surviving 10-run wipe tests. While the nanonodules improved durability, they showed slightly higher contact angles than the bare nanopillar structure.

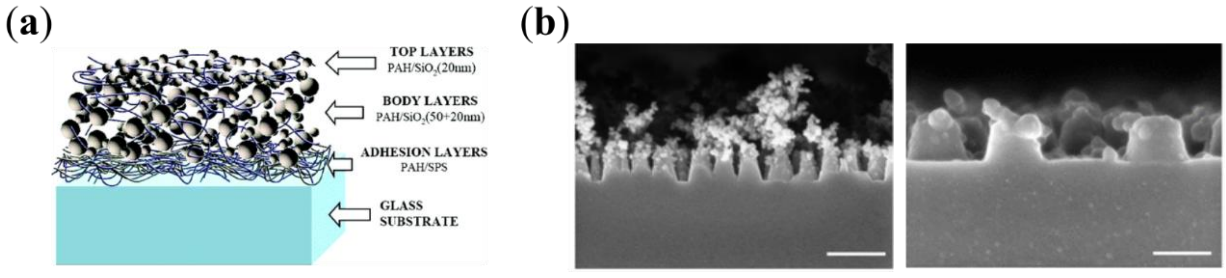

Figure 1.20 Hierarchical nanostructures achieving antireflective properties. (a) schematic of the multilayer film structure. Reprinted with permission from (Bravo et al., 2007). Copyright 2007 American Chemical Society. (b)

SEM images showing (left) branching nanostructures on nanopillars (scale bar: 300 nm) and (right) nanonodules decorating nanopillars (scale bar: 200 nm). Adapted with permission from (Mazumder et al., 2014). Copyright 2014 American Chemical Society.

Mesoporous coatings offer promising functions for multidisciplinary applications across materials science and biotechnology due to their tunable optical properties (Galy et al., 2020). Kim et al. (2002) developed a fabrication technique using thermal decomposition of organic templates to achieve precise control over porosity. This approach allowed simultaneous tuning of both porosity and refractive index (1.18-1.37). Similarly, Bernsmeier et al. (2014) developed a tunable antireflective coating system based on mesoporous MgF_2 films *via* micelle-templated sol-gel deposition on glass and silicon substrates. By using amphiphilic block copolymers as sacrificial templates, the researchers achieved precise control over film porosity (40%-71%), enabling refractive index tuning (1.23-1.11). The coating thickness was independently adjusted by varying the polymer concentration and the withdrawal speed during dip-coating (Figure 21). Optimal antireflective performance (~2% at 480 nm) was achieved when the film's refractive index matched the square root of the substrate's refractive index, while films with a lower refractive index (1.11) showed increased reflectance (~9%) due to suboptimal index matching.

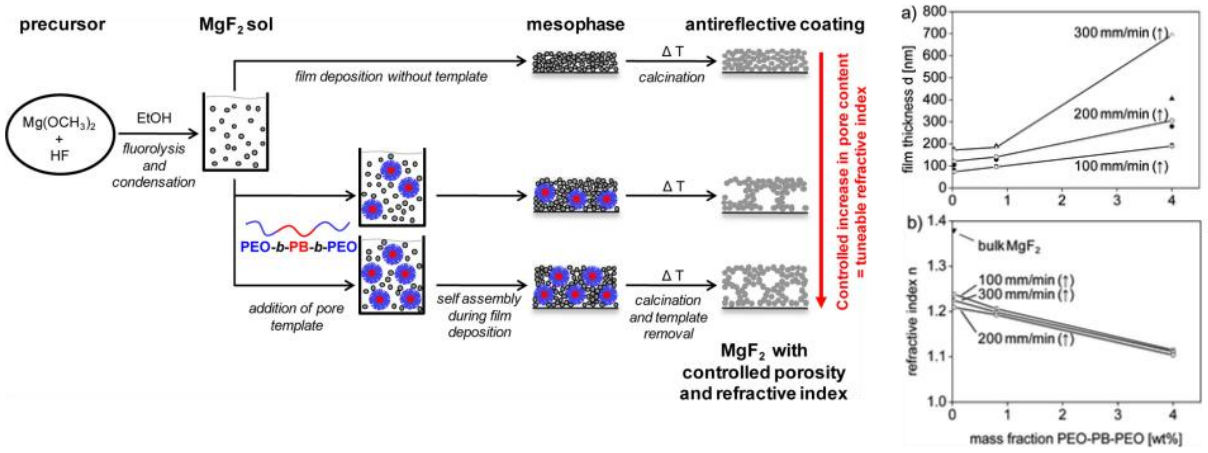

Figure 1.21 Schematic illustration of the synthesis of mesoporous MgF2 films using poly(ethylene oxide)-block-poly(propylene oxide)-block-poly(ethylene oxide) (PEO-PPO-PEO) as a sacrificial template. (a) film thickness as a function of polymer mass fraction at different withdrawal speeds and polymer content. (b) refractive index variation with polymer content. Adapted with permission from (Bernsmeier et al., 2014). Copyright 2014 American Chemical Society.

Overall, biomimetic and nanostructure-based strategies provide a versatile approach for designing transparent, superhydrophobic, and antireflective surfaces. By carefully selecting deposition

methods, tailoring silanization agents, and engineering hierarchical or mesoporous architectures, it is possible to optimize the balance between optical transparency, water repellency, and mechanical durability. Advances in multilayer, hierarchical, and porous coatings provide precise control over surface morphology and refractive index, enabling the fabrication of high-performance, multifunctional surfaces for a wide range of applications.

1.9 Stability and Durability of Hydrophobic and Superhydrophobic Coatings

Hydrophobic and superhydrophobic coatings have demonstrated great potential for various outdoor applications, including self-cleaning (Chen et al., 2021), anti-reflection (Oh et al., 2022), anti-corrosion (Zhang, Li, et al., 2024), anti-biofouling (Wu et al., 2023), and anti-icing (Huang et al., 2022). Despite their versatility, their practical performance is often compromised by long-term exposure to mechanical wear, chemical exposure, and environmental factors. These include sand abrasion, repeated cleaning cycles, UV radiation, thermal cycling, and particulates contamination (Milionis et al., 2016). Diverse laboratory-scale testing protocols have been developed to evaluate their durability (Malavasi et al., 2015b; Verho et al., 2011). Some follow, or are adapted from standards in related industries, including photovoltaics, automotive, construction, and protective coatings (Motamedi et al., 2018a; Raut, 2014; Xu et al., 2014). While industries such as photovoltaic and automotive have well-established durability tests, standardized laboratory test methods for hydrophobic and superhydrophobic coatings still require further development. Such conventional testing procedures would ensure reliable and comparable results across research and industrial applications.

Hydrophobic surfaces are generally fabricated either by roughening the surface or coating it with low-surface-energy materials, leading to the Wenzel wetting state, where water fully penetrates the roughness (Wenzel, 1936). In contrast, superhydrophobic surfaces require both surface roughness and low-surface-energy to achieve extreme water repellency. In this case, air pockets remain trapped beneath water droplets, resulting in a Cassie-Baxter wetting state (Cassie & Baxter, 1944b). The stability of this wetting state is crucial for maintaining superhydrophobicity. However external factors such as mechanical pressure, droplet impact, or chemical degradation can induce an irreversible transition to the Wenzel state. This transition may also occur spontaneously due to evaporation or gravitational forces acting on the droplet (Wang, Fu, et al., 2022). Such changes

lead to liquid infiltration into the surface textures, resulting in a gradual or abrupt decrease in contact angle and an increase in surface adhesion over time.

Recent progress in understanding the wetting transition mechanisms from Cassie-Baxter to Wenzel state (Bormashenko, 2015; Jiang et al., 2020; Ren, 2014) has enabled researchers to design and fabricate robust superhydrophobic coatings. Fabrication of robust superhydrophobic surfaces against mechanical wear is the main focus of researchers nowadays. Several studies have employed hierarchical roughness to stabilize the Cassie-Baxter wetting state. This approach involves using robust microscale protrusions to protect the more delicate nanoscale textures, thereby maintaining surface performance even when minor damage occurs (Balordi et al., 2019; Bhushan & Jung, 2011; Verho et al., 2011; Zhang et al., 2019). Alternative strategies have employed metals and alloys to fabricate durable hierarchical structures capable of withstanding high mechanical stress, including prolonged oscillating sand abrasion (Barthwal et al., 2013; Boinovich et al., 2017; Peng et al., 2014; Yan et al., 2019).

Typically, a primary strategy for developing durable coatings involves enhancing coating-to-substrate adhesion through covalent bonding and crosslinking. Alkyl- and perfluoroalkylsilanes are commonly employed to impart superhydrophobicity to diverse substrates ranging from textile to glass (Artus et al., 2006a; Genzer & Efimenko, 2000; Li et al., 2013; Luo et al., 2022; Zimmermann, Artus, et al., 2007; Zimmermann, Reifler, et al., 2007). Incorporation of binder systems with silica nanoparticles has also been reported to enhance the mechanical performance of superhydrophobic coatings (Ren et al., 2017; Wang, He, et al., 2015; Ye et al., 2011; Zeng & Zhan, 2024). Geng et al. (2015) fabricated transparent superamphiphobic coatings on glass through a multi-step process involving dip-coating, spray-coating, and chemical vapor deposition of PFOTS. Their fabrication process involved sequential deposition of solid and hollow silica nanoparticles, combined with a binder solution containing silica nanosheets and acid-catalyzed silica sol. The resulting coatings demonstrated excellent water and oil repellency, while maintaining high transmittance. Additionally, the coatings were able to withstand tape adhesion, pencil scratching, sand abrasion, and water drop impact. Despite a reduction in contact angles, the tested coatings retained their superhydrophobicity while exhibiting excellent adhesion and high resistance. Furthermore, the coatings maintained their superhydrophobic properties after five months of outdoor exposure.

While substantial progress has been made in durability enhancement, existing methods still fail when wear exceeds critical limits. Emerging solutions focus on regenerative approaches using self-healing or simple repair methods (Zhang, Wang, et al., 2021). Many biological plants, such as Lotus leaves, possess intrinsic self-recovery capabilities that enable functional restoring following surface damage (Wang et al., 2024). Inspired by this fascinating phenomenon, many researchers have constructed healable superhydrophobic coatings (Han et al., 2020; Wang et al., 2011; Weng et al., 2018; Xiang & Liu, 2021; Zhang, Li, et al., 2024). The self-healing of superhydrophobicity relies on the dual-scale roughness and embedded healing-agent reservoir containing low-surface-energy materials such as fluoroalkylsilanes (Zhang, Wang, et al., 2021). Usually, the reservoir consists of a porous polymeric material such as sulfonated poly (ether ether ketone). When physical abrasion or chemical degradation impacts the outer fluoroalkylsilane coating, the exposed surface exhibits increased surface energy than the stored healing agent. The energy differential, when combined with environmental stimuli such as high relative humidity, UV radiation, or thermal energy, drives the migration of stored healing agent to the surface. effectively restoring the superhydrophobic properties through a biomimetic self-repair mechanism (Li et al., 2010). Self-healing coatings based on the healing agent's migration have demonstrated exceptional durability (Esteves et al., 2014; Jin et al., 2013; Wang et al., 2011), however, they also fail when the dual-scale structure is damaged, or the healing agent is depleted after repeated damage cycles (Zhang, Wang, et al., 2021).

1.10 Research Objectives

This doctoral research focuses on the development of stable, durable, and multifunctional hydrophobic and superhydrophobic coatings for glass surfaces intended for solar and other optical applications. The central research question guiding this work is:

« How can organosilane-based coatings be designed to preserve the nano-geometry and optical properties of textured glass while providing long-term hydrophobic stability under environmental stress? »

To address this question, the research was organized into three complementary projects conducted in collaboration with *Edgehog Technologies Inc*., a company specializing in advanced anti-

reflective and self-cleaning glass surfaces. The motivation for this study was driven by the limitations observed in antireflective nanotextured glass developed by Edgehog. While these nanotextures improved optical performance, they degraded over time, leading to gradual loss of performance over time. This highlighted the need for transparent, superhydrophobic protective coatings capable of preserving the nano-geometry and effective refractive index while ensuring long-term durability and environmental stability. The study employed dip-coating, a simple, cost-effective, and scalable technique, to graft commercially available organosilane-based coatings on glass surfaces.

Chapter 2 investigates the influence of silane molecular structure on both hydrophobicity and optical performance of glass surface. Long-chain (C18) alkyltrichlorosilane and short-chain (C8) perfluoroalkyltrichlorosilane were compared as silanizing agents for regular and nanotextured glass. The objectives were to: (i) determine the effect of silane chain length on surface topography, wettability, and optical properties; (ii) assess environmental stability under simulated rainfall and outdoor exposure; and (iii) evaluate the potential of these coatings to protect against dust accumulation and UV-irradiation. This project establishes the relationship between molecular structure and functional performance of superhydrophobic coatings.

Given the environmental concerns associated with fluorinated compounds, Chapter 3 explores the use of non-fluorinated, reactive silanes to achieve superhydrophobicity while enabling post-functionalization for enhanced stability. This project investigates the effect of single-carbon variation between vinyltrichlorosilane (VTCS) and allyltrichlorosilane (ATCS) on surface properties. These short-chain alkenyltrichlorosilanes were applied as primer layers and further functionalized through thiol-ene click chemistry. The objectives were to: (i) develop a fluorine-free route to durable superhydrophobic coatings; (ii) introduce reactive surface groups for versatile post-functionalization; and (iii) evaluate wettability, optical transparency, and stability. Surface characterization was performed using Photo-induced Force Microscopy (PiFM) to assess uniformity and functionalization efficiency.

Chapter 4 focuses on broadening the chemical versatility of glass functionalization through activated alkyne chemistry under mild conditions. The hypothesis was that activated alkynes can provide a universal, stable, and direct functionalization platform for glass surfaces, overcoming the

limitations of traditional silanization and click reactions. The objectives were to: (i) demonstrate covalent grafting of diverse functional groups, including alcohols, azides, and amines on glass; (ii) characterize surface functionalization efficiency using infrared spectroscopy and PiFM; and (iii) explore the potential of this platform for applications requiring tailored interfacial chemistry and enabling sensitive and selective detection. This project emphasizes both the novelty and practical versatility of the approach. Preliminary findings indicate that this approach enables tailored interfacial chemistries suitable for advanced applications such as sensing, selective detection, and optical device integration.

Finally, in Chapter 5 we present the general conclusions and future perspectives of this study, summarizing the key findings and outlining potential suggestions for further exploration.

CHAPTER 2
A COMPARATIVE STUDY BETWEEN ALKYL- AND PERFLUOROALKYL SILANE COATINGS FOR GLASS

Nesrine Khitas, Calvin C.H. Cheng and Ali Nazemi

Department of Chemistry, Université du Québec à Montréal, QC H3C 3P8, Canada
Edgehog Advanced Technologies Inc. 355 Rue Peel, Suite 303, Montréal, QC H3C 2G9, Canada
Corresponding authors: Calvin C.H Cheng (email: calvin@edgehogtech.com) and Ali Nazemi (email: nazemi.ali@uqam.ca)

Published manuscript in: Canadian Journal of Chemistry (https://doi.org/10.1139/cjc-2024-0173)

2.1 Abstract

Surface modification is a crucial strategy to enhance material performance and expand their applications across diverse fields. Among these, nature-inspired hydrophobic coatings have gained attention for their ability to address challenges such as environmental pollution, surface degradation, and efficiency loss in various industries, including optoelectronics, automotive, and outdoor structures. In this work, we present a comparative study of commercial alkyl- and perfluoroalkyl silanes, ($H_3C(H_2C)_{16}H_2CSiCl_3$) and ($F_3C(F_2C)_5(H_2C)_2SiCl_3$), dip-coated on regular glass, with a focus on their stability and performance upon waterfall simulation and outdoor exposure. These coatings' wettability, optical properties, and stability on nanotextured glass were also studied. A video-based goniometer was used to study the wetting properties. Roughness, topography, and optical properties of the resulting surfaces were investigated by atomic force microscopy, and UV-Vis-NIR spectroscopy. At low deposition times, we spot the presence of agglomerated regions of polymerized short perfluoroalkyl chains, leading to a rougher and less uniform film. In contrast, we observed smoother coating with fewer polymerized aggregates for long alkyl chains. We found that an enhancement in hydrophobicity and a decrease in reflectance was achieved with a short perfluorinated alkyl chain. When applied to nanotextured glass, the observed increase in reflectance for both coatings, at 500 nm, was likely due to the coating's thickness effect. Texturing combined with surface roughness significantly increased the water contact angle, while only lowering the surface energy of regular glass without altering its structure resulted in less increase in water contact angle. These coatings can serve as hydrophobic surfaces and protective coatings against outdoor conditions, including dust accumulation, UV irradiation, ice adhesion, and corrosion.

2.2 Introduction

The repulsion of water is a well-known phenomenon observed in many natural environments. It involves nonpolar molecules interacting with water in such a way that they tend to avoid contact (Mezger et al., 2006). In biological and biochemical processes, hydrophobic interactions are essential for cellular function and organization, where it drives crucial phenomena such as protein folding, molecular recognition, and self-assembly of structures (Ben-Naim, 2012; Pieter Rein ten,

2002). In surface science, hydrophobic interactions dictate a surface's ability to repel water, forming hydrophobic and superhydrophobic surfaces. These interactions are crucial for designing surfaces with specific wetting properties (Law, 2014). Inspired by nature, researchers have developed various strategies to replicate multiple natural surfaces with unique wetting characteristics (Wong et al., 2013) for potential applications in biomimetic design and innovative materials (Arzt et al., 2021). These approaches generally combine low surface energy and surface roughness, critical parameters for controlling solid surface wettability (Wong et al., 2013). This involves creating hierarchical micro/nanostructures and chemically modifying the surface with low-surface energy materials (Barthwal et al., 2024; Wang et al., 2023; Xue et al., 2010). Most reported coating methods follow either top-down or bottom-up approaches. The top-down approach relies on constructing micro/nanostructures, often using natural surfaces as templates to transfer their complex patterns onto different substrates (Feng et al., 2010; Lee et al., 2007; Sun, Luo, et al., 2005; Wu et al., 2016) or creating roughness on existing materials, followed by applying low-surface energy coatings (Jafari et al., 2013; Lo et al., 2021; Marquez-Velasco et al., 2010; Rodič et al., 2020; Yang et al., 2019). The bottom-up approach involves mixing ingredients to achieve the desired roughness and low surface energy simultaneously, then applying this mixture to the desired surface (Huang et al., 2020; Saadatbakhsh et al., 2020; Zhao et al., 2018). Due to their wide range of applications, these coatings are usually constructed on a wide variety of substrates such as glass (Zhu & Liao, 2020), silicon (Srinivasan et al., 2011), textile (Berendjchi et al., 2011), wood (Wu et al., 2021), aluminum (Raja et al., 2020), steel (Zhu & Wu, 2020), and others (Liu et al., 2009; Xu et al., 2008).

Alkyl- and perfluoroalkyltrichlorosilanes are widely used molecules for creating hydrophobic and superhydrophobic surfaces and are considered highly effective for reducing a solid's surface energy (Xue et al., 2010). When applied to a substrate, these molecules form self-assembled monolayers (SAMs). Unlike their monofunctional analogs, trichlorosilanes exhibit higher reactivity and can undergo polymerization in the presence of residual water, leading to various surface structures (Fadeev & McCarthy, 2000). The polar head group, $-SiCl_3$, can hydrolyze, generating silanol groups that condense with silanol groups on the solid surface, creating strong covalent bonding through siloxane linkages. This will expose the hydrophobic end groups, CH_3 and/or CF_3, to the solid-air interface, promoting the surface with hydrophobicity, high chemical and mechanical

stability (Banga et al., 1995). Octadecyltrichlorosilane (OTS) and perfluorooctyltrichlorosilane (PFOTS) are among the widely used organosilane derivatives. They have been applied to various surfaces, including silicon wafers (Checco et al., 2014; Song et al., 2009; Wu et al., 2007; Yilbas et al., 2016), aluminum (Arianpour et al., 2017), steel (Zhang et al., 2016), and others (Liu et al., 2009; Seeharaj et al., 2018; Xu et al., 2008). Their efficacy on glass surfaces has been the subject of several investigations exploring the possibilities for preparing monolayer films from OTS and other trichlorosilane derivatives (Banga et al., 1995; Sagiv, 1980a; Tillman et al., 1988). Researchers have developed various strategies for creating hydrophobic and superhydrophobic coatings on multiple glass substrates. These include reacting OTS with water to form hierarchical siloxane aggregates (Zhang, Zhou, et al., 2021), applying coatings to pre-fabricated micro/nano-textured surfaces (Seeharaj et al., 2018; Song et al., 2009; Wang, Yu, et al., 2015; Yilbas et al., 2016), using PFOTS on nanostructured (Xu et al., 2014) and regular glass (Matin et al., 2019a), and employing multi-step processes with silica nanoparticles (Huang & Lin, 2014). To date, coatings to generate such surfaces promise a wide range of applications, from self-cleaning materials (Sethi & and Manik, 2018) to anti-corrosion barriers (Liu et al., 2009; Xu et al., 2008), ice adhesion-resistant materials (Li et al., 2022), and anti-biofouling (Wen & Guo, 2016).

In this study, we present a comprehensive study and comparison of commercially available alkyl- and perfluoroalkyl silanes dip-coated on regular glass. Our research is aiming to evaluate the impact of structural differences on hydrophobicity, investigate the coating uniformity, and evaluate the durability of these coatings under simulated rainfall and real outdoor conditions. Initially, the coating protocols were applied to regular glass surface, then reproduced on nanotextured glass surface. While we examine the hydrophobic properties and durability on nanotextured glass, it should be noted that this study does not include an analysis of the surface morphology or topography of the nanotextured substrate or its coatings. We study the effect of immersion time on the hydrophobic character of the surface, and we investigate the wetting properties using a video-based goniometer. Atomic force microscopy (AFM) and UV-Vis-near infra-red (NIR) spectroscopy are used to investigate roughness, topography, and optical characteristics of the resulting coatings. Our findings reveal that PFOTS tends to form polymerized aggregates at shorter deposition times, resulting in a rougher and less uniform film. As deposition time increases, these aggregates merge creating a smoother and more uniform surface. On the other hand, OTS shows

smoother coating with fewer polymerized aggregates, leading to a decrease in surface roughness over time. In addition to being hydrophobic, short perfluoroalkyl chains improved reflectivity and may serve as protective coatings against outdoor exposure conditions, including dust accumulation, UV irradiation, ice adhesion, and corrosion. Their versatility makes them suitable for various substrates, such as glass, metals, ceramics, polymers, and textiles. These coatings can also find potential applications in diverse fields, including optoelectronic devices, automotive and marine industries as well as membrane separation applications.

2.3 Materials and Chemicals

Regular soda-lime glass slides (27 mm x 46 mm x 1.16 to 1.27 mm thick) were supplied by Lakeside Microscope Accessories (Monee, IL, US). Nanotextured fused silica glass wafers (254 mm diameter x 0.5 mm thick) were provided by *Edgehog Advanced Technologies Inc.* The glass samples were cut into 10 mm x 8 mm pieces before use. Octadecyltrichlorosilane (OTS) and Trichloro(1H,1H,2H,2H-perfluorooctyl)silane (PFOTS), concentrated sulfuric acid (H_2SO_4, 98%) and hydrogen peroxide (H_2O_2, 30%) were purchased from Sigma Aldrich. Hexane, toluene, and methanol were all of reagent grade and used as received.

2.4 Activation of the Glass Surface

Before coating, it was essential to clean the glass samples to remove any surface contamination. Cleaning was conducted with standard piranha solution (H_2SO_4/H_2O_2) (7:3 v/v) (Song et al., 2009). Since this is a strong acidic and oxidizing solution, it hydroxylates the surface, rendering it superhydrophilic. The glass slides were dipped in piranha solution for 1 h at 50 °C. Then, they were thoroughly rinsed sequentially with deionized water, toluene, and deionized water again, and finally blown dry with compressed air and annealed for 1 h at 200 °C.

2.5 General Coating Procedure of the Activated Glass Surface

The first modification reaction on regular glass samples was conducted using OTS by employing the dip-coating technique. This process was conducted in closed vials during the reaction but exposed to air when solution and sample were introduced. Properly cleaned glass samples were rapidly immersed in a freshly prepared OTS solution in hexane (25 mM) and maintained at room temperature for varying durations ranging from a few minutes to hours. The coated samples were

rinsed with toluene and methanol to remove excess deposits (Sagiv, 1980a), then gently air-dried. Later, we replaced OTS with PFOTS to enhance hydrophobicity and durability. To do this, cleaned glass samples were rapidly immersed in a freshly prepared PFOTS solution in toluene (25 mM) following the same reaction conditions as for OTS coating. The coated samples were rinsed with hexane, methanol, hexane again, gently air-dried, and then annealed at 100 °C for 30 min. A schematic representation of alkyl- and perfluoalkyl-silane coatings on glass substrates is shown in Scheme 1.

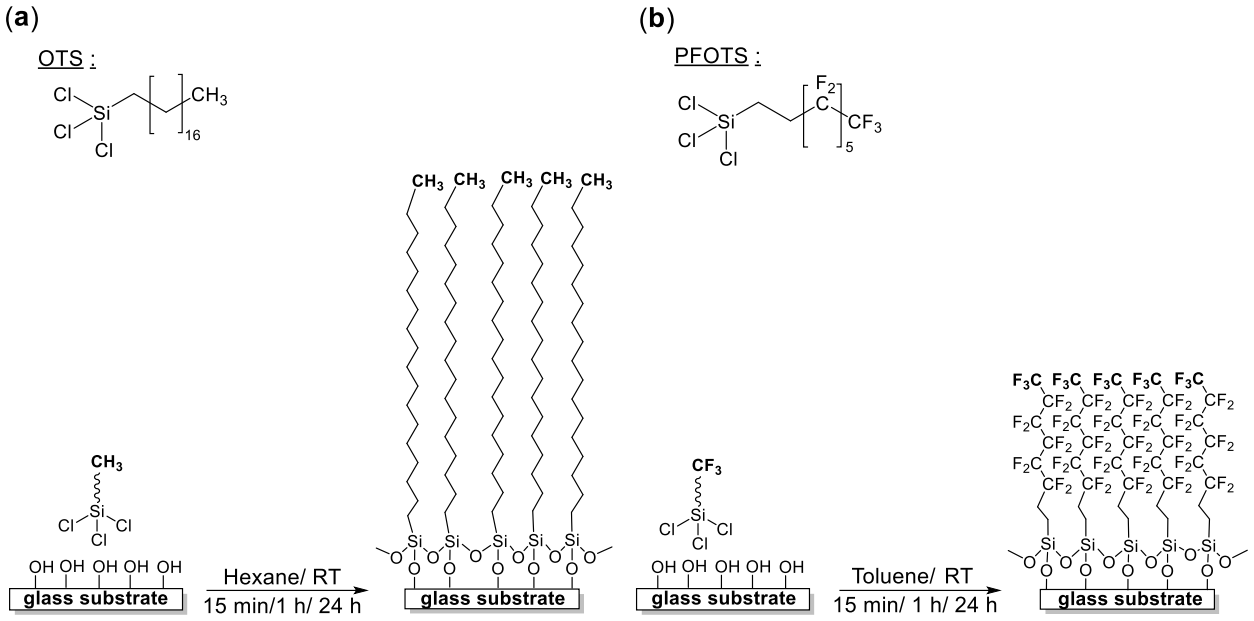

Scheme 2.1 (a) Alkyl- and (b) perfluoroalkylsilane coatings on glass substrate.

2.6 Characterization

The wettability of the bare and coated glass samples with OTS and PFOTS was measured by static water contact angle at ambient temperature through a contact angle goniometer (OneAttension). During this procedure, a volume of 4 μL of deionized water droplets was used for each measurement. The reported value for each sample represents an average of measurements taken at three different positions on the surface. The topography and surface roughness parameters were measured by Bruker's MultiMode8 microscope and Gwyddion software. UV-Vis analysis was conducted using a PerkinElmer Lambda 750 spectrometer.

2.7 Results and Discussion

2.7.1 Wettability, Optical Properties, and Surface Coverage of Modified Regular Glass Surfaces

To investigate the effect of the coating time on the hydrophobicity, and consequently, the growth of the organosilane on the modified regular glass surface, a series of reaction times were tested (15 min, 1 h, and 24 h). Using the same concentration of OTS and PFOTS (25 mM), we observed that extending the reaction time did not significantly alter the hydrophobicity of the samples (Figure 2.1a). Perfluoroalkyl silanes are known to be more hydrophobic than alkyl silanes because of their high fluorine content surrounding the carbon backbone. This effect creates extremely strong bonds to carbon, rendering it chemically inert. Moreover, due to the high electronegativity of fluorine atoms, the polarizability of the C–F bond is reduced. This reduction limits the susceptibility of perfluorinated materials to van der Waals interactions, resulting in their remarkable low surface energies. Consequently, the interaction between PFOTS-coated surfaces and water is minimized due to their extremely low surface energy, resulting in an increased water contact angle values compared to those resulting from non-perfluoroalkyl silanes (Barry, 2011; Chambers et al., 2021; Cheng et al., 2013). In our study, despite the longer chain length of OTS (18 carbons) compared to PFOTS (8 carbons), OTS- and PFOTS-modified samples exhibited similar levels of hydrophobicity overall, with a slightly higher water contact angle difference for PFOTS at 1 h reaction time, likely due to the high fluorine content enhancing hydrophobicity. To better understand the relationship between wettability and surface roughness of a non-ideal surface, we refer to the fundamental models developed by Wenzel (1936), Cassie and Baxter (1944b) and Cassie (1948b). These models describe the water contact angle on a real surface that can have chemical heterogeneity and roughness. In our study, the chemical modification approach of regular glass samples resulted in a wetting behavior consistent with Wenzel wetting, based on qualitative observations and contact angle hysteresis measurements. In this context, these samples exhibited contact angles characteristic of hydrophobic surfaces with a sticky behavior as revealed by the contact angle hysteresis values, measured using the tilt method (20 µL of DI water at 20°/min), ranging from 20.8° to 43.9°. This indicates that the surfaces are most likely in the Wenzel state or at least in a mixed wetting state (Katasho et al., 2015; Raza et al., 2012; Raza et al., 2015), as Cassie-Baxter surfaces generally exhibit much lower hysteresis (<10°) (Li, Reinhoudt, et al., 2007; Zhang et al., 2008). We were also interested in investigating the effect of these coatings on the

transparency of the samples, given that hydrophobicity and transparency are often competing properties (Karunakaran et al., 2011). Increasing surface roughness to enhance hydrophobicity typically reduces transparency due to light scattering. Therefore, the surface roughness of the films should be precisely controlled, keeping it less significant than approximately ¼ of the visible light wavelength range (400-800 nm), preferably less than 80 nm (Nakajima, 2004b; Wong et al., 2012). When light travels through different media (air, coating, and glass), reflection occurs at interfaces where there is an abrupt change in refractive index. The results presented in Figure 2.1b,c reveal that both coatings generally improved the transparency of the glass. However, no significant differences were observed between the two coatings in terms of their impact on transparency. On the other hand, while both coatings improved reflectance of surfaces compared to bare glass, the PFOTS-coated surfaces exhibited slightly better anti-reflective properties, characterized by their slightly more pronounced reduction in reflectance compared to the OTS-coated surfaces, particularly after a coating time of 1 h. This observation can be attributed to the lower refractive index of PFOTS ($n \approx 1.35$) compared to that of OTS ($n \approx 1.46$). The PFOTS coating creates a gradual change in refractive index between air ($n \approx 1$) and regular glass ($n \approx 1.5$), effectively reducing reflections at the air-coating, coating-glass, glass-coating, and coating-air interfaces. This gradient in refractive index allows for better light transmission through the coated glass. Thus, this demonstrates that it is possible to enhance hydrophobicity and transparency simultaneously. We would also like to note that slight fluctuations in the data points in Figure 2.1b, particularly for PFOTS, could be due to sample-to-sample variation, measurement conditions, or inherent variability in coating application.

(a)

As prepared coatings	
	WCA (θ)
Bare glass	26±6.1
OTS 15 min	113±2.1
OTS 1 h	108±4.0
OTS 24 h	116±4.4
PFOTS 15 min	116±0.9
PFOTS 1 h	118±0.4
PFOTS 24 h	117±1.4

(b)

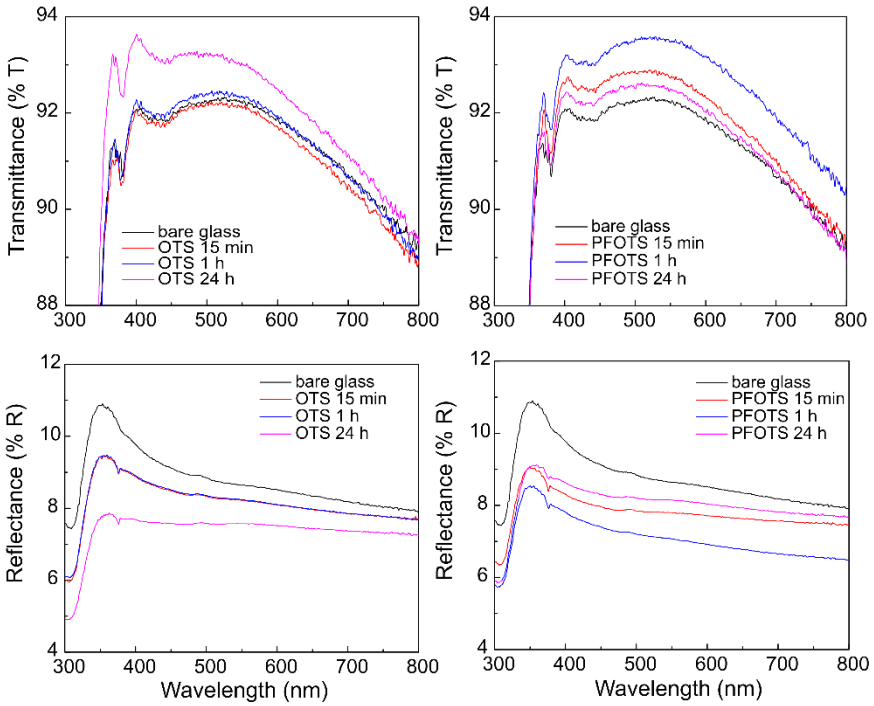

Figure 2.1 (a) Water contact angle (WCA), (b) transmittance and reflectance spectra of OTS- and (c) PFOTS-modified regular glass surfaces of varying coating durations.

The formation of a self-assembled monolayer (SAM) involves the adsorption process and an increase in surface coverage over time, leading to the evolution of molecular order (Schwartz, 2001). A previous study examined the influence of surface coverage on the packing of long-chain molecules and the rate of monolayers formation (Banga et al., 1995). It was reported that OTS monolayers (less than 2.6 nm) form after 90 min of immersion, while PFOTS monolayers (less than 1.6 nm) form after 5 min. Herein, the impact of the adsorption of long-chain OTS and PFOTS molecules on the surface coverage is investigated using AFM, as shown in Figure 2.2. For the glass surfaces modified with OTS (Figure 2.2a-c), the results showed a heterogeneous surface coverage consisting of few aggregates and densely packed molecules at the shorter immersion time (15 min), and high-density aggregates at longer immersion time (24 h), resulting in an increase in the mean roughness (R_a) (from 4.45 nm to 9.27 nm) and root-mean-square roughness (R_q) (from 7.22 nm to 16.08 nm) from 15 min to 24 h. After 1 h of immersion, the aggregates merged, resulting in a smoother surface, as evidenced by the decrease in R_a (4.01 nm) and R_q (5.16 nm) (Table 2.1). Similar behavior was reported by Banga et al. (1995), who observed that low silane coverage on the substrate leads to the formation of islands. As the coverage approaches a monolayer, these

islands merge to form a smooth surface. However, disordered molecular islands were observed above monolayer coverage.

For glass surfaces modified with PFOTS (Figure 2.2d-f) at 15 min, adsorbed molecules formed a randomly distributed array of spherically-shaped islands on the surface, likely due to polymerized aggregates deposited on the surface (Banga et al., 1995; Li & Horton, 2002b). After 1 h of reaction, the resulting film formed a closely packed array of smaller islands with a relatively uniform distribution. The surface roughness analysis revealed a reduction in both R_a (from 15.24 nm to 4.86 nm) and R_q (from 19.97 nm to 7.40 nm), indicating a decrease in surface roughness from 15 min to 1 h of coating formation. This is consistent with findings reported by Matin et al. (2019a) who investigated glass surfaces coated with PFOTS using a 1 h dip-coating method. While Matin et al. achieved a R_q of 7.40 nm and a ~120° using a higher concentration of PFOTS in hexane (100 mM) (Matin et al., 2019a), we obtained comparable results using only 25 mM PFOTS in toluene. Subsequently, at prolonged coating time (24 h of dip coating), a heterogeneous coverage of closely packed molecules, alongside a few emerged spherically shaped islands with lower R_a (3.62 nm) and R_q (7.79 nm), were observed.

Traditionally, chlorosilane derivatives are believed to react too quickly with water, forming large aggregates that hinder the creation of high-quality monolayer coatings (Angst & Simmons, 1991; McGovern et al., 1994; Silberzan et al., 1991; Wang & Lieberman, 2003). This led to the belief that strict humidity control was necessary when using these compounds. However, OTS's long alkyl chain slows down its reaction with water (Sagiv, 1980a). We observed that the formation of polymerized OTS molecules occurred more slowly than that of PFOTS (at 24 h compared to 15 min) (Figure 2.2c,d). This is likely due to the relative rate of hydrolysis of the silane molecules. The Si-Cl groups in PFOTS undergo hydrolysis more rapidly than those of OTS. This increased rate is attributed to the significant electron-withdrawing effects of the CF_3 and CF_2 groups in PFOTS compared to the CH_3 and CH_2 groups in OTS (Banga et al., 1995). As a result, the PFOTS were hydrolyzed faster than the OTS, allowing the silane's silanol groups to condense with the substrate's silanol groups. Consistent with previous findings reported by Banga et al. (1995), the R_a values for both coatings (Table 2.1), except when large aggregates were present, were smaller than those for bare glass. This smoothing effect can be attributed to the formation of a highly ordered arrangement of OTS molecules. Moreover, the hydrolysis and subsequent condensation of

trichlorosilane groups result in the formation of siloxane linkages (Si–O–Si). This molecular arrangement fills in the irregularities on the glass, resulting in a more uniform and smoother surface which contributes to a decrease in surface roughness compared to the bare glass substrate (Siedlecki et al., 1994).

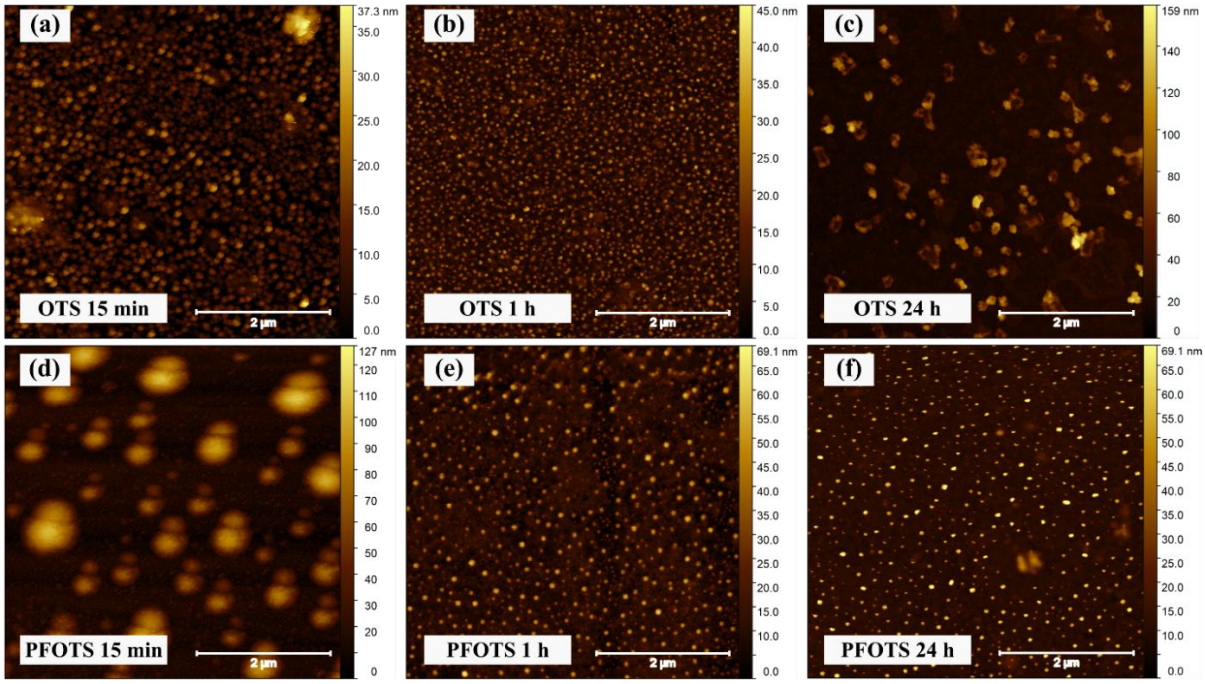

Figure 2.2 2-dimensional AFM images of OTS and PFOTS modified glass surfaces (5×5 µm).

Table 2.1 The roughness parameters of bare and modified regular surfaces determined by AFM measurements.

As prepared coatings	Mean roughness Ra (nm)	Root-mean-square roughness Rq (nm)
Bare glass	5.57	1.30
OTS 15 min	4.45	7.22
OTS 1 h	4.01	5.16
OTS 24 h	9.27	16.08
PFOTS 15 min	15.24	19.97
PFOTS 1 h	4.86	7.40
PFOTS 24 h	3.62	7.79

2.7.2 Stability of Modified Regular Glass Surfaces

Organosilanes are essential for creating hydrophobic and superhydrophobic films widely used for practical applications due to their remarkable mechanical and chemical stability. Their stability primarily results from the strong immobilization provided by siloxane bonds (Darband et al., 2020). Simplicity and cost-effectiveness are important parameters of the manufacturing process and are of great importance, as is the stability for practical applications. To respond to the application versatility, the stability of these films is considered a crucial criterion (Darband et al., 2020; Tian et al., 2016; Wen & Guo, 2016). It is essential that these coatings can withstand harsh weather conditions, including intense sunlight, heavy rain, snow, and temperature fluctuations. The stability of the modified regular glass samples was studied under simulated rainfall and actual outdoor conditions. Rainfall simulation was conducted in the laboratory using a custom-made waterfall setup. The samples, placed on a fixed support, were positioned within 30 cm distance from the rainfall source. The system consisted of a shower head connected to a submersible pump. The pump was submerged in a tank filled with deionized water, and the flow rate was adjusted to a low level. The samples were exposed to simulated light rain for 1 h, 3 h, and 24 h at room temperature, with a flow rate of 25 mL per hour over a 10 cm × 10 cm surface area (equivalent to 2.5 mm/h over 1 m^2) measured using the gauging method. Subsequently, the same samples were exposed to outdoor conditions in Montreal, Quebec, Canada, for 8 weeks from October 10th, 2021, to December 20th, 2021. During this period, they experienced a mix of rainy, snowy, and sunny days with temperatures ranging from 24 °C to -16 °C (*Daily Data Report for October to December 2021*). Before each measurement, the samples were cleaned with deionized water and gently air-dried. After 8 weeks of outdoor exposure, the PFOTS-coated samples maintained relatively stable contact angles on average, as shown in Figure 2.3a. In contrast, the OTS-coated samples displayed more variation, with the OTS 24h sample showing a notable decline in contact angle. Furthermore, the reflectance spectra of both OTS- (Figure 2.3b) and PFOTS-modified (Figure 2.3c) samples revealed slight improvement after outdoor exposure compared to as-prepared samples. Overall, PFOTS-modified samples demonstrated slightly higher stability and resistance to both simulated and real environmental tested conditions compared to OTS samples. This can be attributed to the strong bonding energy (486 kJ/mol) of its C–F bonds (Cheng et al., 2013).

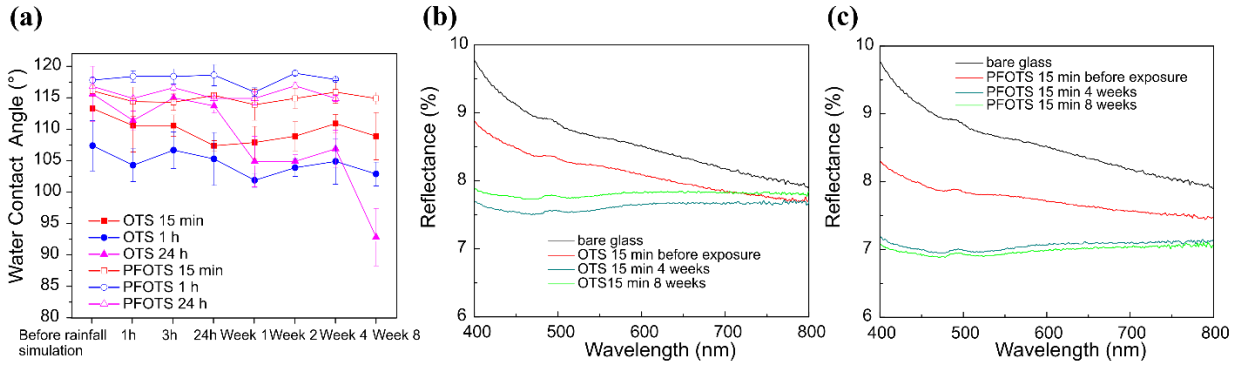

Figure 2.3 (a) Variation in water contact angle on OTS- and PFOTS-modified glass surfaces before and after exposure to simulated rainfall for 1 h, 3 h, and 24 h, followed by 8 weeks of outdoor exposure. (b) reflectance spectra of OTS- and (c) PFOTS-modified regular glass surfaces with a 15 min coating duration, measured before and after rainfall simulation followed by 4 and 8 weeks of outdoor exposure. All samples were subjected to light rainfall simulation prior to outdoor exposure. Note for (a): The PFOTS 1 h and 24 h samples were not analyzed at the Week 8 timepoint due to damage, presumably caused by a squirrel, during Week 7 under outdoor exposure conditions.

2.7.3 Nanotextured Glass Surfaces

Nanotextured glass surfaces have gained significant interest due to their unique physical properties and promising applications (Liapis et al., 2017; Sahraei et al., 2020). These surfaces are engineered with nanosized textures that mimic natural structures like lotus leaves and moth eyes, enabling them to repel water, reduce glare, and enhance optical performance (Motamedi et al., 2018a). Their potential applications include ultra-transparent encapsulation layers for solar panels, optical systems, and other optoelectronic devices (Liapis et al., 2017; Yu, Kim, et al., 2015). In our study, we used a cone-like nanotextured glass substrates provided by *Edgehog Advanced Technologies Inc*. Initially, we applied the coating protocols to regular glass surface and then reproduced them on the nanotextured glass. These surfaces have approximately a 50 nm pitch distance (peak to peak) and a height of 250 nm, which their morphology is presented in their scanning electron microscopy (SEM) image in Figure 2.4.

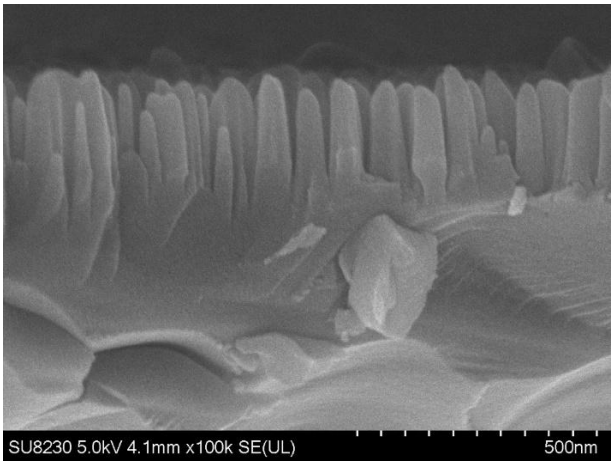

Figure 2.4 SEM image of the cone-like nanotextured glass substrate provided by *Edgehog Advanced Technologies Inc.*

2.7.4 Wettability and Optical Properties of Modified Nanotextured Glass Surfaces

As mentioned earlier, after optimizing the cleaning and coating procedures on regular glass, we reproduced the same protocol on nanotextured glass, provided by *Edgehog Advanced Technologies Inc.* These bare nanotextured glass are superhydrophilic with a water contact angle of 2.1° ± 1.4. As shown in Figure 2.5a, after 15 min of coating time, the OTS and PFOTS coatings transformed the nanotextured surface from superhydophilic to superhydrophobic with a maximum average water contact angle of 162.5° ± 1.6 and 157.4° ± 2.9, respectively. After 1 h and 24 h, while the OTS-coated samples did not exhibit any significant changes in their water contact angles, those modified with PFOTS demonstrated lower values. This indicates that prolonged coating times do not significantly enhance the hydrophobicity and may even reduce it, likely due to the formation of thicker coatings. The measured sliding angle (SA) was approximately around 5°. The increase in water contact angle is due to the combination of roughness generated by the nanotextures and surface modification with low surface energy materials (Song et al., 2009). The modification of nanotextured glass samples led to a heterogeneous wetting behavior, where air is trapped underneath the liquid and inside the asperity cavities (Cassie-Baxter state). In Figure 2.5b,c, we assume that the observed increase in reflectance of the modified nanotextured surfaces, at 500 nm, is likely due to the coating's thickness effect, which masked the nanotextures' index gradient and, thus, resulted in a diminished anti-reflection effect.

(a)

As prepared coatings	
	WCA (θ)
Bare nanotextured glass	2.1±1.4
NT OTS 15 min	162.5±1.6
NT OTS 1 h	161.8±4.6
NT OTS 24 h	158.4±8.6
NT PFOTS 15 min	157.4±2.9
NT PFOTS 1 h	151.4±4.0
NT PFOTS 24 h	140.8±6.3

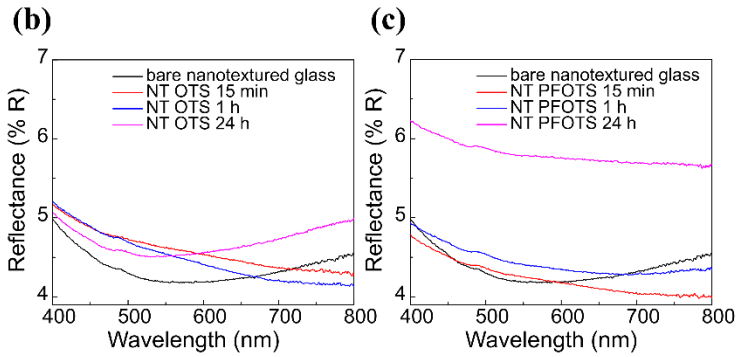

Figure 2.5 (a) Water contact angle (WCA), (b) reflectance spectra of OTS- and (c) PFOTS-modified nanotextured surfaces of varying coating durations.

2.7.5 Stability of Modified Nanotextured Glass Surfaces

Nanotextured glass samples underwent outdoor exposure in Montreal, Quebec, Canada, from February 11th, 2022, to June 17th, 2022. During this period, the samples experienced a mix of snowy, rainy, and sunny days with temperatures ranging from -21 °C to 32 °C (*Daily Data Report for February to June 2022*). After 17 weeks, the OTS-modified samples exhibited an average decrease of 20° in the water contact angle, while PFOTS-modified samples showed an average decrease of 14° in the water contact angle (Figure 2.6a). This difference in stability is attributed to the higher bond dissociation energy of the C–F bonds in PFOTS (544 kJ/mol) compared to the C–H bonds in OTS (413 kJ/mol), explaining the greater stability of PFOTS-modified samples (Nayshevsky et al., 2020). Over time, the wetting behavior of the glass samples shifted from the Cassie-Baxter state (where the surface exhibits superhydrophobicity) to Wenzel state (where the surface exhibits hydrophobicity) due to the observed decrease in water contact angle (Lin et al., 2008). Additionally, the reflectance of the coated samples for stability studies was investigated and the selection of a 15 min coating duration was based on previous observations. These samples provided an optimal water contact angle increase while minimizing potential coating thickness effects that could diminish the anti-reflection properties of the nanotextured surfaces. After 17 weeks of outdoor exposure (Figure 2.6b), a slight increase in reflectance was observed. Overall, the modified nanotextured glass exhibited less than ~0.5% increase for OTS and less than ~1% for PFOTS.

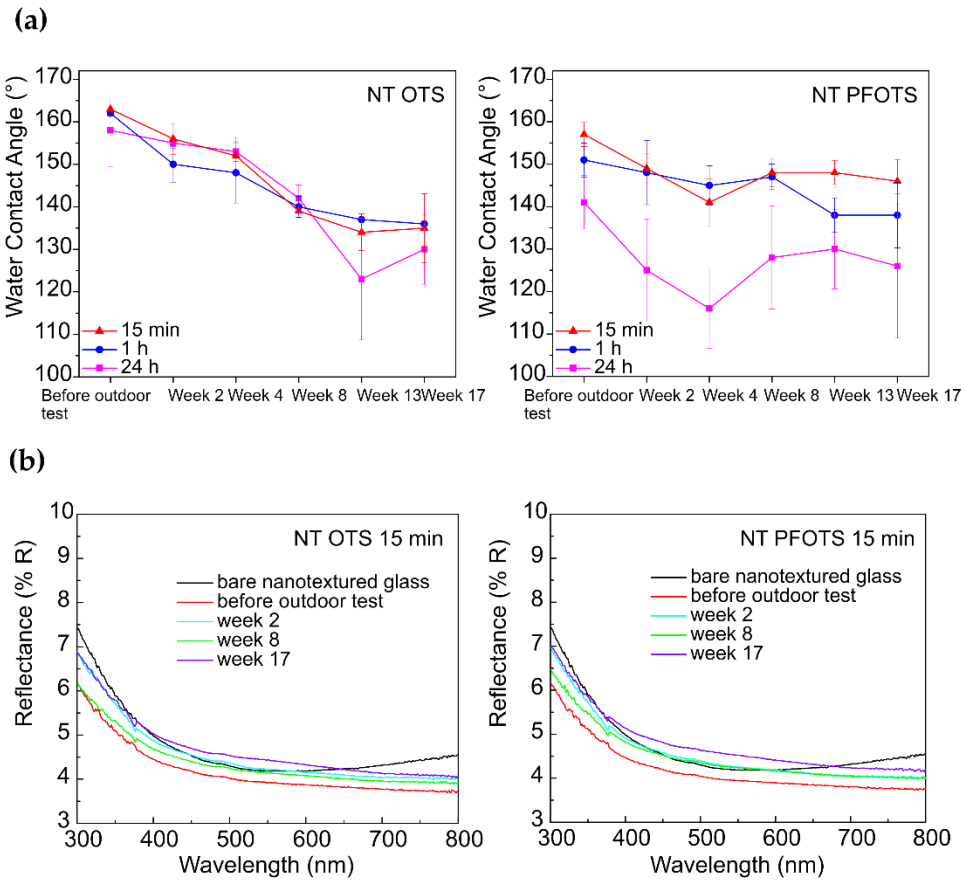

Figure 2.6 (a) Water contact angle and (b) reflectance spectra of OTS- and PFOTS-modified nanotextured glass surfaces before and after outdoor exposure.

Overall, for both regular and nanotextured glass surfaces, the samples coated for 15 minutes demonstrate comparable average water contact angles after 8 weeks of outdoor exposure. Specifically, on regular glass, OTS- and PFOTS-modified surfaces exhibit water contact angles of 109.3° ± 3.8 and 114.9° ± 1.0, respectively. On nanotextured glass, these values are higher, with OTS- and PFOTS-coated surfaces achieving contact angles of 138.9° ± 0.6 and 148.4° ± 3.4, respectively, after 8 weeks in outdoor condition. This suggests that despite differences in initial hydrophobicity and stability, the long-term performance of these coatings converges under outdoor conditions. This observation underscores the potential robustness of both coatings for extended applications. We also note that the effects of non-water-soluble organic molecules and airborne oxidants on the stability of the coatings for both regular and nanotextured glass were not investigated, as this falls outside the scope of the current study. Nonetheless, we recognize that these factors could be impactful and deserve consideration.

2.8 Conclusion

In summary, we evaluated the effects of commercially available alkyl- and perfluoroalkyltrichlorosilanes on surface coverage for regular glass, wettability, optical properties, and durability under simulated rainfall and real outdoor conditions for both regular and nanotextured glass. By varying the immersion times during dip coating on regular glass, we observed that the self-assembly of OTS and PFOTS molecules affects the surface coverage. For PFOTS, short immersion times (15 min) led to heterogeneous surface coverage with polymerized aggregates, while longer immersion times (1 h and 24 h) resulted in smoother surfaces as aggregates merged. In contrast, the formation of polymerized aggregates for OTS occurred more slowly due to the difference in electron-withdrawing effects between both molecules. Consequently, PFOTS hydrolyzed faster than OTS allowing the silane's silanol groups to condense with the substrate's silanol groups. Moreover, our findings demonstrate that replacing OTS with PFOTS results in superior hydrophobicity, stability, and improved optical properties. On regular glass, the shorter PFOTS chain length led to an enhancement in hydrophobicity and a decrease in reflectance. Lowering the surface energy without modifying the glass surface structure resulted in a moderate increase in water contact angle, while extending reaction times does not significantly alter hydrophobicity. When applied to nanotextured glass, both OTS and PFOTS coatings transformed the surfaces from superhydrophilic to superhydrophobic surfaces. PFOTS-modified samples exhibited higher stability during extended outdoor exposure due to the stronger C–F bonds. The modified nanotextured glass maintained its enhanced properties, highlighting the potential of PFOTS coating for durable and practical applications.

2.8.1 Acknowledgments

This research was funded by MITACS in collaboration with *Edgehog Advanced Technologies Inc* (project number: IT13352). We thank Prof Luc Stafford from Université de Montréal and NanoQAM for providing the equipment for the characterization of the glass surface coatings.

CHAPTER 3

FROM VINYL TO ALLYL: HOW A SINGLE-CARBON DIFFERENCE ALTERS GLASS SURFACE ARCHITECTURE, REACTIVITY AND FUNCTION

Nesrine Khitas[a], Maziar Jafari[a], Calvin C.H. Cheng[b], Mohamed Siaj[a] and Ali Nazemi[a]

[a] Department of Chemistry, Université du Québec à Montréal, QC H3C 3P8, Canada

[b] Edgehog Advanced Technologies Inc., Montréal, H3C 2G9, QC, Canada

Corresponding authors: Mohamed Siaj (siaj.mohamed@uqam.ca), Ali Nazemi (email: nazemi.ali@uqam.ca)

Published manuscript in: RSC Applied Interfaces (https://doi.org/10.1039/D5LF00162E)

3.1 Abstract

Natural non-wettable surfaces, such as lotus leaves, exhibit exceptional self-cleaning properties due to their unique micro- and nanostructures. This has inspired researchers to develop artificial superhydrophobic materials, particularly on mica and SiO_2-based substrates, such as glass, using organosilanes to achieve tailored properties. This study focused on modifying glass surfaces with vinyltrichlorosilane (VTCS) and allyltrichlorosilane (ATCS) to create coatings with enhanced optical properties, wettability, and stability. We employed a two-step surface modification strategy: dip-coating followed by functionalization with 1-decanethiol through radical-initiated thiol-ene click reaction to functionalize these surfaces with a long alkyl chain to enhance hydrophobicity and improve chemical stability. The morphology, structure, and chemical composition of the coatings were characterized by using a combination of techniques, including scanning electron microscopy, atomic force microscopy, attenuated total reflectance-Fourier transform infrared spectroscopy, and photo-induced force microscopy (PiFM). PiFM was specifically employed to assess the uniformity of surface functionalization, both at the surface and throughout the film's depth, and to quantify the efficiency of the thiol-ene click reaction.

Keywords: Hydrophobic; superhydrophobic; thiol-ene click chemistry; alkenylsilanes; organofunctional silanes; photo-induced force microscopy

3.2 Introduction

The remarkable self-cleaning properties of some plant surfaces (Barthlott & Ehler, 1977; Barthlott & Neinhuis, 1997), especially the lotus leaf (Barthlott & Neinhuis, 1997; Neinhuis & Barthlott, 1997b), have attracted the attention of researchers and have inspired the development of artificial hydrophobic and superhydrophobic surfaces (Liu & Li, 2012; Motamedi et al., 2018b; Su et al., 2016a; Sun, Watson, et al., 2009; Wagner et al., 1996; Watson, Green, et al., 2015; Youngblood & Sottos, 2008; Zhu et al., 2021). These natural surfaces combine micro- and nanostructures with a waxy coating, resulting in high water contact angles and low sliding angles (Barthlott & Neinhuis, 1997; Guo & Liu, 2007). The unique combination of surface topography and surface chemistry is responsible for water repellency and self-cleaning properties (Gao & McCarthy, 2006a), making them ideal models for replication (Yu, Guo, et al., 2015). In parallel, surface modification of inorganic materials using organosilanes has emerged as a practical approach to achieve tailored

surface properties that mimic the natural non-wettable surfaces (Fadeev & McCarthy, 2000). While this modification technique applies to various oxide surfaces (Pesek & Matyska, 1997b), the most studied systems include alkyl trichlorosilanes on SiO_2-based substrates (Kondo et al., 2013), including silicon wafer (Wasserman et al., 1989) and glass (Jumrus et al., 2020b; Nanda et al., 2017a; Zhang, Li, et al., 2014b), as well as layered silicates such as mica (Carson & Granick, 1989b; Huang et al., 2017a; Kessel & Granick, 1991; Schwartz et al., 1992).

The reactivity of the trichlorosilane precursors is highly dependent on the choice of their chemical composition, functional groups, reaction conditions, and substrate properties. Under proper conditions, the silane precursors will self-assemble into monolayers through horizontal polymerization. Subsequently, they react with existing surface silanols, resulting in the formation of covalently bonded monolayers. Additionally, silane precursors have demonstrated a capacity to condense with water and surface silanols, leading to the formation of covalently attached, crosslinked polymeric layers through vertical polymerization (Fadeev & McCarthy, 2000). Early investigations in this field predominantly focused on silanes and siloxanes with relatively simple molecular structures, where silicon atoms were primarily bound to short (Gao & McCarthy, 2006c; Jumrus et al., 2020b; Khoo & Tseng, 2008) or long-chain alkyl groups (Banga et al., 1995; Matin et al., 2019b; McGovern et al., 1994; Noll, 2012; Sriram et al., 2020). These nonreactive functional groups are often challenging to functionalize and may require harsh conditions (Kim et al., 2008; Stojanovic et al., 2010; Zahner et al., 2011). However, current trends in chemistry have shifted towards silanes with functionalizable groups such as amines, thiols as well as alkenes (Indumathy et al., 2023). This shift has opened up new possibilities for tailoring material properties under mild conditions, expanding their potential applications across diverse technological sectors (Zhang, Ji, et al., 2024) such as optoelectronics (Li et al., 2019; Suzuki et al., 2017), microfluidics (Lee & Ram, 2009), and biosensing (Chen et al., 2020; Zhu et al., 2021). While vinyl- and allyltrichlorosilanes have demonstrated utility in organic synthesis (Moskalik & Shainyan, 2024), their application to glass surface modification remains less studied (Babik et al., 2012; Li et al., 2015b) compared to other organosilanes (Menawat et al., 1984) such as alkyl- and perfluoroalkyltrichlorosilanes including alkoxysilanes (Artus et al., 2006b; Banga et al., 1995; Guo-hua & Higashitani, 2000; Jeong et al., 2001; Jin et al., 2011a; Jumrus et al., 2020b; Khoo & Tseng, 2008; Matin et al., 2019b; McGovern et al., 1994; Sriram et al., 2020; Wong & Yu, 2013a). These short-chain alkenylsilanes

are of particular interest due to their reactive terminal C=C bond, enabling functionalization *via* thiol-ene click chemistry under mild conditions. The use of vinyl- and allyltrichlorosilanes started gaining attention in the mid-20th century (Erickson, 1970). These compounds were initially explored due to their ability to form covalent bonds with oxide surfaces, particularly glass (Pujari et al., 2014a). Modification of oxide surfaces with organosilanes enabled various applications, including the improvement of adhesion of organic materials, the increase of the wear resistance of coatings and further chemical modifications (Materne et al., 2012). In the 1940s and 1960s, researchers began investigating the use of these organosilanes as coupling agents for improving binding between inorganic materials and organic polymers. For instance, studies demonstrated the improved properties of polyester laminates treated with these silanes, showing significant strength improvements over their saturated derivatives (ethyl- and propyltrichlorosilanes) Erickson (1970).

Early studies on allyltrichlorosilane (ATCS)-modified glass surfaces have shown their potential for subsequent functionalization. These modifications enable fine control over multifunctional surface properties such as inertness, wettability, and photoactivity, with applications ranging from gas chromatography capillaries (Novotný & Bartle, 1970) to nanotechnology (Cheawchan et al., 2016). The functionalization strategies offer complementary modifications, with one study increasing surface polarity through oxidation of the unsaturation in the allyl group, while another enhances hydrophobicity through a catalyst- and solvent-free 1,3-dipolar cycloaddition reaction, enhancing the surface's versatility for various applications (Cheawchan et al., 2016; Novotný & Bartle, 1970). Vinyltrichlorosilane (VTCS)-modified glass surfaces similarly allow for post-functionalization reactions through photoinduced disulfide-ene and thiol-ene click reactions (Li et al., 2015b). Such approaches provide stable and tunable interfaces for biosensing and diagnostic applications while preserving the integrity of the silane layer. The developed VTCS-derived coatings achieved dual thiol/disulfide-ene reactivity, persistent superhydrophobicity, and direct protein conjugation.

Herein, we investigate glass surfaces modified by commercially available VTCS and ATCS *via* dip coating. We explore how a single-carbon variation in the used silanizing agent affects the resulting surface properties. We also investigate how functionalizing the surface with a long alkyl chain thiol through a thiol-ene click reaction enhances the stability of the superhydrophobic coatings. Our study includes in-depth surface analyses using a combination of attenuated total reflectance-Fourier transform infrared spectroscopy (ATR-FTIR), photo-induced force microscopy

(PiFM), atomic force microscopy (AFM), scanning electron microscopy (SEM), water contact angle measurements, and UV-Vis spectroscopy techniques. Notably, this study presents a novel application of PiFM to quantify the efficiency of the thiol-ene click reaction and to map the spatial distribution of functionalization both across the surface and throughout the depth of the films. These findings offer new insights into how subtle structural differences between silanizing agents can significantly influence surface properties.

3.3 Materials and Methods

3.3.1 Materials

As substrates, soda-lime glass slides (27 mm × 46 mm × 1.2 mm thick) were supplied by Ward's Science (USA). Trichlorovinylsilane ($Cl_3SiCH=CH_2$, 97%) (VTCS), allyltrichlorosilane ($Cl_3SiCH_2CH=CH_2$, 95%) (ATCS), 1-decanethiol (DSH) ($CH_3(CH_2)_9SH$, 96%), concentrated sulfuric acid (H_2SO_4, 98%) and hydrogen peroxide (H_2O_2, 30%) were purchased from Sigma-Aldrich and used without further purification. Benzene, toluene, ethanol, methanol, tetrahydrofurane were all reagent grade and used as received.

3.3.2 Glass Silanization Procedure

Firstly, the glass slides were cleaned using piranha solution (H_2SO_4 : H_2O_2), following the activation protocol of glass described in our previous study (Khitas et al., 2025b). Then, the glass substrates were annealed at 200 °C for 1 h. Once cooled to room temperature, the activated glass samples were dip-coated in 8 mL of freshly prepared VTCS and ATCS solutions (40 mM) in benzene for 24 h. Under optimal humidity conditions (RH 40-60%), the reactions were carried out in closed vials with brief exposure to air during the introduction of the solutions and samples. When the ambient humidity is high (RH > 70%), the vials containing the activated glass samples were first purged with argon until cooled to room temperature before adding the solvent. The closed vials were only briefly exposed to air when adding silanizing agents. Finally, the vials were placed in a desiccator to minimize moisture exposure and limit humidity. The modified glass samples were rinsed with toluene, ethanol, and methanol, gently air-dried, and finally annealed for 10 min at 100 °C.

3.3.3 Surface Post-Modification Reaction *via* Thiol-ene Click Reaction

Glass surfaces with short-chain alkene-containing functionalities (*i.e.* vinyl and allyl) were investigated towards post-modification *via* thiol-ene click reaction using DSH to enhance the stability of the coatings. The silanized glass samples were immersed in a 20% (v/v) solution of DSH in tetrahydrofuran (THF), with ~0.05 eq. of azobisisobutyronitrile (*AIBN*) relative to the thiol. The reaction was conducted overnight under an inert atmosphere at 80 °C. The samples were then withdrawn from the solution, rinsed with hexane, ethanol, and methanol, gently air-dried, and finally annealed for 10 min at 100 °C. A schematic representation of the VTCS and ATCS coatings on the glass substrate followed by the thiol-ene click reaction is shown in Scheme 1. Notably, the dip-coating process enabled uniform functionalization across the entire glass substrate. For illustrative simplicity, the reactions of VTCS and ATCS with the glass substrate are depicted on a single surface. However, all optical characterizations account for modification on both sides, and any observed changes reflect functionalization across the entire substrate.

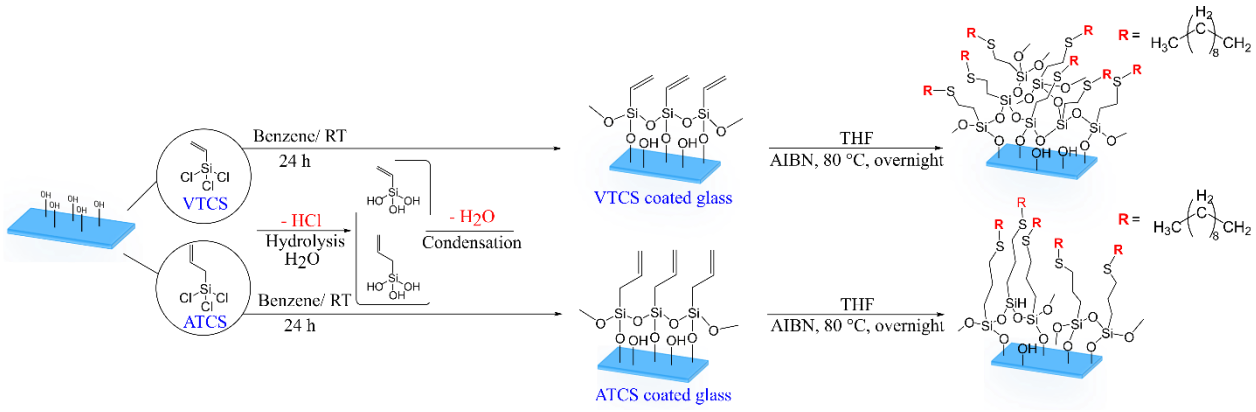

Scheme 3.1 The reactions of VTCS and ATCS on glass substrate followed by thiol-ene click reaction.

3.4 Characterization

An Attension Theta Optical Tensiometer (Biolin Scientific) was employed to study the wettability of the coated glass surfaces. Static water contact angles (θ) (WCAs) were measured at ambient temperature using 10 µL of deionized water. The reported values represent the average of three measurements taken at random positions on each sample. Sliding angles of the control samples were measured using the same instrument with 10 µL droplets. A Lambda 750 UV/Vis/NIR spectrophotometer (PerkinElmer, USA) was used to study the transmittance and reflectance of the coatings. A Nicolet iS50 Fourier transformed infrared spectrometer (Thermo Scientific, USA) was

used to confirm the fixation of the silanization agents on the glass surface and the functionalization of alkenes. Surface topography and roughness were analyzed using a multimode 8 (Bruker, USA) atomic force microscope (AFM). A JEOL JSM-7600F scanning electron microscope (SEM) (Japan) was used to examine the morphology of the coatings. Chemical identities, topography, and quantification of the surface coverage were determined using a photo-induced force microscope (PiFM) on a VistaScope instrument (MolecularVista, Inc., USA). PiFM spectra and images result from deconvoluting a summed heterodyne signal ($f_1 + f_2$). This signal is observed by lock-in amplifiers tracking two different cantilever resonant modes, termed f_1 and f_2, where $f_1 < f_2$. The f_2 frequency is exclusive to topographic imaging. PiFM imaging is slightly more complex, as there are two principal origins which depend on the pulsing frequency (f_m) of the source irradiation. The more straightforward method, also termed *direct mode*, is to pulse the IR laser at the cantilever frequency (f_1). Direct mode enables laser penetration deep into the sample, triggering a stronger photothermal expansion effect which is sensed by the tip. This mode is ideal for bulk surface characterization with nanometer lateral spatial resolution. The *sideband* mode is the image resulting from the laser pulsing at the differential frequency $f_m = f_2 - f_1$. The laser pulsing at midpoint between the two cantilever modes has been proven to yield surface-sensitive (~10 – 20 nm depth) spectroscopy and chemical imaging, generated by the contributions of sample molecule induced-dipoles and photothermal expansion (Vista).

3.5 Results and Discussion

The glass surfaces were coated with VTCS and ATCS, short-chain alkenylsilanes chosen for their reactive terminal double bonds, which allow further surface modification. The coating process involved the hydrolysis and condensation of VTCS and ATCS, forming covalent siloxane bonds with the glass surface while preserving the alkene functionality. FTIR spectroscopy was carried out to confirm the covalent bonding of VTCS and ATCS coatings on the glass surfaces. These short alkenylsilanes were interesting because their unsaturated bond functionality allows further surface modification (Li & Horton, 2002a; Li et al., 2015b; Rollings & Veinot, 2008). The transmittance ATR-FTIR spectra of bare glass, VTCS- and ATCS-modified glass samples were recorded in the 4000-650 cm^{-1} range. Due to the strong absorption of the glass substrate at wavenumbers below 1200 cm^{-1}, which can be seen as the broad peak in the transmittance spectrum (Figure S1), an entire spectral range was not represented. Consequently, it is inconvenient to determine the presence of

any peaks below 1200 cm^{-1} in the spectra that could be associated with the VTCS or ATCS coatings. Therefore, peaks associated with the silicon head group, Si–CH_2, Si–O–Si or Si–C overlap with the absorption of the glass substrate and are not observed in the lower frequency ranges of these spectra.

3.5.1 VTCS and ATCS Fixation on Glass Surfaces

To the best of our knowledge, the only infrared spectroscopy study of VTCS-coated glass was previously reported by Harrop (1978), revealing key features at 1639 cm^{-1}, 1450 cm^{-1}, and 971 cm^{-1}, corresponding to C=C stretching, –CH_2 in-plane bending, and –CH_2 out-of-plane bending modes, respectively. However, this study does not discuss the full mid-infrared region (4000-400 cm^{-1}), particularly the C–H stretching region (3100-2800 cm^{-1}), which is crucial for a more comprehensive analysis of the organosilane coating. This research gap highlights the need for a more complete spectral analysis to fully characterize the VTCS coating on glass surface. Later on, Shen and co-workers (2001) conducted a detailed vibrational analysis of VTCS using infrared and Raman spectroscopy, supported by computational calculations (*ab initio*). While their studies focused only on the bare forms of VTCS (gaseous, solid, liquid, and dissolved in liquid xenon), their findings provide valuable insights into the vibrational behavior of VTCS, which may contribute to a better understanding of the vibrational behavior of VTCS on glass.

In the current study, the characteristic vibrational frequencies of VTCS and ATCS were assigned, as shown in Figure 3.1. Considering the spectral regions 3150-2800 cm^{-1} (top) and 1730-1230 cm^{-1} (bottom), the ATR-FTIR spectra in Figure 3.1a confirm the functionalization of glass surfaces with VTCS and ATCS. The spectrum of the bare glass shows no prominent peaks associated with specific functional groups, indicating their absence on the surface. In the bare glass, the peak at 1630 cm^{-1} is attributed to the bending vibration of adsorbed molecular water (δ H–O–H) (Amma et al., 2016; Zarubin, 1999). This band is observed in the spectra of VTCS-modified glass surfaces. After functionalization with DSH, the intensity and position of the H–O–H bending vibration remain relatively unchanged. In the case of ATCS-modified samples, this peak overlaps with the C=C stretching vibration at 1632 cm^{-1}, making it difficult to determine whether molecular water is still present. These observations indicate that water molecules may be re-adsorbed from ambient humidity, even after surface modification. The VTCS-modified glass spectrum indicates two

separate C–H stretching peaks, likely influenced by Fermi resonance and combination bands involving the C=C stretch and C–H bending modes (Shen et al., 2001). The peak at 3062 cm^{-1} corresponds to the asymmetric C–H stretching vibration of the vinyl group, while the peak at 2984 cm^{-1} represents the symmetric C–H stretching of the vinyl group. The peaks at 3024 cm^{-1} and 2958 cm^{-1} are assigned to symmetric and asymmetric C–H stretching of the vinyl group, respectively. Further, the peak at 1602 cm^{-1} corresponds to C=C stretching vibration, confirming the presence of vinyl groups. The peaks at 1409 cm^{-1} and 1276 cm^{-1} are attributed to in-plane deformations and bending modes of $=CH_2$ and =CH bonds, respectively.

On the other hand, while there is no literature precedent for the infrared spectroscopic characterization of ATCS molecules attached to glass surfaces, most studies have focused on the bare forms of ATCS or VTCS (Bailey & Pines, 1954; Durig & Hellams, 1968; Guirgis et al., 1998; Scott & Frisch, 1951; Shull et al., 1956; Smith, 1960) or their fixation to other substrates, such as aluminum (Li, Vecchio, et al., 2007), mica (Li & Horton, 2002a), or silicon wafers (Rollings et al., 2007). Similarly, the FTIR spectrum of ATCS-modified glass exhibits the characteristic vibrational modes that confirm the covalent bonding of allyl groups. As shown in Figure 3.1a, the peaks at 3082 cm^{-1} and 2977 cm^{-1} are attributed to $=CH_2$ stretching, while the peak at 2930 cm^{-1} corresponds to CH_2 asymmetric stretching. The peak at 1632 cm^{-1} is assigned to C=C stretching. Additionally, the peaks at 1452 cm^{-1} and 1419 cm^{-1} are associated with CH_2 bending vibration, with the peak at 1387 cm^{-1} corresponding to $=CH_2$ bending. The peak at 1265 cm^{-1} represents the CH_2 bending modes of the terminal $=CH_2$ groups. These absorptions confirm the covalent bonding of vinyl and allyl groups from VTCS and ATCS onto the glass surface.

3.5.2 Functionalization of the VTCS- and ATCS-Modified Glass Surfaces

The terminal alkene groups in VTCS- and ATCS-modified glass surfaces enable versatile modifications through thiol-ene click chemistry. This approach allows fine surface functionalization without compromising the integrity of the coating while simultaneously improving coating stability. Significant changes were observed following the thiol-ene click reaction between the VTCS-modified glass surface and DSH (Figure 3.1b). Two new peaks at 2924 cm^{-1} and 2855 cm^{-1} are observed, corresponding to asymmetric and symmetric C–H stretching in methylene groups. These peaks are characteristic of the alkyl chain from DSH incorporated during

the functionalization reaction. An increase in peak intensity at 2958 cm^{-1}, associated with the asymmetric CH stretching in the -CH_2 groups, was also observed. This increase in intensity is likely due to the asymmetric stretching of alkyl groups (methylene or methyl) from the DSH chains. A new peak at 1467 cm^{-1}, attributed to the deformation of newly formed –CH_2– groups, indicates the conversion of some of the C=C bonds to C–C bonds. Concurrently, a decrease in the peaks at 3062 cm^{-1}, 3024 cm^{-1}, 2984 cm^{-1}, 1602 cm^{-1}, 1409 cm^{-1}, and 1276 cm^{-1} were noted, further confirming the partial conversion of surface alkenes and the fixation of the DSH molecules on the VTCS-modified glass surface. The partial conversion of surface alkenes was further supported by the persistence of the characteristic C=C peaks after functionalization, as a complete reaction would have resulted in the total disappearance of such peaks.

Similarly, distinct changes were observed in the IR spectrum of ATCS-modified glass surface upon its reaction with DSH (Figure 3.1c). The spectrum shows a new peak at 2853 cm^{-1}, indicative of symmetric C–H stretching vibrations in the methylene groups, while the intensity of the peak at 2927 cm^{-1} increases, corresponding to asymmetric C–H stretching in the methylene groups. These peaks are characteristic of the alkyl chains introduced by DSH during the click reaction. Simultaneously, slight decreases in the peak intensities at 1632 cm^{-1}, 1419 cm^{-1}, 1387 cm^{-1}, and 1268 cm^{-1} are observed. These reductions likely result from the partial conversion of C=C bonds into C–C bonds during the click reaction. The increase in peak intensity at 1452 cm^{-1} is associated with CH_2 bending and thus confirms the covalent bonding of alkyl chains from DSH. The spectral changes in the VTCS and ATCS systems after reacting with DSH exhibit distinct differences. In addition, the incomplete disappearance of VTCS and ATCS original peaks suggests that only a certain percentage of alkene functionalities were reacted with DSH during the click reaction. The VTCS system shows more pronounced spectral changes, suggesting a greater extent of thiol-ene click reaction. In contrast, the changes in the ATCS system are relatively less significant, indicating a more limited reaction. This may be attributed to numerous factors, such as steric hindrance and accessibility of the reactive groups.

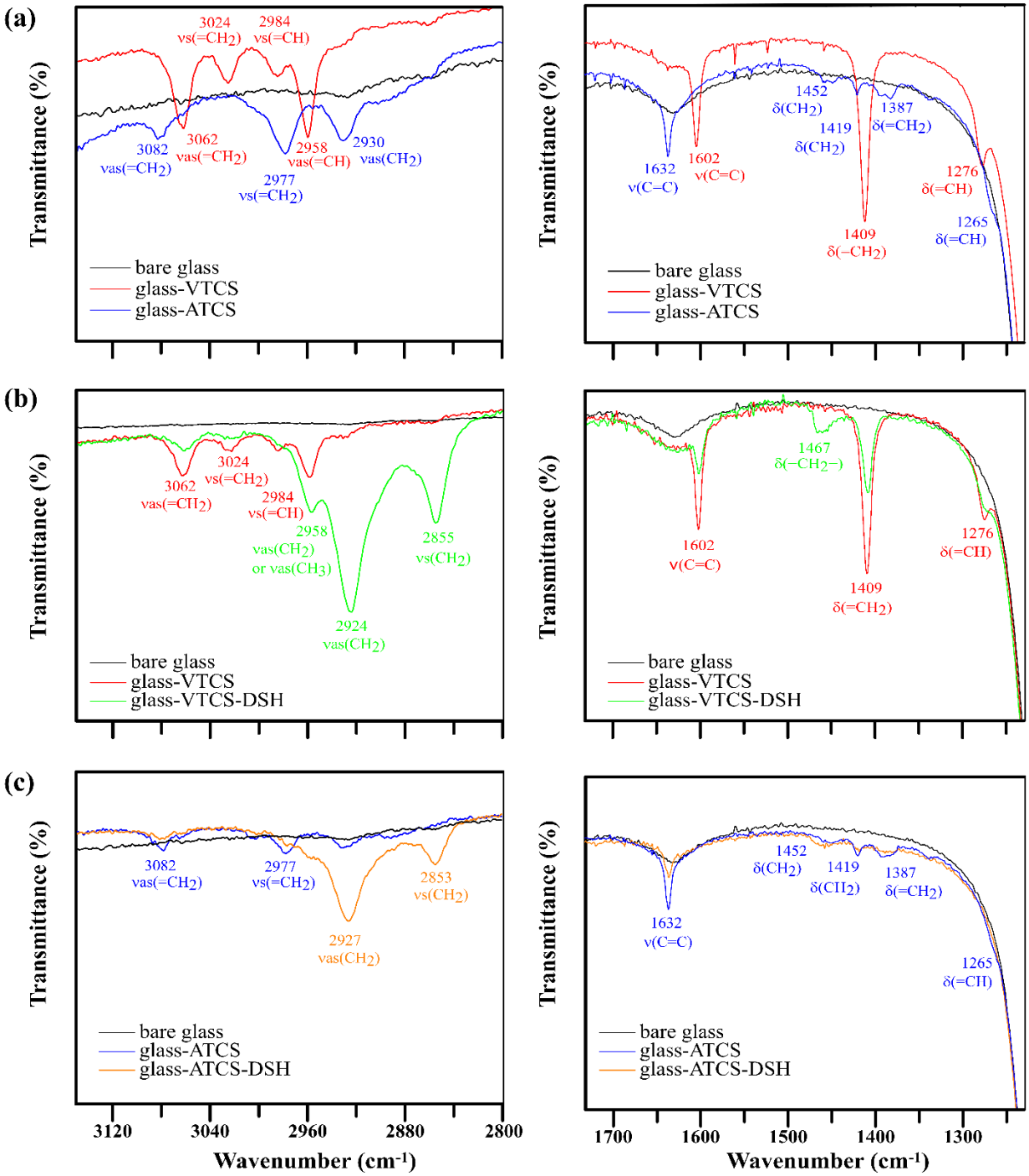

Figure 3.1 ATR-FTIR spectra of (a) bare glass, VTCS-, and ATCS-modified glass showing characteristic peaks of the vinyl and allyl groups. Transmittance spectra of VTCS- (b) and ATCS-coated glass surfaces (c) after functionalization with DSH, highlighting changes in peak intensities. The partial reduction in C=C stretching vibrations (1602 cm^{-1} for VTCS and 1632 cm^{-1} for ATCS) confirms the partial conversion of surface alkenes, indicating incomplete functionalization.

3.5.3 Light Interaction and Nanoscale Topography

Developing hydrophobic or superhydrophobic coatings for practical use is often challenging due to the need to balance surface roughness with optical transparency (Choi & Huh, 2010; Nakajima et al., 2000). An increase in surface irregularities would increase water repellency but simultaneously lower the optical performance due to the enhanced light scattering effect (Karunakaran et al., 2011). Achieving optimal balance between both properties requires precise control over the surface topography. This balance can typically be achieved when the surface features are kept below ¼ of the visible light wavelength range (400-800 nm) and ideally below 80 nm (Nakajima, 2004a; Nakajima et al., 1999; Wong et al., 2012). In practice, transparency is measured in terms of transmittance using UV-Vis spectroscopy. Another crucial parameter is the fraction of the incident light lost due to scattering and reflection, which is a function of the surface roughness and abrupt changes in refractive index at the interfaces (Nakajima, 2004a; Yu, Guo, et al., 2015).

Figure 3.2 demonstrates the optical properties of the modified glass surfaces before and after functionalization. The average transmittance of the bare glass substrate is 92%, with approximately 8% of incident light lost due to reflection. VTCS and ATCS coatings improved the average transmittance of the substrate by ~3.0% and ~1.0%, respectively at 550 nm (Figure 3.2a,b top). DSH functionalization further enhanced the optical transmittance of both modified substrates. The VTCS-modified substrate had an enhancement in transmittance of ~3.7 % (Figure 3.2a top), while for the ATCS-modified substrate, the enhancement was ~1.4% (Figure 3.2b top) at 550 nm. Comparable optical improvements have been reported in earlier studies (Wong et al., 2012; Wong & Yu, 2013a; Zhang & Seeger, 2013; Zimmermann et al., 2008). Li and co-workers (2015b) reported a multifunctional surface where VTCS was polymerized on glass. Their surface maintained about 83% transparency above 400 nm, comparable to their reference glass. Our results demonstrate superior optical performance compared to this previous study. Reflectance data (Figure 3.2a,b bottom) revealed a reduction for both VTCS- and ATCS-modified glass substrates. Furthermore, VTCS modification resulted in an average reflectance reduction of ~3.6% (Figure 3.2a bottom), while ATCS modification led to an average decrease of ~1.4% at 550 nm (Figure 3.2b bottom). DSH functionalization further decreased reflectance by ~4.3% for the VTCS-modified glass and ~1.5% for the ATCS-modified glass at 550 nm. The observed decrease in

reflectance is attributed to the antireflective properties of the films (Diedenhofen et al., 2009). This is likely due to the low refractive indices of the coatings ($n_{VTCS} \approx 1.43$ and $n_{ATCS} \approx 1.44$) and their morphology, which together create a gradient interface between air (n≈1) and glass (n≈1.5).

Water contact angle (WCA) measurements were carried out to characterize the wettability of the studied surfaces. The WCA of bare glass is 26° ± 6. The VTCS-modified glass surface exhibited superhydrophobic behavior with a WCA of 168° ± 2 and a sliding angle of 2°. After functionalization with DSH, the samples exhibited a WCA of 170° ± 4 with a sliding angle of 1°. This was achieved despite the absence of perfluoroalkyl chains, which are known for their low surface energy and ability to enhance hydrophobicity (Dalvi & Rossky, 2010; Liang et al., 2023). In contrast, ATCS-modified glass showed WCAs of 109° ± 4 and 113° ± 4 before and after functionalization with DSH, respectively. These negligible contact angle changes likely reflect the fact that the additional, chemically grafted DSH layer does not substantially alter the surface energy, particularly when DSH chains are embedded within the coating network or when thiol coverage, as in our case, is modest. Moreover, AFM measurements (Table 1) show only minor variations in surface roughness after functionalization, indicating that the surface morphology, an important determinant of wettability, was largely preserved. Finally, it is worth noting that contact angle measurements are inherently less sensitive than spectroscopic methods to subtle changes in surface chemistry, especially when surface morphology and roughness remain essentially unchanged.

Despite these changes in wettability, both surfaces remained optically transparent. While longer alkyl chains generally increase hydrophobicity due to greater van der Waals interactions (Arianpour et al., 2016), the slightly longer chain of ATCS may have introduced more conformational flexibility due to the additional methylene group. Infrared and Raman spectroscopy studies reported by several groups (Guirgis et al., 1998; Li, Vecchio, et al., 2007) indicated that only the gauche conformer was present in all three physical states of ATCS. This could potentially affect how molecules arrange on the surface, leading to less ordered structures, which may reduce hydrophobicity compared to VTCS.

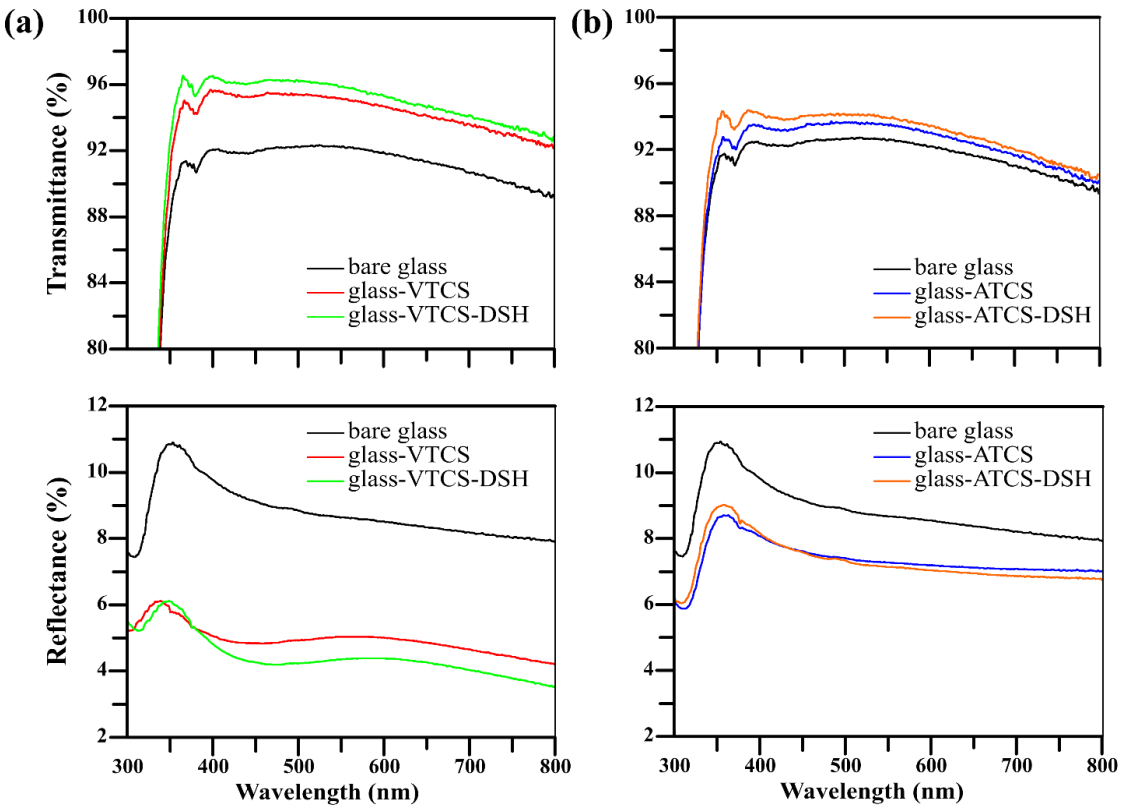

Figure 3.2 UV-Vis transmittance and reflectance spectra of VTCS- and ATCS-modified glass before and after functionalization. (a) VTCS-modified glass (top) transmittance and (bottom) reflectance spectra. (b) ATCS-modified glass (top) transmittance and (bottom) reflectance spectra. In each panel, spectra of the modified surfaces are shown with the bare glass for comparison.

Figure 3.3 shows the nanoscale surface topography and morphology of the modified glass surfaces before and after functionalization, along with the size distribution of the surface features. In the 2-dimensional (2D) AFM images (Figure 3.3i-a), the VTCS-modified glass shows a nanofilament-like dense network. This is consistent with observations reported by Li and co-workers (2015b). After functionalization with DSH (Figure 3.3ii-a), these nanofilament-like structures become thicker, with less pronounced gaps in between and slightly increased roughness. In contrast, the ATCS-modified glass (Figure 3.3iii-a) shows irregular agglomerated structures distributed across the surface, making the coating less uniform and smoother than the VTCS-modified surface. These features suggest that ATCS forms discrete domains instead of a continuous layer, resulting in a heterogeneous surface topography. After functionalization with DSH (Figure 3.3iv-a), the aggregates become more defined. This change in topography gives evidence of a possible growth of the aggregates after thiol-ene click reaction by increased molecular interactions in the modified regions.

SEM images (Figure 3.3b) further confirm these observations, revealing a well-defined nanofilament network for VTCS (Figure 3.3i-b and ii-b), which generates a highly porous surface instead of a densely packed coating. The size distribution analysis (Figure 3i-c) indicates a relatively narrow filament diameter size range between 32 and 42 nm with an average diameter of 37 ± 1 nm. These results explain our superior optical performance compared to those reported by Li and co-workers (2015b), whose silicon nanofilaments measured ~30 - 50 nm in diameter. Furthermore, the notable reflectance reduction from 8.6% for bare glass to 5.0% and 4.4% at 550 nm achieved by the VTCS-modified glass before and after functionalization, respectively, is primarily attributed to its porous nanofilament network (Bravo et al., 2007). This network reduces the abrupt refractive index change between glass and air. It creates a gradual index transition, minimizing Fresnel reflections through effective index matching, thereby enhancing the optical performance of the glass surface (Diedenhofen et al., 2009). Similar improvements have been reported for polymethylsiloxane nanofilament coating, with filament diameters of 20 to 50 nm, where ellipsometry revealed a refractive index as low as 1.12 (Artus et al., 2006b). After functionalization with DSH (Figure 3.3ii-c), the diameter distribution shifted towards larger sizes, with most filaments measuring between 45 to 65 nm and an average diameter of 52 ± 2 nm. The measured sub-65 nm diameters of these porous nanofilaments further confirm their role in reducing the reflected fraction of visible light and enhancing transparency (Rahmawan et al., 2013). The high surface roughness of the porous VTCS nanofilament network (Table 1) contributes significantly to the surface architecture, supporting the development of the observed superhydrophobic behavior, which is discussed in detail in a later section (Rahmawan et al., 2013).

ATCS (Figure 3.3iii-b) shows a distribution of irregular agglomerates with smaller particle-like structures across the surface, which is suspected to be a thinner coating than the layer underneath the aggregate features (Figure S2). The equivalent circular area diameter (ECAD) (Heywood, 1937) is defined as the diameter of the particle's projected image based on its area and is represented by (d_a). The ECAD of ATCS-glass particles exhibits a broad distribution, with most particles having a diameter below 150 nm and a few extending up to 210 nm (Figure 3.3iii-c). This reflects the heterogeneous nature of the ATCS coating with an average ECAD of around 80 ± 4 nm. The d_a was calculated using the following equation:

$$d_a = 2 \times \sqrt{\frac{A}{\pi}}$$ Equation (3.1)

where A is the area of the particle measured by ImageJ, representing the number of pixels or calibrated unit (nm) within the particle boundary

Following functionalization with DSH, the particle distribution becomes more concentrated around 100 nm, with a few particles extending up to 425 nm, suggesting further aggregation growth. The particle ECAD distribution (Figure 3.3iv-c) shows a narrower range, with most particles still below 150 nm and a mean diameter of approximately 96 ± 1 nm. This suggests shifting towards slightly larger particles after the click reaction.

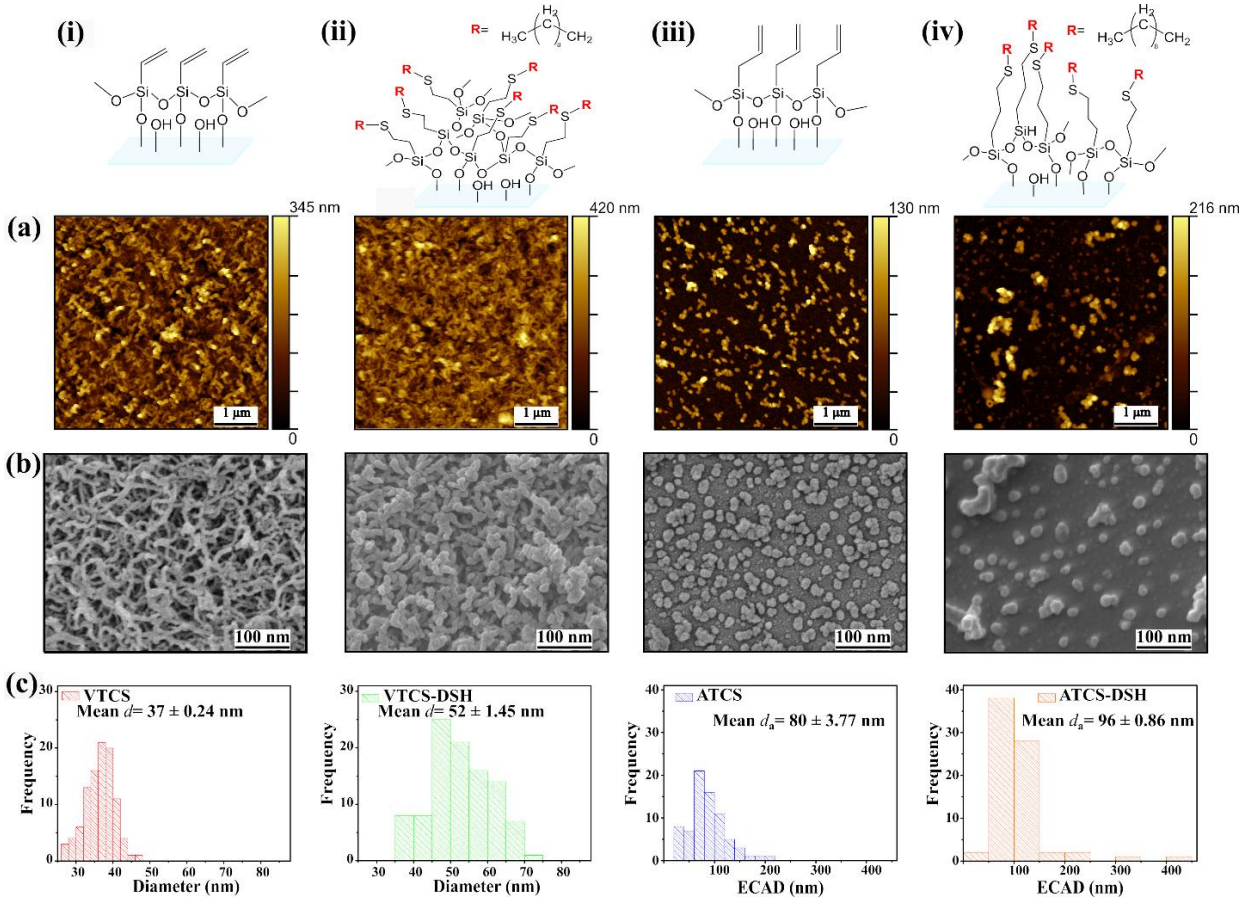

Figure 3.3 Surface characterization of VTCS- and ATCS-modified glass before and after functionalization. Molecular structures of (i) VTCS, (ii) VTCS-DSH, (iii) ATCS, and (iv) ATCS-DSH. (a) 2D AFM images of VTCS- and ATCS-modified glass surfaces (i and iii) before and (ii and iv) after functionalization. (b) SEM images showing scale bars of 100 nm. (i and ii) VTCS-modified glass with nanofilaments and (iii and iv) ATCS-modified glass with

particle-like morphology, both before and after functionalization. (c) Size distribution of (i and ii) VTCS nanofilaments and (iii and iv) ATCS particles, both before and after functionalization.

Roughness parameters, measured by AFM analysis, presented in Table 1 for the VTCS- and ATCS-modified surfaces before and after functionalization provide valuable insights into the evolution of surface topography. The VTCS-modified surfaces, characterized by a porous nanofilament network, show minor changes upon functionalization. The relatively constant mean roughness (R_a) (from 50.6 nm to 50.2 nm) and root mean square roughness values (R_q) (from 63.3 nm to 64.2 nm) indicate that the general network structure was preserved upon functionalization. On the other hand, the functionalization resulted in more pronounced changes for the ATCS-modified surfaces. While the R_a values showed some variation (19.2 nm to 25.6 nm), the R_q values increased more significantly (26.0 nm to 37.9 nm). This increase suggests that the functionalization caused more pronounced surface features due to aggregate growth or coalescence without altering the average surface height.

Table 3.1 The roughness parameters of bare and modified glass surfaces determined by AFM measurements.

As prepared coatings	Mean roughness R_a (nm)	Root-mean-square roughness R_q (nm)
Bare glass	1.1	1.3
Glass-VTCS	50.6	63.3
Glass-VTCS-DSH	50.2	64.2
Glass-ATCS	19.2	26.0
Glass-ATCS-DSH	25.6	37.9

3.5.4 Chemical Mapping and Spectral Analysis of Surface Modification using Photo-induced Force Microscopy (PiFM)

Infrared results highlighted the need for a more sensitive quantitative technique to investigate surface chemistry and accurately quantify the functionalization reaction conversion of the studied surfaces. In this context, PiFM (Amini et al., 2024; Davies-Jones & Davies, 2022; Jafari et al., 2024) local point infrared spectroscopy was selected as an emerging technique to support our initial findings. This technique represents a high-resolution spectroscopy technique, enabling the observation and mapping of chemical changes with nanoscale resolution and offering a complete investigation of the functionalization process. It should be noted that local point infrared spectral acquisitions were collected over all the analyzed surfaces, and an average of these spectra was then

presented. Bare soda-lime glass produced a distinct mid-infrared PiFM spectra with no visible peaks in the 1700-1250 cm^{-1} range (Figure S5a). The PiFM local point infrared spectra of VTCS- and ATCS-modified glass surfaces (Figure 3.4a,b and Figure 3.5a,b, respectively) showed peaks attributed to the stretching and bending vibrations of the vinyl (1602 cm^{-1}, 1467 cm^{-1}, 1409 cm^{-1}, and 1276 cm^{-1}) and allyl (1632 cm^{-1}, 1452 cm^{-1}, 1387 cm^{-1}, and 1265 cm^{-1}) groups. These findings were in good agreement with the ATR-FTIR spectroscopy results for both samples (Figure 3.1) and further supported the expected functional groups on the modified glass surfaces. Notably, the absence of a peak around 1467 cm^{-1} (Figure 3.4a) indicates the absence of C–C single bonds in the initial VTCS structure. Significant spectral changes are observed following the thiol-ene click reaction with DSH (Figure 3.4b), providing additional evidence for the partial surface functionalization. The intensity of the C=C stretch decreased considerably, indicating the consumption of a certain percentage of the vinyl groups. The peaks at 1409 cm^{-1} and 1276 cm^{-1} also decreased with approximately the same range, further confirming the loss of C=C functionality and suggesting that these double bonds have been converted into C–C bonds upon thiol-ene click reaction. The appearance of a new peak at 1467 cm^{-1} provides additional evidence for this conversion, signifying the presence of CH_2 groups in C–C single bonds.

To evaluate the spatial distribution of the DSH functionalization in VTCS and ATCS films, we performed PiFM chemical mapping in both sideband and direct modes. As expected, since the PiFM spectrum of bare soda-lime glass did not show any signals overlapping with those of VTCS or ATCS, the corresponding PiFM maps of its surface displayed uniformly low intensity, as illustrated in Figure S4b at the C=C band (~1632 cm^{-1}). The resulting chemical maps (Figure 3.4c,d; Figure 3.5c,d; Figure S3c,d; and Figure S4c,d) revealed a distinct contrast between the control and functionalized samples, providing supported evidence that functionalization occurred both at the surface and within the film depths. High-intensity zones in these maps correlated with the locations of filament-like structures and particles observed in the topography scans of VTCS- and ATCS-modified glass surfaces, respectively.

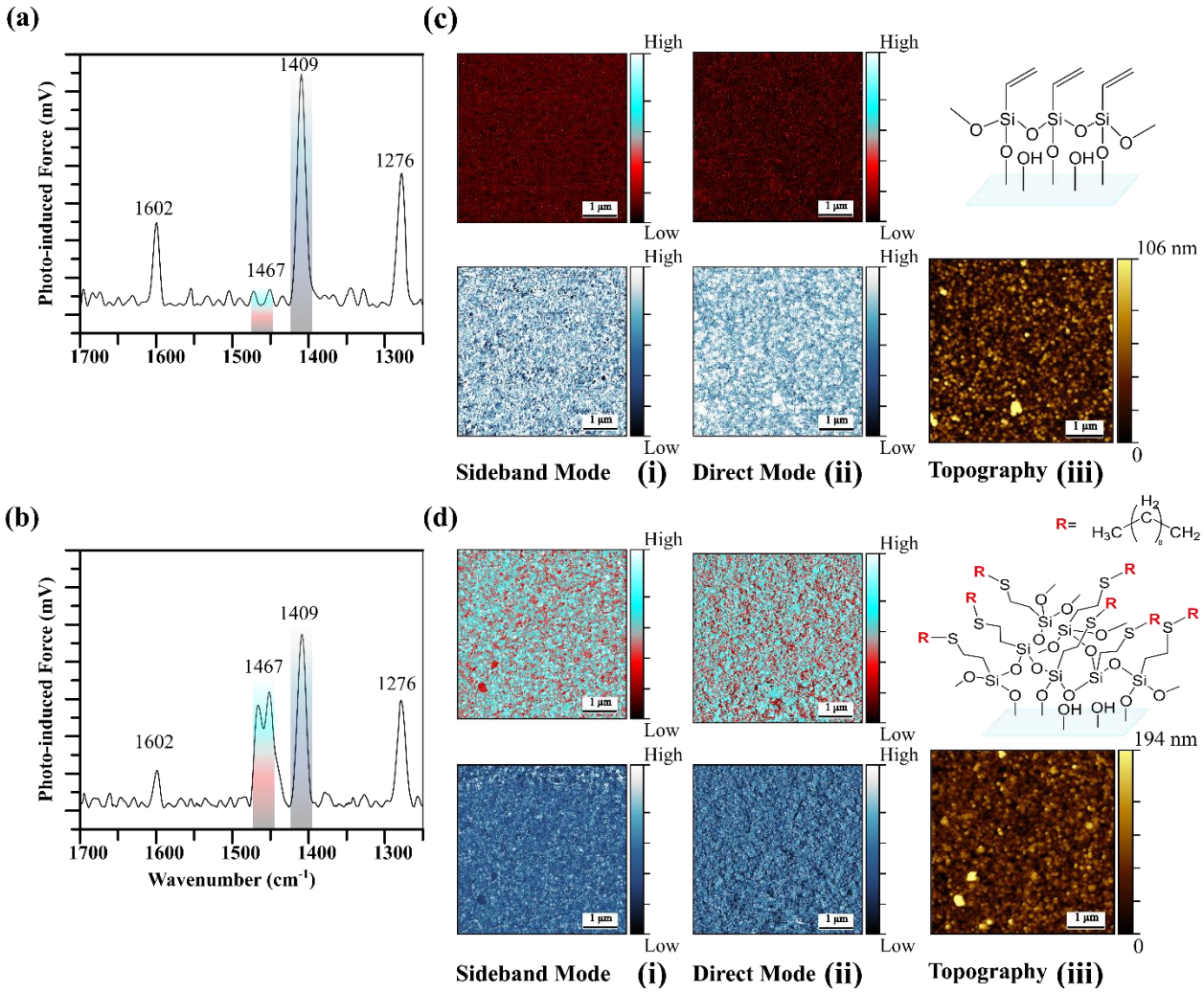

Figure 3.4 PiFM spectra, chemical mapping, and topography images of glass surfaces modified with VTCS. PiFM spectra of VTCS-modified glass before (a) and after (b) thiol-ene click reaction. PiFM chemical mapping images before (c) and after (d) functionalization, collected at 1467 cm^{-1} and 1409 cm^{-1} in (i) sideband and (ii) direct modes. (iii) Topography images of the corresponding analyzed surface.

For VTCS-modified surfaces (Figure 3.4c and d), pre-functionalization maps at 1409 cm^{-1} (δ ($=CH_2$)) showed higher contrast in the sideband mode (Figure 3.4ci) compared to the direct mode (Figure 3.4cii). The in-depth mode (Figure 3.4cii) reveals a more uniform filament-like structure with high-intensity signal distribution, representing areas rich in vinyl groups. However, gaps between these structures indicate regions with lower molecular concentrations. Post-functionalization maps, collected at 1409 cm^{-1} (δ ($=CH_2$)) (Figure 3.4d), 1276 cm^{-1} (δ (=CH)) (Figure S3), and 1602 cm^{-1} (ν (C=C)) (Figure S3), show a decrease in intensity, particularly in the areas surrounding the features. This indicates that the regions originally rich in C=C bonds have been effectively converted, leaving fewer double bonds and a more uniform surface. A similar

pattern is observed at the surface level, with homogeneous functionalization indicating good molecular permeability of the molecules as they diffused into the VTCS layer. These findings confirm the functionalization of the modified glass surface both at the surface level and within the film. In contrast, ATCS-modified glass (Figure 3.5a and b) demonstrated moderate changes in the peak intensities. Following the functionalization reaction (Figure 3.5b), we observed a mild decrease in peak intensities at 1632 cm^{-1} (ν (C=C)), 1265 cm^{-1} (δ (=CH)), and 1387 cm^{-1} (δ ($=CH_2$)), indicative of the partial loss of C=C bonds. Concurrently, the increase in intensity of the preexisting peak at 1452 cm^{-1} (δ (CH_2)) supports the formation of C–C bonds resulting from the thiol-ene reaction with DSH. These spectral changes provide strong evidence for the partial thiol-ene click reaction.

To confirm the uniformity of the functionalization across the ATCS-modified surfaces, we also employed PiFM in sideband (Figure 3.5ci) and direct modes (Figure 3.5cii) analyses. Before functionalization (Figure 3.5c), in-depth and surface PiFM mapping revealed that the entire substrate is uniformly coated, not just regions with visible aggregates. The in-depth PiFM maps collected at 1632 cm^{-1} (ν (C=C)) (Figure 3.5cii) and 1265 cm^{-1} (δ (=CH)) (Figure S4) show a higher signal intensity in the aggregate regions due to the higher molecular concentration in these areas compared to the surrounding surface areas. However, surface mapping reveals a relatively more homogeneous signal distribution with low-intensity signals in the regions between aggregates. The underneath layer is composed of a lower molecular concentration than the aggregates. After functionalization (Figure 3.5d), the PiFM images collected at 1632 cm^{-1} (ν (C=C)), 1387 cm^{-1} (δ ($=CH_2$)), and 1265 cm^{-1} (δ (=CH)) (Figure S4) show a decrease in signal intensity, while certain regions remained at high intensity uniformly across the surface. The in-depth PiFM results (Figure 3.5dii) further support this finding, as the signal intensity, pre-functionalization was initially localized to the aggregates becomes more evenly distributed across the surface. However, some regions exhibit lower saturation levels compared to the pre-functionalized surface (Figure 3.5cii). This indicates that certain C=C bonds remain unconverted across the substrate. This confirms that functionalization occurred at both levels: on the aggregates and surrounding areas across the entire substrate, with some C=C bonds remaining unconverted. These results provide valuable insights into surface chemistry and the distribution of the functionalization.

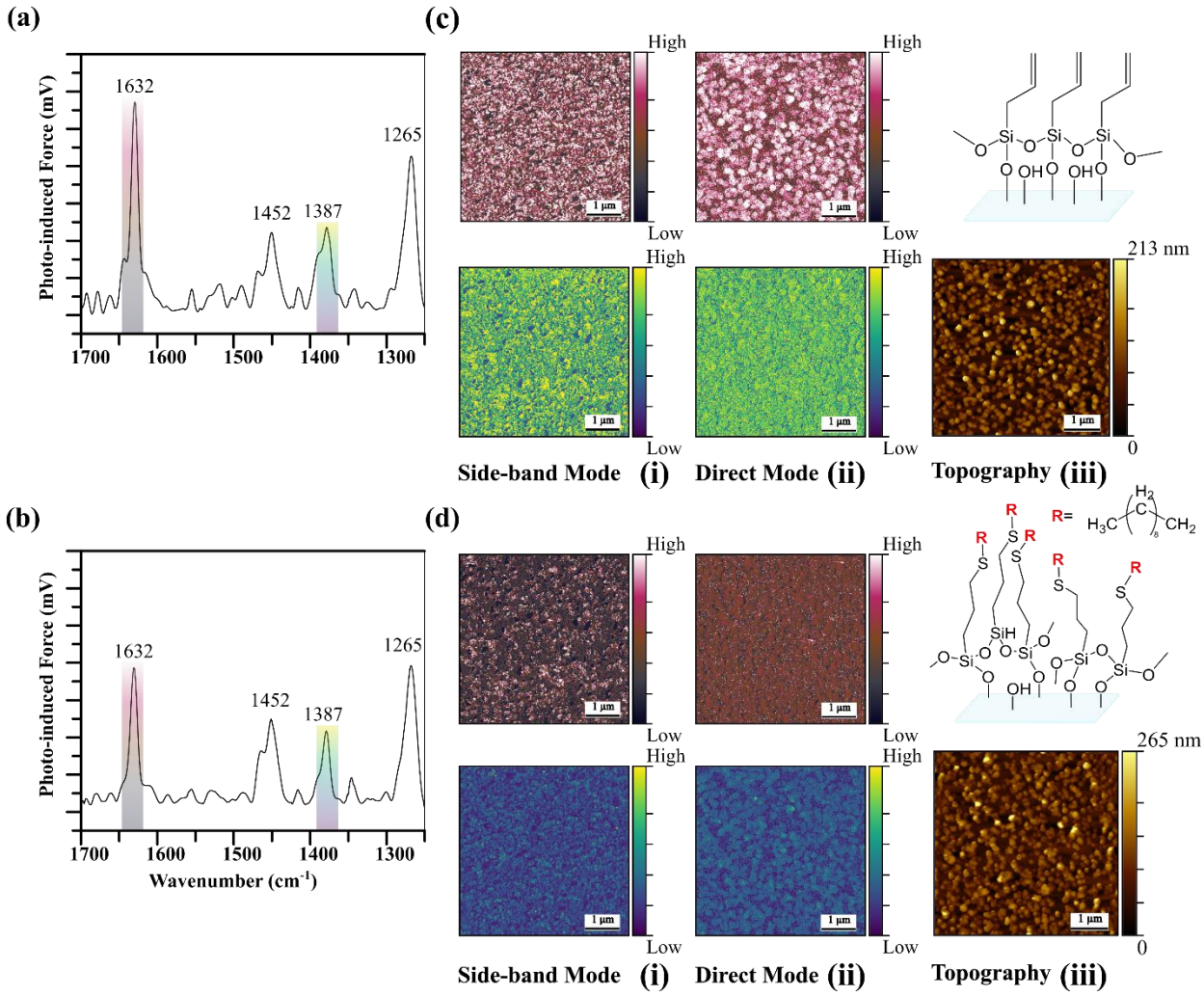

Figure 3.5 PiFM spectra, chemical mapping, and topography images of glass surfaces modified with ATCS. PiFM spectra of ATCS-modified glass before (a) and after (b) thiol-ene click reaction. PiFM chemical mapping images before (c) and after (d) functionalization, collected at 1632 cm^{-1} and 1378 cm^{-1} in (i) sideband and (ii) direct modes. (iii) Topography images of the corresponding analyzed surface.

3.5.5 Why Does VTCS Form Porous Nanofilament Networks but Not ATCS?

Previous research on VTCS coatings has been limited, with only a few studies exploring their potential for creating 3D nano-architectures. Rollings and co-workers (2007) as well as Rollings and Veinot (2008) were the first to investigate VTCS as a coating, reporting the formation of nanofibers through surface-induced vapor-phase polymerization on silicon wafers. Later on, Li and co-workers (2015b) demonstrated the formation of VTCS-porous nanofilaments through the phase separation technique on glass substrates. It is known that under optimized conditions, organosilanes condense with water and surface silanols, creating covalently attached, crosslinked polymeric

layers through vertical polymerization (Fadeev & McCarthy, 2000). In our study, VTCS condensation with water and glass surface silanols resulted in a porous nanofilament network. This has likely occurred due to the covalent bonding of VTCS followed by crosslinking into polymeric layers through vertical polymerization. Among the key factors governing the production of nanofibers are the concentration of the surface hydroxyl groups and the adsorbed water layer, which serve as nucleation sites for vertical polymerization (Rollings & Veinot, 2008).

Under ambient conditions in our study, when VTCS is introduced to the reaction vial, it hydrolyzes either in solution or upon adsorption on the glass substrate (Babik et al., 2012; Sagiv, 1980b; Wasserman et al., 1989). Subsequently, the hydrolyzed VTCS is attached to the surface due to the condensation reaction of its one (or possibly more) silanol groups with the glass hydroxyl groups. At this point, the remaining silanol groups are available for coupling with other physisorbed hydrolyzed VTCS moieties (Wasserman et al., 1989). Subsequently, the alkyl chains of each VTCS crosslinking must rearrange into a configuration that minimizes their interaction from overlapping van der Waals radii (3.5 Å) (Stevens, 1999). This is because the maximum bond length of a Si–O–Si, even when stretched to its limit, is 3.2 Å (Grigoras & Lane, 1988). The residual hydroxyl groups maintain specific orientation away from the substrate to guide further condensation reactions with other hydrolyzed VTCS moieties (Stevens, 1999). The nanofilament growth is initiated by the first anchored hydrolyzed VTCS, followed by the nucleation site. Therefore, vertical polymerization produces a porous cross-linked nanofilament network. Hence, the key point for nanofilament formation is the initial nucleation and subsequent vertical growth of the polymeric islands perpendicular to the surface (Rollings & Veinot, 2008). In contrast, research on ATCS coatings is even more limited. Li and Horton (2002a), studied the assembly process of ATCS on mica under an inert atmosphere to minimize the water vapor effect on the polymer formation in the monolayers. They found that, at room temperature, ATCS forms homogeneous and continuous overlayers of only 1 to 2 molecules thick. At -78 °C, polymerized aggregates formed due to water condensation within the reaction chamber. Additionally, nanoindentation technique was employed to evaluate the mechanical properties of the coatings, distinguishing between ordered SAM and polymerized aggregates on the surface. In our study, both VTCS and ATCS have double bonds at the end of their alkyl chain. However, ATCS contains an additional methylene group, leading to a slightly longer chain with increased flexibility. While VTCS readily forms nanofilaments, ATCS

exhibits different assembly due to its structural constraints. The additional methylene group introduces steric hindrance which combined with the formation of charged centers due to the partial C=C polarization, disrupts the lateral crosslinking required for filament growth (Li & Horton, 2002a). Instead, ATCS adopts two distinct morphologies, an ordered SAM and irregular polymerized aggregates, which were suggested to be physiosorbed in the nanoindentation study of Li and Horton (2002a).

3.5.6 Quantification of the Thiol-ene Click Reaction Conversion

The peak integration method was applied to both ATR-FTIR and PiFM spectra (Figure 3.6) to quantify the thiol-ene click reaction conversion. The method involves measuring the area under the peaks associated with the C=C bond before and after functionalization. The conversion (%) of the thiol-ene click reaction is then calculated using the following equation:

$$\text{Conversion (\%)} = \frac{A_{initial} - A_{final}}{A_{initial}} \times 100 \qquad \text{Equation (3.2)}$$

Where $A_{initial}$, represents the area of the C=C peak before functionalization, and A_{final} after functionalization.

Based on ATR-FTIR analysis, the click reaction conversion was estimated to be approximately 63% and 40% for VTCS- and ATCS-functionalized glass surfaces, respectively. These values are slightly higher than those obtained *via* PiFM analysis which yielded conversions of about 56% and 33% for VTCS- and ATCS-functionalized glass surfaces, respectively. This difference is attributed to differences in resolution and sampling depth between the two techniques.

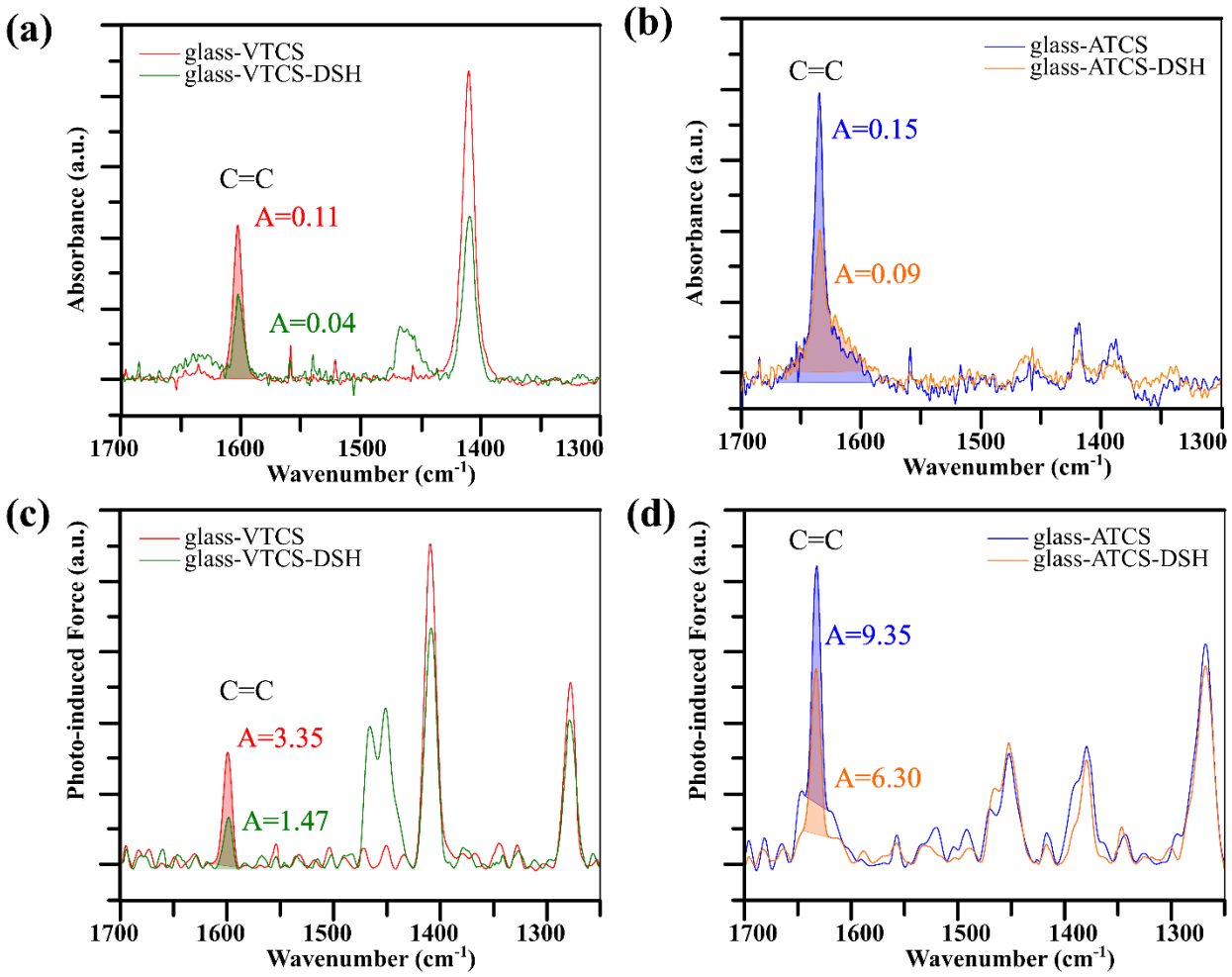

Figure 3.6 Quantifying the thiol-ene click reaction conversion *via* ATR-FTIR (a and b) as well as PiFM (c and d) spectra of VTCS- and ATCS-modified glass before and after functionalization. (a and c) VTCS- and (b and d) ATCS-modified surfaces, highlighting the C=C bond peak area reduction.

Thiol-ene click reaction is widely used as a general route to functionalize organosilanes for surface coating applications (Li et al., 2015b). This reaction is typically known for its high efficiency, resulting in quantitative to near-quantitative yields (Kaczmarek et al., 2023b; Tucker-Schwartz et al., 2011b). The conversion values obtained in our study from both ATR-FTIR and PiFM are relatively low, which is unexpected for this reaction. While Li and co-workers (2015b) performed click reactions of glass substrates bearing vinyl groups, they did not provide quantitative analysis of the reaction yields. In contrast, Campos and co-workers (2010) achieved 45-75% surface coverage for multiple functional thiols attached to alkene-terminated oxide-free Si(111) substrates *via* thiol-ene click chemistry. This reaction is typically known for its high efficiency, resulting in quantitative to near-quantitative yields (Kaczmarek et al., 2023b; Tucker-Schwartz et al., 2011b).

Our click reaction conversions for VTCS and ATCS are relatively low at 56% and 33%, respectively, which is unexpected for this reaction. Furthermore, Zhang and co-workers (2020) have employed wettability measurements to confirm the covalent bonding of diverse thiols to an allyl-containing copolymer grafted onto metal surfaces. Additionally, the researchers demonstrated the practical efficiency of the coating by applying it to a porous membrane. They achieved 99.2% separation efficiency, which also confirmed the functionalization's effectiveness. Kaczmarek and co-workers (2023b) reported the complete disappearance of the characteristic peaks corresponding to thiol and the C=C stretching vibration of polyether. Their reaction was performed at the molecular level, which likely facilitated higher efficiency.

Similarly, the study by Tucker-Schwartz and co-workers (2011b) involved the synthesis of fifteen trialkoxysilanes. These chemicals were produced by reacting either alkenes with mercaptoalkyltrialkoxysilanes or thiols with allyltrialkoxysilanes. The reaction was carried out in the presence of a photo-initiator in molecularly dissolved state. A key difference in our work was the heterogenous nature of the reactions in solid-liquid interface and the use of a surface-sensitive approach to quantify the reaction yield. Unlike conventional techniques that provide averaged bulk signals, PiFM spectra deliver quantitative surface chemical information with molecular resolution. This high spatial sensitivity likely enabled us to distinguish between reacted and unreacted molecules, subtleties that earlier methods may have overlooked.

Furthermore, the reaction yields are highly dependent on the availability of surface-exposed C=C bonds. In the case of VTCS, the formation of nanofilaments during self-assembly on the glass surface likely traps a fraction of C=C bonds within the internal network, rendering them unavailable for subsequent reactions. Similarly, ATCS coating form aggregates with disordered arrangements, which may sterically obstruct access to a fraction of C=C bonds, preventing their reaction with decanethiol. However, the conversions were incomplete, likely due to steric hindrance preventing some double bonds that are buried within the polymerized VTCS nanofilaments and ATCS aggregates from reacting.

Thus, a fraction of alkene molecules not positioned at the coating-solution interface remain inaccessible to react with thiols due to limited molecular penetration. The lower conversion observed for ATCS (33%) compared to VTCS (56%) suggests that ATCS aggregates adopt a more

compact morphology that buries allyl groups more effectively than the VTCS filament-network. Biggs and co-workers (2016) have quantified polymer grafting efficiency on acrylate silane functionalized glass substrates through quartz crystal microbalance with dissipation (QCM-D) using gold, plain, and coated silicon sensors. They reported that steric hindrance was the limiting factor for poly[oligo(ethylene glycol)methyl ether methacrylate] grafting on gold sensors, while that of poly(*N*-isopropylacrylamide) was dependent on chain length. Grafting on silicon-coated sensors exhibited lower efficiency than on gold, which was attributed to the acrylate group density and spacing. Thus, steric hindrance and molecules accessibility are decisive factors in thiol-ene reaction yields on functionalized glass surfaces.

3.5.7 Chemical Stability and Mechanical Durability of the Surfaces

VTCS-modified glass surfaces demonstrated superior properties to ATCS coatings, making them more promising candidates for practical applications. The VTCS coatings consist of a well-defined nanofilament network exhibiting desired transparency, superhydrophobicity, self-cleaning ability, and antireflective properties. In contrast, while ATCS coatings are transparent, they demonstrate hydrophobicity with lower contact angles. They are comprised of irregular structures, which may compromise their long-term performance. Consequently, we were interested in evaluating the chemical stability and mechanical durability of the prepared superhydrophobic VTCS-modified glass surfaces before and after functionalization with DSH through their static water contact angle.

The durability and stability testing comprised three protocols, each involving three freshly prepared samples tested over three successive cycles. Each cycle lasted 2 hours except for the thermal cycling test, where each cycle lasted for 6 h. Our protocols were guided by literature (Darband et al., 2020; Malavasi et al., 2015a; Motamedi et al., 2018b) and two testing standards for photovoltaic panels: ASTM B117-16 (*Standard Practice for Operating Salt Spray (Fog) Apparatus*, 2016) for immersion in an ionic solution and IEC 61215-2 (*Terrestrial Photovoltaic (PV) Modules – Design Qualification and Type Approval – Part 2: Test Procedures*, 2021) for thermal cycling. We believe these test conditions are relevant for evaluating the durability of superhydrophobic surfaces on a laboratory scale. However, further refinement of the proposed protocols is welcomed to effectively assess the aging characteristics of different types of superhydrophobic surfaces at an industrial scale. Other parameters may also need to be considered for various applications.

To evaluate the durability of superhydrophobic surfaces under simulated environmental conditions, we developed a custom-designed waterfall-impact setup similar to that used in our previous study (Khitas et al., 2025b) with a moderate flow (4.3 mm/h) (equivalent to 4.3 mm/h over 1 m^2). All experiments were conducted under laboratory conditions at room temperature. The coating's resistance in an ionic environment was also examined. Before and after functionalization with DSH, three samples of the modified glass were submerged in a 5 wt% sodium chloride solution, following ASTM B117 (*Standard Practice for Operating Salt Spray (Fog) Apparatus*, 2016) guidelines for the salt spray testing standard. This solution's pH was measured at 5.7, simulating the combined effects of salt exposure and slightly acidic rainwater (Xuan et al., 2021). The samples were soaked in the solution for multiple cycles, rinsed with deionized water, and finally air-dried.

The waterfall impact test (Figure 3.7a) shows a significant initial drop of contact angles from ~170° to ~140°, both before and after functionalization. Subsequently, this decrease reached and maintained a plateau at ~140° for the following three cycles. The initial contact angle of ~170° with the sliding angle of 2° confirms the Cassie-Baxter state, where air is trapped within the nanofilament network, enabling water repellency (Cassie, 1948a; Cassie & Baxter, 1944a). However, the significant decrease to ~140° and the observed droplet pinning during measurements suggest a transition toward the Wenzel state (Papadopoulos et al., 2013). This suggests a loss of superhydrophobicity due to surface degradation caused by water impact.

The salt solution immersion (Figure 3.7b) highlighted the superior stability of the DSH-functionalized surfaces. The functionalized samples demonstrate higher resistance to degradation, maintaining their superhydrophobicity throughout the experiments. In contrast, the unfunctionalized samples exhibit a notable decrease in WCAs when subjected to chemical degradation. The salt immersion test revealed a gradual decline in hydrophobicity, with functionalized surfaces maintaining superhydrophobic properties to a minimum extent of ~150°.

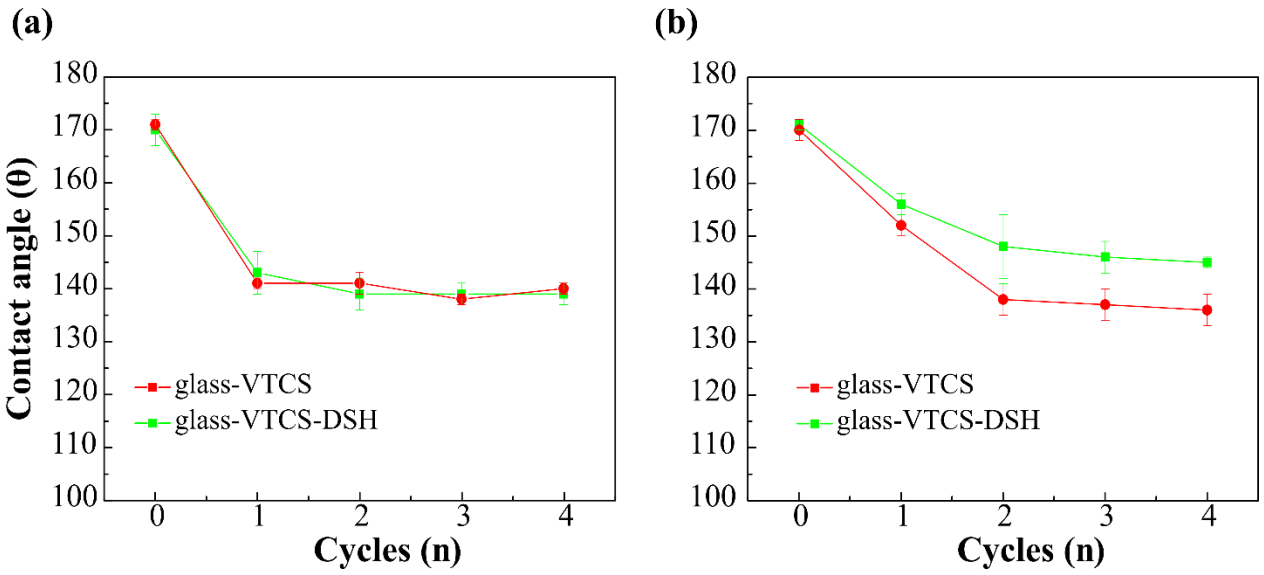

Figure 3.7 Evolution of the water contact angle of the VTCS-modified glass samples before and after functionalization with DSH over multiple cycles under (a) a custom-designed waterfall impact test, and (b) a salt solution immersion test following ASTM B117 (*Standard Practice for Operating Salt Spray (Fog) Apparatus*, 2016).

The protocol for the thermal cycling test was designed based on the MQT11 thermal cycling test specified in IEC 61215-2 (*Terrestrial Photovoltaic (PV) Modules – Design Qualification and Type Approval – Part 2: Test Procedures*, 2021). Each cycle of this test involved exposing the sample to temperature variations ranging from -20 °C to 100 °C, with transitions at room temperature. The lower temperature limit (-20 °C) was achieved using a laboratory freezer (General UF 17CW1, USA), while the upper-temperature limit (100 °C) was attained using a laboratory oven (Fisher Scientific Isotemp 200 Series, USA). During transitions between extreme temperatures, samples were allowed to equilibrate to room temperature through heat exchange with the ambient environment on a bench. The thermal cycling profile (Figure S6) followed these steps: cooling to -20°C and holding for 2.5 h, equilibration to room temperature for 1 h, heating to 100 °C and holding for 2.5 h, and finally equilibration to room temperature. It should be noted that this protocol derives from the standard IEC 61215-2:2021 (*Terrestrial Photovoltaic (PV) Modules – Design Qualification and Type Approval – Part 2: Test Procedures*, 2021) test conditions, which specify temperature extremes of -40 °C and 85 °C. Our modified approach accommodated our equipment limitations while subjecting the samples to significant thermal stress. While our thermal cycling protocol was conducted under ambient atmospheric condition, we acknowledge that performing such tests under inert and low-humidity environments may offer further insight into the

stability of reactive surface groups such as vinyl. This remains an important direction for future work.

The thermal cycling test (Figure 3.8) highlighted the superior stability of the functionalized surfaces. The functionalized samples demonstrate higher resistance to degradation, maintaining their superhydrophobicity throughout the experiments. In contrast, the unfunctionalized samples exhibit a notable decrease in WCAs when subjected to chemical and thermal degradation. The salt immersion test revealed a gradual decline in hydrophobicity, with functionalized surfaces maintaining superhydrophobic properties to a minimum extent ~150°. Similarly, the functionalized samples retained higher and more stable contact angles during thermal cycling, indicating enhanced thermal durability. These findings confirm the effectiveness of DSH functionalization in preserving the superhydrophobic properties under salt immersion and thermal cycling tests.

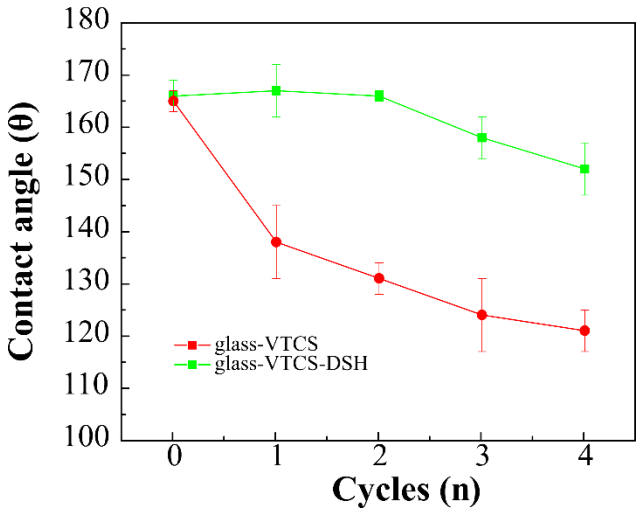

Figure 3.8 Evolution of the water contact angle of the samples before and after functionalization over multiple cycles for thermal cycling test.

3.6 Conclusions

This study demonstrates that the initial molecular arrangement of VTCS and ATCS, prepared under the same reaction conditions, forming the coating structure on the glass surface, mainly determines the properties of the resulting coatings. VTCS developed a porous nanofilament network with superhydrophobic properties and enhanced transparency. In contrast, ATCS produced irregular aggregates with hydrophobic properties and enhanced transparency. Upon functionalization with

DSH, the properties of the modified surfaces improved, preserving the initial coating structure with only slight modifications. For VTCS coating, functionalization increased superhydrophobicity from 168° ± 2 to 170° ± 4 and enhanced optical properties, increasing the transmittance by 4% compared to the bare glass. The ATCS contact angles increased from 109° ± 4 to 113° ± 4 after functionalization, with a 2% increase in transmittance. Indeed, functionalized VTCS-modified surfaces demonstrated superior thermal and chemical stability, remaining superhydrophobic during the experiments. However, superhydrophobicity was not preserved during the water impact testing, as evidenced by a drop in WCA after the first cycle. Compared with VTCS, ATCS has an additional methylene group that increases its steric hindrance and flexibility, resulting in a heterogeneous coating with lower hydrophobicity. This structural difference led ATCS to form irregular aggregates. PiFM provided valuable insights into the spatial distribution of functionalization and reaction yield. From ATR-FTIR analysis, the thiol-ene click reaction conversion was estimated to be approximately 63% for VTCS- and 40% for ATCS-functionalized glass surfaces. Slightly lower conversions (56% for VTCS- and 33% for ATCS-) obtained by PiFM were attributed to variations in spatial resolution and sampling depth differences between the techniques. The lower yield for ATCS may be attributed to the inaccessibility of double bonds caused by the aggregate morphology. These findings highlight the importance of molecular structure in determining the coating properties and functionalization efficiency.

Aknowledgements: This research was funded by MITACS, in collaboration with *Edgehog Advanced Technologies Inc*. We thank Prof. Luc Stafford from Université de Montréal and NanoQAM for providing the equipment for the characterization of the glass surface coatings.

CHAPTER 4

VERSATILE GLASS SURFACE ENGINEERING THROUGH ACTIVATED ALKYNE CHEMISTRY

4.1 Abstract

Glass surfaces are widely used in scientific and industrial applications due to their optical transparency and chemical stability. However, their utility in advanced applications remains limited by challenges in achieving stable, tunable, and efficient surface functionalization. Current methods predominantly rely on silanization or thiol-ene/-yne radical-mediated reactions, while the use of activated alkynes, particularly propiolic acid (PA) derivatives, remains unexplored. Herein, we propose a versatile functionalization strategy using PA, an activated alkyne suitable for subsequent metal-free click reactions under mild conditions. Two approaches were explored: direct acid-catalyzed esterification of surface silanols and an indirect grafting involving silanization followed by hydroboration-oxidation and subsequent esterification. While direct functionalization showed limited spectroscopic characterization, the indirect method demonstrated improved stability and efficiency. Surface functionalizations through the indirect approach were confirmed by infrared spectroscopy *via* characteristic C=C, O–H, C=O, and C≡C stretching vibrations. Contact angle measurements further confirmed the functionalization, revealing tuned wettability from hydrophilic (26°) to superhydrophobic (165°) and moderately hydrophobic (91°). Furthermore, preliminary Photo-induced Force Microscopy (PiFM) results revealed low but detectable molecular coverage. These findings present promising avenues for future investigations to expand the practical utility of glass surfaces in applications enabling sensitive and selective detection.

4.2 Introduction

Glass is among the most studied substrates due to its chemical stability, optical transparency, heat resistance, and widespread availability. Despite these advantages, the presence of surface silanol groups renders it hydrophilic, limiting its direct use in many advanced applications (Kruszelnicki et al., 2022). In the early history of glass technology, efforts to enhance its performance focused primarily on composition and bulk material processing (McCamy et al., 2018; Musgraves et al., 2019). However, since the mid-20th century, advancements in surface chemistry and engineering have enabled tailored interfacial properties through surface modification approaches (McCamy et al., 2018). This has significantly expanded the use of glass into high-performance fields such as biomedicine, optoelectronics, and biosensing (Hu et al., 2023; Neděla et al., 2017; Sandhyarani, 2019).

To meet the growing functional needs imposed by these high-end applications, various strategies have been developed, including plasma treatments (Gogolides et al., 2015), self-assembled monolayers (Mathew & Sandhyarani, 2014), silanization (Prakash et al., 2007), and polymer grafting (Zhang et al., 2020). Silanization using organosilanes has gained significant interest due to its ability to form stable and tunable self-assembled monolayers (SAMs) (Wang et al., 2021). These SAMs can be further modified *via* post-functionalization, imparting multifunctional properties to glass surfaces and enhancing their utility in applications such as self-cleaning and antireflective coatings for solar panels (Sakhuja et al., 2011; Wu et al., 2022).

Silanization and subsequent post-functionalization have enabled notable performance enhancements. Kaczmarek et al. (2023a) developed anti-fog glass surfaces using a poly(ethylene glycol)-functionalized silane (PEG-silane). Their modified surfaces ensured superhydrophilicity and excellent optical transparency, preventing light scattering by spreading condensed water into a uniform film. Gidi et al. (2018) demonstrated that grafting PEG-silane monolayers onto glass in a single step effectively reduced biofouling. Haritha et al. (2024) reported a sol-gel derived anti-reflective double layer coating on glass surfaces. They employed a silica-titania high refractive index bottom layer and an organosilane-modified silica lower refractive index top layer. The top layer was functionalized with octyl-silane, rendering the surface moderately hydrophobic compared to the bare glass. Additionally, Sypabekova et al. (2025) reported an optimal silanization approach using 3-aminopropyltriethoxysilane (APTES) to achieve more effective analyte binding and reduced background noise in biosensor applications.

Beyond silanization, recent advances have focused on click chemistry as a versatile platform for surface functionalization (Wang et al., 2021). Introduced by Sharpless and his co-workers (Kolb et al., 2001), click reactions have emerged as a modular synthetic approach with broad applications in organic synthesis, materials science, and polymer chemistry (Chen et al., 2024; Kluger, 2010; Moses & Moorhouse, 2007; Xi et al., 2014). These reactions are characterized by high efficiency, selectivity and yield, proceeding under mild conditions and producing minimal and easily removable byproducts (Kolb et al., 2001). Rather than representing a specific class of organic reactions, click chemistry encompasses broad reactions inspired by the simplicity, selectivity, and efficiency of biological processes. Thus, any reaction capable of efficiently assembling complex

molecules from smaller components under mild conditions can be defined as a click reaction (Ramapanicker & Chauhan, 2016).

Click chemistry is extensively employed in polymer synthesis (Lowe, 2010, 2014; Resetco et al., 2017) and surface modifications of metallic and inorganic nanoparticles for advanced materials applications (Geng et al., 2021; Ghosal et al., 2024; Xi et al., 2014). Among click reactions, thiol-ene and thiol-yne radical-mediated reactions (Hoyle & Bowman, 2010; Hoyle et al., 2004), have proven a powerful surface functionalization approach (Haensch et al., 2010). Studies by Li et al. (Li et al., 2015a), highlighted the effectiveness of employing thiol-ene and disulfide-ene photoinitiated reactions in functionalizing superhydrophobic vinyltrichlorosilane-modified glass. They demonstrated that vinyl-terminated glass surfaces allow precise photolithographic patterning, resulting in distinct superhydrophobic–hydrophilic structures. Additionally, they revealed that the developed transparent, photoactive, and superhydrophobic coating can serve as a versatile platform for biofunctionalization. Similarly, Kaczmarek et al. (2023a) developed anti-fog glass coatings by covalently attaching polyether-modified alkoxysilane onto surfaces *via* UV-induced thiol-ene chemistry. Thiol-yne click reactions on the other hand, expand click chemistry versatility by enabling dual functionalization. While thiol-ene couples one thiol to a single alkene (Tucker-Schwartz et al., 2011a), thiol-yne allows sequential addition of two thiols to an alkyne (Lowe et al., 2010). Veerbeek et al. (2018) demonstrated the material-selective functionalization of silicon nanowires over silicon oxide substrates using thiol-yne click chemistry. Their study achieved precise selectivity, critical for biosensing applications, while highlighting the versatility of thiol-yne reactions in surface modification for nanoscale surface modification.

Beyond traditional radical-mediated pathways, click reactions involving activated alkynes have recently gained attention for the development of functional materials (Hu et al., 2018). The enhanced electrophilicity of activated alkynes enables metal-free, efficient, regioselective nucleophilic additions with thiols, amines, hydroxyls, and azides under mild conditions (Worch et al., 2021). This approach offers a sustainable alternative to copper-catalyzed azide-alkyne cycloaddition (CuAAC), addressing limitations associated with cytotoxicity and the need for rigorous purification methods (Fantoni et al., 2021). Propiolic acid has been used to functionalize H-terminated Si(111) surface (Imanishi et al., 2008; Liu et al., 2005) and silicon nanowire (Henriksson et al., 2011). However, despite their versatility, activated alkynes remain

underexplored for glass surface modification. Current methods predominantly rely on silanization or thiol-ene/-yne radical-mediated reactions, while the use of activated alkynes, particularly PA, remains unexplored. Herein, we introduce a novel strategy for glass surface functionalization using PA. Two approaches are explored in a preliminary manner: the first method involves direct acid-catalyzed esterification between surface silanols groups (≡Si−OH) and propiolic acid. The second method employs indirect functionalization *via* vinylsilane-terminated glass, followed by hydroboration-oxidation to generate organic hydroxyl groups (−C−OH), and subsequent esterification with propiolic acid. The resulting alkyne-terminated surface offers a chemically versatile platform for subsequent click reactions with thiols, amines, azides, or alcohols under mild conditions. The proposed approach enables the fabrication of functional glass surfaces for diverse applications.

4.3 Materials and Methods

4.3.1 Materials

Soda-lime glass slides (27 mm × 46 mm × 1.2 mm thick) were supplied by Ward's Science (USA). Propiolic acid (HOOCC≡CH, 95%) (PA), trichlorovinylsilane ($Cl_3SiCH{=}CH_2$, 97%) (VTCS), borane-tetrahydrofuran complex (1.0 M in THF) ($BH_3{\cdot}THF$) (Borane-THF), concentrated sulfuric acid (H_2SO_4, 98%), and hydrogen peroxide (H_2O_2, 30%) were purchased from Sigma-Aldrich and used without further purification. Benzene, toluene, ethanol, and methanol were of reagent grade and used as received.

4.3.2 Activation of the Glass Substrates

The glass slides were first cleaned using piranha solution (H_2SO_4/H_2O_2) (7:3, v/v) following our previously reported glass activation protocol (Khitas et al., 2025a). After cleaning, the glass substrates were annealed at 200 °C for 1 h.

4.3.3 Direct Grafting of PA onto Glass *via* Acid-Catalyzed Esterification

The functionalization of the hydroxylated glass surfaces with PA was achieved through an acid-catalyzed esterification (Scheme 4.1). The reaction was performed in a (1:1 v/v) mixture of toluene and benzene, using 250 mM of PA and 50 µL drop of concentrated sulfuric acid (H_2SO_4) at 116 °C

for 16 h. A Dean-Stark apparatus was employed to remove the produced water byproduct and drive the reaction toward completion.

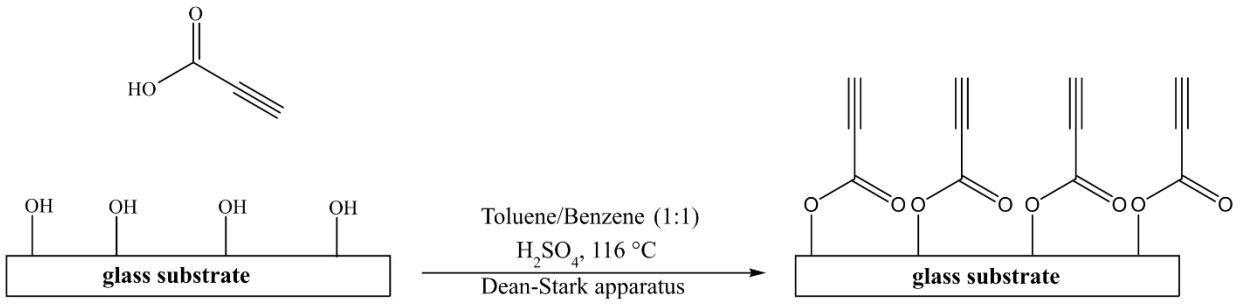

Scheme 4.1 Schematic representation of direct grafting of PA onto a hydroxylated glass surface *via* acid-catalyzed esterification.

4.3.4 Indirect Grafting of PA onto Glass *via* Sequential Surface Modifications

The hydroxylated glass surface was initially functionalized with VTCS. Hydroboration-oxidation with borane-THF (Soderquist & Brown, 1980) was then employed to convert the surface vinyl groups (–CH=CH_2) into hydroxyl groups (–CH_2–OH), as illustrated in Scheme 4.2. Subsequently, the surface was reacted with PA *via* acid-catalyzed esterification (Scheme 4.2b) following the same reaction conditions as those used for the direct grafting of PA onto glass.

In the silanization step, a glass sample was immersed in 8 mL of a freshly prepared 40 mM VTCS solution in benzene for 24 h. Under optimal humidity conditions (relative humidity, RH 40-60%), the reaction was conducted in a closed vial with brief air exposure only during the addition of the VTCS solution and glass substrate. When the ambient humidity was high (RH > 70%), the vial containing the activated glass was first purged with argon and allowed to cool to room temperature before adding the solvent. VTCS was then added with only brief air exposure. The vial was subsequently placed in a dessicator to maintain controlled humidity. After silanization, the functionalized glass sample was rinsed with toluene, ethanol, and methanol, gently air-dried, and finally annealed at 100 °C for 10 min.

In the hydroboration-oxidation step, the vinyl-functionalized glass was converted into a hydroxyl-terminated substrate *via* a two-step reaction (Wasserman et al., 1989). First, the sample was placed

in a Schlenk flask sealed with a rubber septum. The system was purged with argon for 20 min to ensure an inert atmosphere. A 1 M solution of borane-tetrahydrofuran complex (BH_3·THF) was introduced *via* a cannula until the substrate was fully covered (~4 mL). The hydroboration reaction was allowed to proceed under argon for approximately 16 h at room temperature. After removing the borane solution, the substrate was rinsed with THF. After removing THF, oxidation was then performed by introducing a mixture of (1:1 v/v, 3 mL) 30% H_2O_2 and 0.1 M NaOH. This reaction was allowed to proceed for 4 h at room temperature. The substrate was then rinsed multiple times with deionized (DI) water and ethanol to remove residual reagents and was subsequently air dried. Subsequently, the acid-catalyzed esterification with PA was carried out under the same reaction conditions as those used for the direct grafting of PA onto glass.

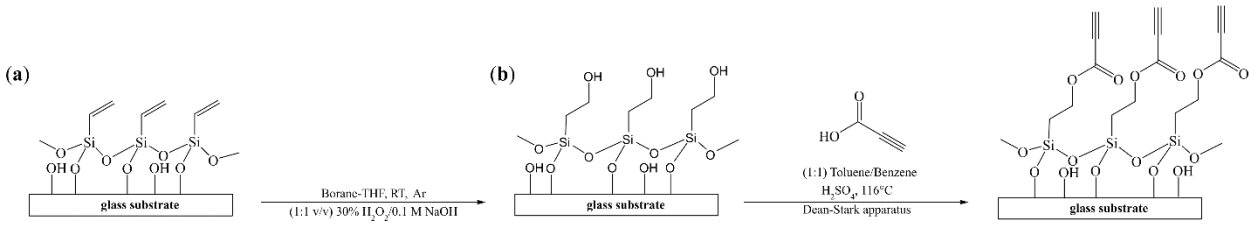

Scheme 4.2 Schematic representation of the grafting of PA onto glass *via* silanization, hydroboration-oxidation reaction, and acid-catalyzed esterification.

4.4 Characterization

Wettability measurements were conducted using an Attension Theta Optical Tensiometer (Biolin Scientific). Static water contact angles (θ) (WCAs) were measured at ambient temperature using 10 µL of DI water. The reported values represent the average of three measurements taken at random positions on each sample. Chemical analysis *via* Nicolet iS50 Fourier transformed infrared spectrometer (Thermo Scientific, USA) confirmed the sequential surface modifications, including VTC functionalization, vinyl to hydroxyl groups conversion through hydroboration-oxidation, and subsequent functionalization with PA. Nanoscale chemical mapping was performed using Photo-induced Force Microscop (PiFM), which provided ~10-20 nm surface sensitivity through the simultaneous detection of molecular induced-dipole interactions and photothermal expansion effects (Vista). This analysis verified the spatial distribution of PA groups grafted *via* direct grafting to the surface.

4.5 Results and Discussion

Initially, our primary approach involved direct grafting of PA onto glass *via* acid-catalyzed esterification, aiming to achieve covalent grafting through the –COOH group with the terminal alkyne oriented outward. However, characterization of the resulting sub-nanometer monolayer proved challenging due to limitations of conventional spectroscopic techniques. Our employed ATR-FTIR spectrometer, equipped with a diamond crystal, was unable to reliably detect signals resulting from functionalized glass surfaces. Due to the extremely low thickness of the resulting potential organic layer (~1 nm), the signal is either very weak or obscured by background noise. Based on this limitation, future studies should prioritize the use of a germanium ATR crystal, which offers enhanced signal-to-noise ratios for detecting organic monolayers on glass (Kim, 2010). Germanium with a higher refractive index (~4.0) compared to diamond (~2.4), provides better sensitivity, enhancing interfacial signal intensity while reducing the penetration depth from 1.66 to 0.65 µm (BRUKER, 2025). Similarly, Raman spectroscopy proved ineffective for detecting the monolayer. This limitation arises because the Raman signal intensity is directly proportional to the concentration of the analyzed materials. The strong background signal from the glass substrate interferes with the weak monolayer signals (Mikoliunaite et al., 2015). Polarization Modulation Infrared Reflection Absorption Spectroscopy (FTIR-PM-IRRAS) was also considered. However, this technique is applicable only to highly reflective metallic substrates. Consequently, it is unsuitable for glass, which reflects only ~4% of incident light at each surface.

The absence of detectable signals can be attributed to two possible explanations. First, surface functionalization may have occurred, but the employed spectroscopic techniques were unable to detect the grafted monolayer. Alternatively, the reaction may have failed to proceed or may have formed an ester bond that was too unstable, resulting in a hydrolytic degradation. The inherent instability of the ester bond formed between a caproic acid and silica surface has been reported by Azizova et al. (2015). Experimental studies revealed that nearly 46% of surface-grafted esters hydrolyze within 1 h under humid conditions at room temperature. Additionally, the resulting acids remained adsorbed on the surface despite vacuum treatment. As an alternative to conventional spectroscopic techniques, Photo-induced Force Microscopy (PiFM) was explored during the final phase of this PhD. However, due to time constraints, in-depth investigations could not be conducted. Figure 4.1 presents spatially localized PiFM spectra collected from a PA-functionalized glass

surface. The observed signal intensity is notably weak, suggesting a low molecular concentration on the surface. Further studies are required to confirm the covalent grafting and to optimize the reaction conditions to further enhance signal detection. Despite the encountered challenges, the preliminary results demonstrate the potential of PiFM for future investigations.

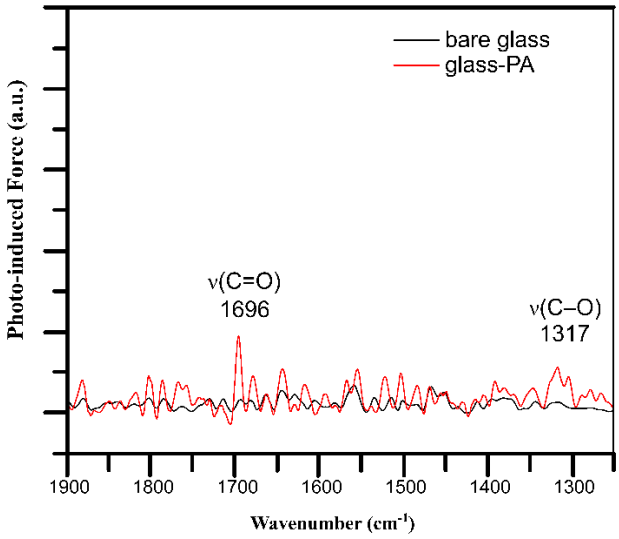

Figure 4.1 PiFM spectrum of the glass surface functionalized with PA *via* direct grafting. The PiFM reveals the chemical composition at the nanoscale, a low molecular concentration on the surface.

An alternative indirect approach was proposed to improve the stability and efficiency of surface functionalization. ATR-FTIR spectroscopy was employed to characterize the sequential surface modifications leading to the grafting of PA on glass (Figure 4.2). Spectral measurements were taken over the 4000-650 cm^{-1} range for all samples. However, due to the strong absorption of glass substrate below 1200 cm^{-1} (as shown in Figure S1, Appendix A), signals from functional groups such as Si–CH_2, Si–O–Si, or Si–C are difficult to observe, as substrate absorption overlaps with these peaks. After silanization (Figure 4.2a), the spectrum exhibits a C=C stretching vibration at 1602 cm^{-1}, along with C_{sp2}–H stretching vibrations in the 3060-2956 cm^{-1} range, and in-plane deformations and bending modes of =CH_2 and =CH bonds at 1409 cm^{-1} and 1276 cm^{-1}, respectively. Following the hydroboration-oxidation reaction step, the disappearance of the C=C stretching peak and the emergence of a broad O–H stretching band at 3384 cm^{-1} confirms the conversion of alkene groups (C=C) into hydroxyl groups (O–H). Subsequent esterification with propiolic acid results in the appearance of a carbonyl (C=O) stretching vibration at 1718 cm^{-1} and a weak alkyne (C≡C) stretching vibration at 2117 cm^{-1}, along with C_{sp}–H stretching vibrations at 3282 cm^{-1}, confirming

covalent grafting *via* ester bond formation. Notably, the intensity of the O–H stretching band decreased significantly after esterification, supporting the consumption of surface hydroxyl groups during the reaction. The persistence of the alkyl stretching and bending vibrations supports the stability of the initial silane-derived coating throughout the modification steps. Additionally, changes observed in the 1320-1220 cm^{-1} region further support the loss of vinyl moieties and the formation of ester groups, highlighting the effectiveness of each functionalization step.

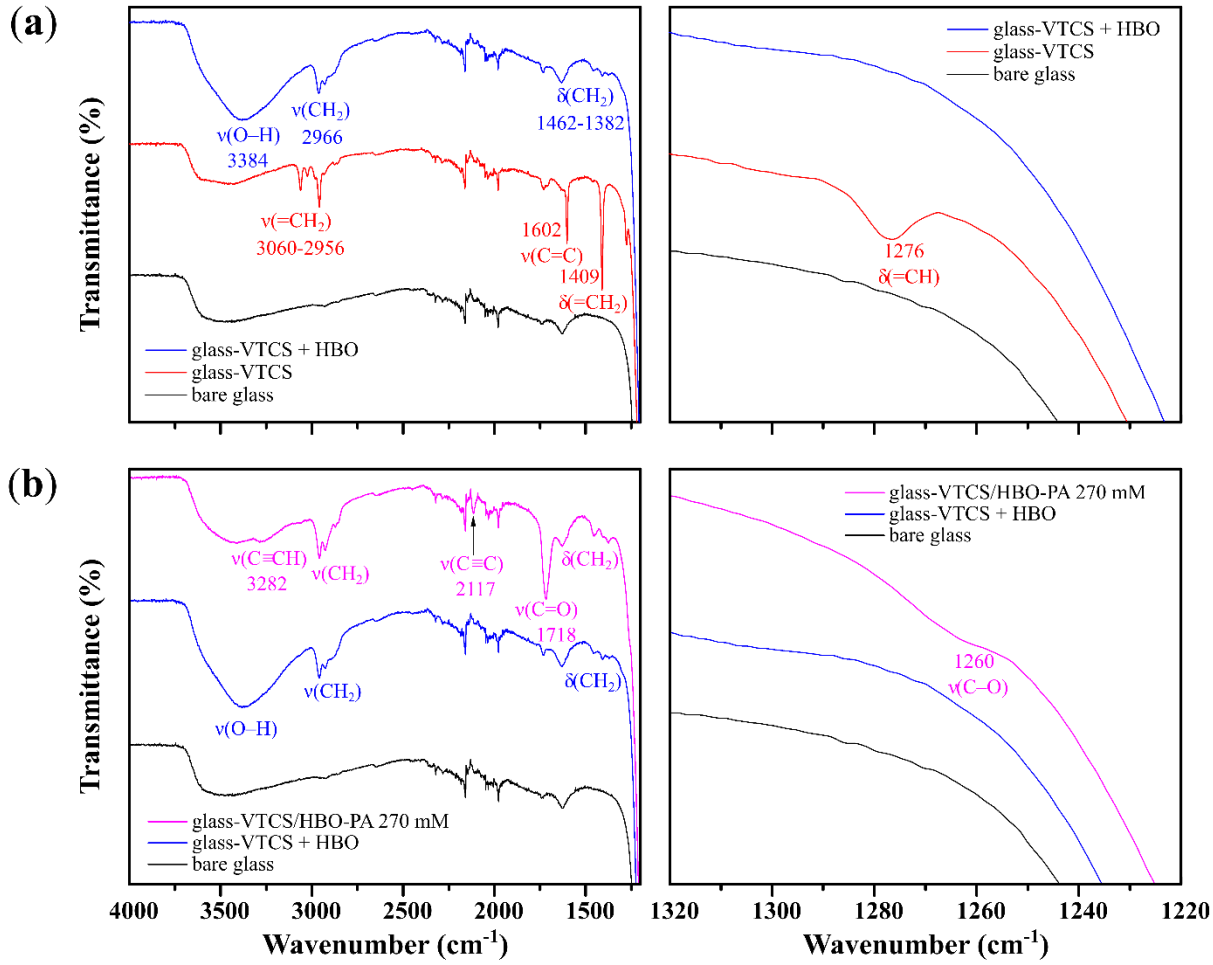

Figure 4.2 ATR-FTIR spectra illustrating the sequential functionalization of glass surfaces. (**a**) comparison of bare, silanized, and hydroboration-oxidized glass surfaces, showing the disappearance of the vinyl C=C stretching band at 1602 cm^{-1} and the emergence of hydroxyl O–H stretching band at 3384 cm^{-1}, indicating oxidation of surface vinyl groups. (**b**) spectra after functionalization with PA *via* acid-catalyzed esterification of the surface hydroxyl groups, revealing the emergence of characteristic C=O (1718 cm^{-1}), terminal alkyne C≡CH (3282 cm^{-1}), and C≡C (2117 cm^{-1}), confirming ester formation.

Surface wettability of bare and functionalized glass surfaces was assessed after each functionalization step by measuring the water contact angle, as summarized in Table 4.1. Bare glass exhibited a low WCA of 26 ± 6°, indicating high hydrophilicity due to surface silanol groups. Upon direct functionalization with propiolic acid (glass-PA), the surface became moderately hydrophobic with a WCA of 84 ± 2°. In the indirect modification route, silanization with VTCS (glass-VTCS) rendered the surface superhydrophobic, as evidenced by a WCA of 165 ± 2°. This increase in WCA is attributed to the presence of nonpolar vinyl groups, which is also supported by the appearance of C=C and C–H stretching bands in the ATR-FTIR spectra (Figure 4.2a). Subsequent hydroboration-oxidation (glass-VTCS-HBO) converted these vinyl groups to hydrophilic hydroxyl groups, resulting in a decrease in WCA to 41 ± 5°. This is supported by the emergence of the O–H stretching band at 3384 cm^{-1}. Finally, esterification with propiolic acid (glass-VTCS-HBO-PA) increased the WCA to 91 ± 3°, reflecting the incorporation of hydrophobic ester functionalities, as indicated by the C=O and C≡C stretching bands observed in the ATR-FTIR spectra (Figure 4.2b).

Table 4.1 Summary of water contact angles of bare glass and PA functionalized glass surfaces *via* direct and indirect grafting approaches, including direct esterification, silanization with VTCS followed by hydroboration/oxidation, and amide coupling, respectively.

Sample type	bare glass	glass-PA	glass-VTCS	glass-VTCS-HBO	glass-VTCS-HBO-PA
WCA (°)	26 ± 6	84 ± 2	165 ± 2	41 ± 5	91 ± 3

The promising preliminary results in functionalizing glass surfaces with PA have demonstrated the feasibility of introducing terminal alkyne groups under mild conditions. The stability of the silane-derived coating ensures its reliability for subsequent modifications. This strategy holds significant promise due to the broad compatibility of terminal alkynes with diverse functionalities, including thiols, hydroxyls, amines, and azides.

4.6 Conclusion

This study investigated two strategies for covalently functionalizing glass surfaces with propiolic acid: direct esterification and an indirect route involving silanisation, followed by hydroboration-oxidation, and subsequent esterification. The direct grafting approach yielded inconclusive

spectroscopic results due to the limitations of the ATR-FTIR equipped with a diamond crystal and the Raman spectroscopy in detecting sub-nanometer monolayers. In contrast, the indirect approach provided clear evidence of surface functionalization through infrared spectroscopy and wettability analyses. We were able to confirm the disappearance of vinyl groups (ν(C=C) at 1602 cm^{-1}) after hydroboration-oxidation. We also confirmed the emergence of hydroxyl groups (ν(O–H) at 3384 cm^{-1}), and subsequent esterification (ν(C=O) at 1718 cm^{-1}, ν(C≡C) at 2117 cm^{-1}). Water contact angle measurements supported these findings, with VTCS rendering the surface superhydrophobic (165° ± 2), hydroboration-oxidation increasing hydrophilicity (41° ± 5), and final PA esterification restoring moderate hydrophobicity (91° ± 3). Preliminary PiFM results supported the presence of molecular features, suggesting promise for future investigations.

GENERAL CONCLUSIONS

Through this project, we demonstrated how organosilane-based surface modification can tailor glass surface properties and enhance its performance for practical applications such as self-cleaning and anti-reflection coatings. The main objective was to develop coatings that preserve the nano-geometry and optical properties of glass while providing long-term hydrophobic stability under environmental stress. The research was structured into complementary studies exploring silanization chemistry, surface functionality, and coating performance, collectively addressing the central research question. We also introduced a novel method for glass functionalization using activated alkynes under mild conditions to expand the practical utility of glass surfaces in applications enabling sensitive and selective detection.

Our investigations demonstrated that the chemical nature of silanes and their molecular architecture critically determine coating properties. Through comparative studies of OTS and PFOTS coatings on regular and nanotexture glass, we demonstrated that perfluorinated chains govern hydrophobicity more effectively than long alkyl chains. This is due to the stronger electron-withdrawing nature of fluorine atoms, which lowers the surface energy more effectively than alkyl groups. Furthermore, PFOTS coatings not only enhanced water repellency of the modified regular glass surface but also contributed to decreased reflectance, while nanotexturing further amplified these effects. Notably, despite differences in initial hydrophobicity and stability, the long-term performance of both coatings converged under outdoor conditions.

Given the environmental concerns associated with fluorinated compounds, we further explored fluorine-free strategies using VTCS and ATCS. Subtle variations in molecular structure led to distinct nanoscale morphologies and functionality. Under similar deposition conditions, VTCS self-assembled into a porous 3D nanofilament network, achieving superhydrophobicity and reduced reflectance through a refractive index gradient, without requiring perfluorinated compounds. ATCS, in contrast, formed disordered aggregates with a relatively uniform underlying thin film. The introduction of post-functionalization via thiol-ene click chemistry, validated by ATR-FTIR and PiFM, not only confirmed uniform functionalization throughout the film but also enhanced chemical and thermal stability.

Building on these findings, we explored activated alkyne chemistry as a mild, versatile and effective strategy for covalent glass surface functionalization. While direct PA grafting proved inconclusive, the indirect sequential approach provided clear evidence of surface functionalization. Sequential surface modifications were confirmed by infrared spectroscopy and supported by wettability analyses. Preliminary PiFM further suggested molecular-level features. Compared to conventional methods (silane-based self-assembly), our proposed approach offers superior efficiency and versatility for applications enabling sensitive and selective detection.

Despite the investment of considerable experimental effort, some aspects remained unexplored due to time constraints, while some approaches proved to be unrewarding, leaving certain questions partially addressed. The long-term environmental durability of non-fluorinated coatings and optimization of alkyne-based functionalization under varied conditions require further investigation. The coatings developed through this thesis show potential to enhance photovoltaic performance through self-cleaning and anti-soiling effects. However, further studies are required to evaluate their scalability, long-term durability, and compatibility with anti-reflection layers to ensure integration with real-world solar panels.

In summary, this thesis demonstrates: (i) the critical role of silane chemistry and molecular structure in designing durable, transparent superhydrophobic coatings, (ii) the potential of fluorine-free approaches with tunable post-functionalization, and (iii) the development of an activated alkyne-based platform enabling versatile chemical modification under mild conditions. Collectively, these contributions offer a foundation for future innovation in designing high-performance, durable, and multifunctional glass surfaces for optical, self-cleaning, and sensing applications.

PERSPECTIVES

The results of this project suggest several promising avenues for future investigations to expand the practical applications of glass surfaces:

Among the major challenges encountered during the realization of this project was the reproducibility of transparent and superhydrophobic coatings, particularly under high ambient humidity. To address this, future studies should prioritize strict humidity control. As an example, incorporate a humidity-controlled chamber, equipped with an inert gas system and Teflon beakers. to prevent side interactions during coatings.

Since organosilanes, especially trichlorosilanes are highly reactive, residual unreacted chains can accelerate degradation kinetics. Annealing the coated sample post coating is recommended to improve coating adhesion and stability. Employing X-ray photoelectron spectroscopy (XPS) is crucial for confirming the absence of residual chlorine atoms from unreacted trichlorosilanes. Hence, preventing undesired hydrolysis and ensuring the long-term durability of the functionalized surface.

Ellipsometric analysis is also recommended for evaluating and optimizing optical properties, porosity, and thickness, particularly for the VTCS-derived porous nanofilament coating. This would enable better control over its performance in optoelectronic and anti-reflective applications. Subsequent post functionalizations are preferred over leaving the vinyl groups exposed.

To further enhance the optical properties of glass-coatings, especially for applications requiring high transparency and minimal reflectance, replacing conventional soda-lime glass with low-iron glass is recommended. Although moderately more expensive, its use can significantly enhance the energy performance and sensitivity of optoelectronic and biosensing devices.

Propiolic acid was explored as versatile alternative for imparting multifunctionality to glass surfaces. Preliminary results are promising and further optimizations and analyses using XPS or Photo-induced Force Microscopy (PiFM) to confirm covalent grafting are recommended.

Analyzing glass surfaces directly coated with PA *via* XPS or PiFM to confirm the covalent grafting of PA. Wether the monolayer of propylic acid on the surface or the silane precoatings, both are interesting to explore for further analyses and characterizations.

An alternative to VTCS, (e.g., (3-aminopropyl)triethoxysilane)) (APTES), is less humidity sensitive. The proposed surface functionalization can be simplified by employing amine-terminated organosilanes, followed by amide coupling with PA. This approach simplifies our initial four-step protocol (silanisation, hydroboration, oxidation, and esterification with PA) to a more efficient two-step process (silanisation with amine-terminated organosilanes and amide coupling with PA).

Future works may involve subsequent post-functionalizing the alkyne-terminated glass surfaces with thiol, hydroxyl, azide, and amine molecules under mild conditions. These modifications could be thoroughly characterized using complementary spectroscopic and surface analysis techniques. One molecule of particular interest is tetraphenylethylene (TPE), which exhibits aggregation-induced emission (AIE). TPE becomes highly fluorescent when aggregated or immobilized on a surface (as in the case of glass functionalization). This property makes it interesting for developing fluorescent surfaces for sensing applications.

Finally, integrating micro/nanopatterning techniques such as microcontact printing can be explored to create a multifunctional array on the same glass surface for applications enabling sensitive and selective detection.

APPENDIX A
SUPPORTING INFORMATION - PAPER 2

FROM VINYL TO ALLYL: HOW A SINGLE-CARBON DIFFERENCE ALTERS GLASS SURFACE ARCHITECTURE, REACTIVITY AND FUNCTION

Nesrine Khitas[1], Maziar Jafari[1], Calvin C.H. Cheng [2], Mohamed Siaj[1], Ali Nazemi[1,*]

[1] Department of Chemistry, Université du Québec À Montréal, Montréal, H3C 3P8, QC, Canada

[2] Edgehog Advanced Technologies Inc., Montréal, H3C 2G9, QC, Canada

[*] Correspondence : siaj.mohamed@uqam.ca and nazemi.ali@uqam.ca

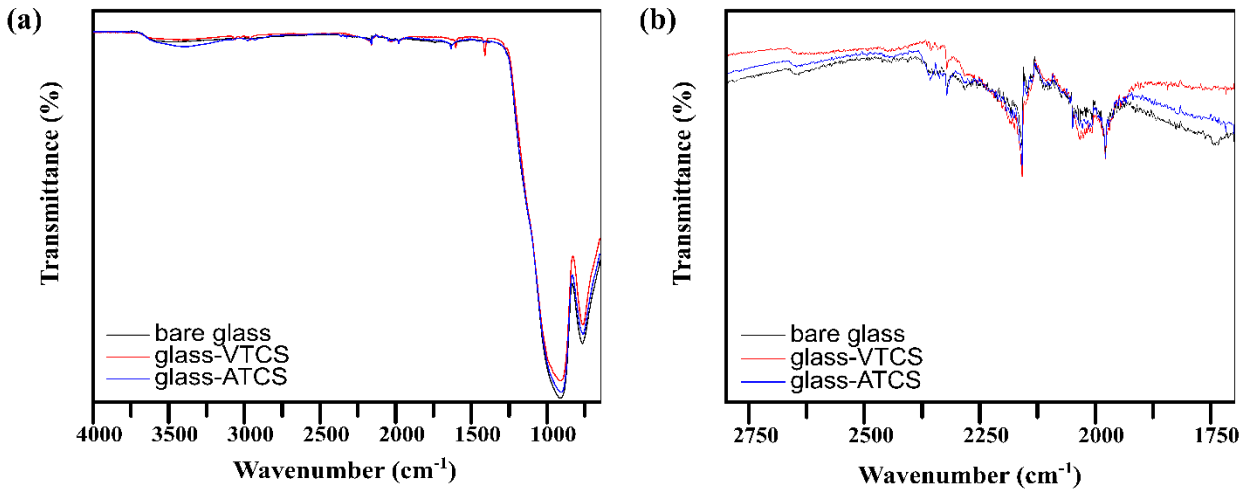

Figure S 1 ATR-FTIR of bare glass, VTCS-, and ATCS-modified glass: (a) full spectral range (4000-650 cm^{-1}) highlighting the absorption of the glass substrate and (b) focus on 2800-1730 cm^{-1} highlighting the absence of any characteristic vibrational peak

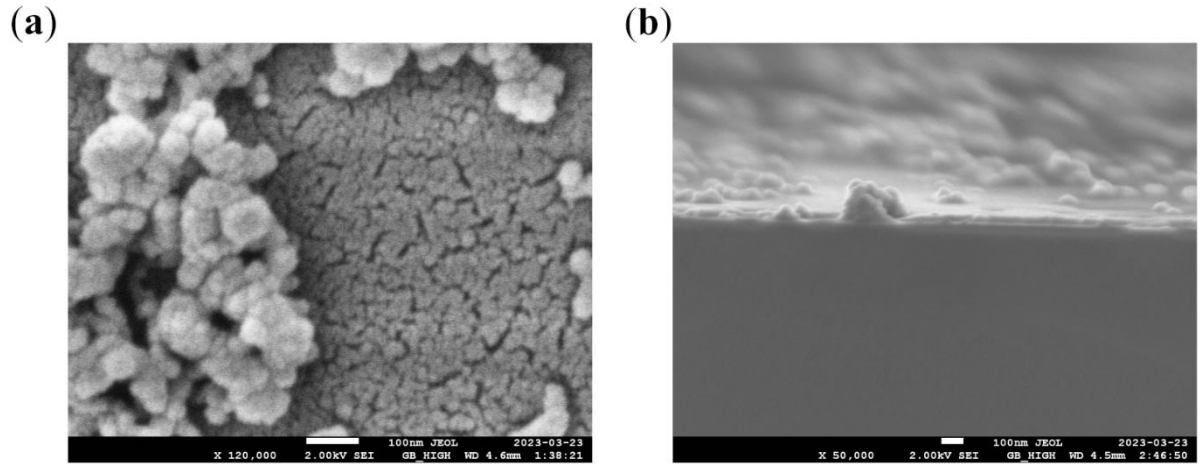

Figure S 2 SEM images of the ATCS -modified glass surface showing (a) a magnified top-view and (b) a cross-sectional view.

Photo-induced Force Microscopy

The modified glass samples were attached to 12 mm *d* magnetic sample holding discs with double sided adhesive tape. The sample surface nanometer resolved simultaneous topography and infrared spectroscopy were examined with the VistaScope (MolecularVista.Inc, CA, USA) scanning probe microscope. The plasmonic probe was a coated PtIr atomic force microscope Si3N4 cantilevered tip. The infrared spectra wave-range was from 1250 to 1910 cm^{-1} and signals corresponding to the uppermost molecules were mapped to correspond the localization of the molecules within the topographical feature at a laser intensity of 5% the total laser power, ≤ 1 mW. The samples were scanned a total of 256 lines at 1 Hz in non-contact mode.

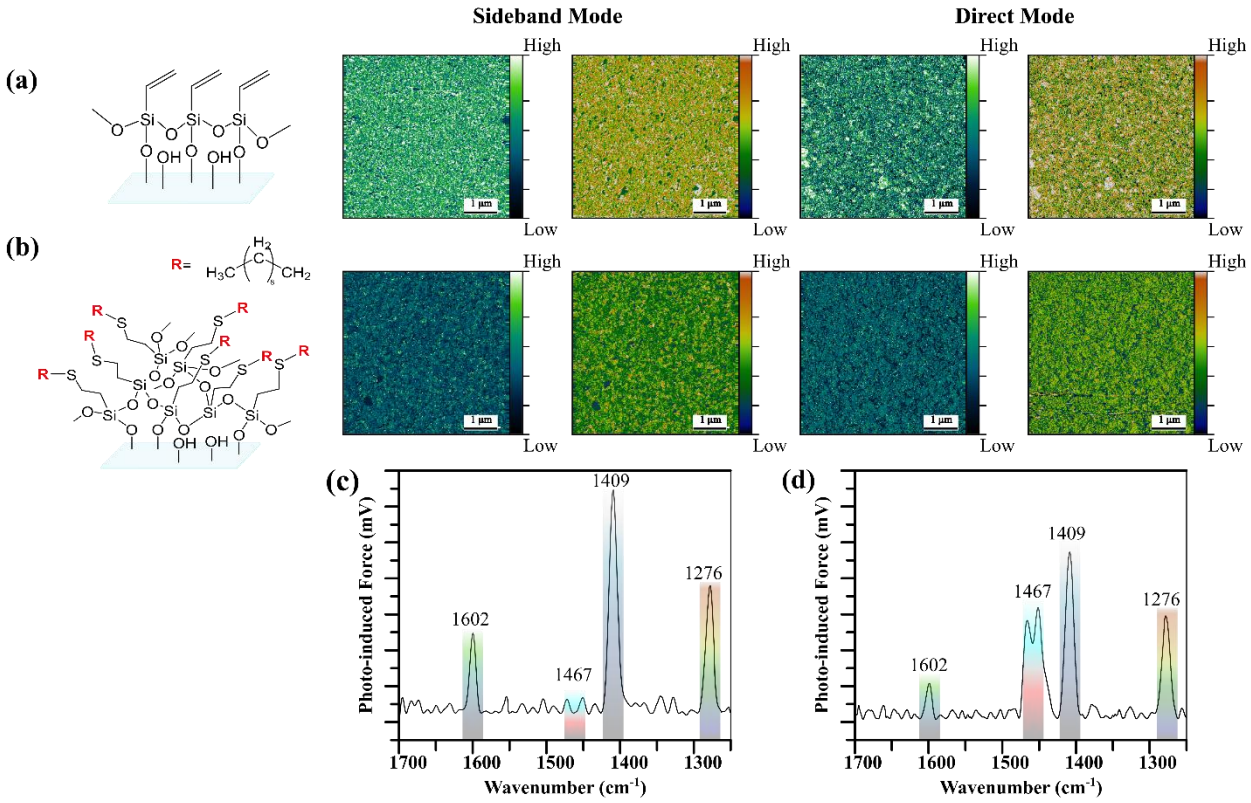

Figure S 3 PiFM chemical mapping and spectra images of glass surfaces modified with VTCS. (a) PiFM chemical mapping images before and (b) after functionalization, collected at 1602 cm^{-1} and 1276 cm^{-1} in sideband and direct modes. (c) PiFM spectra of VTCS-modified glass before and (d) after thiol-ene click reaction.

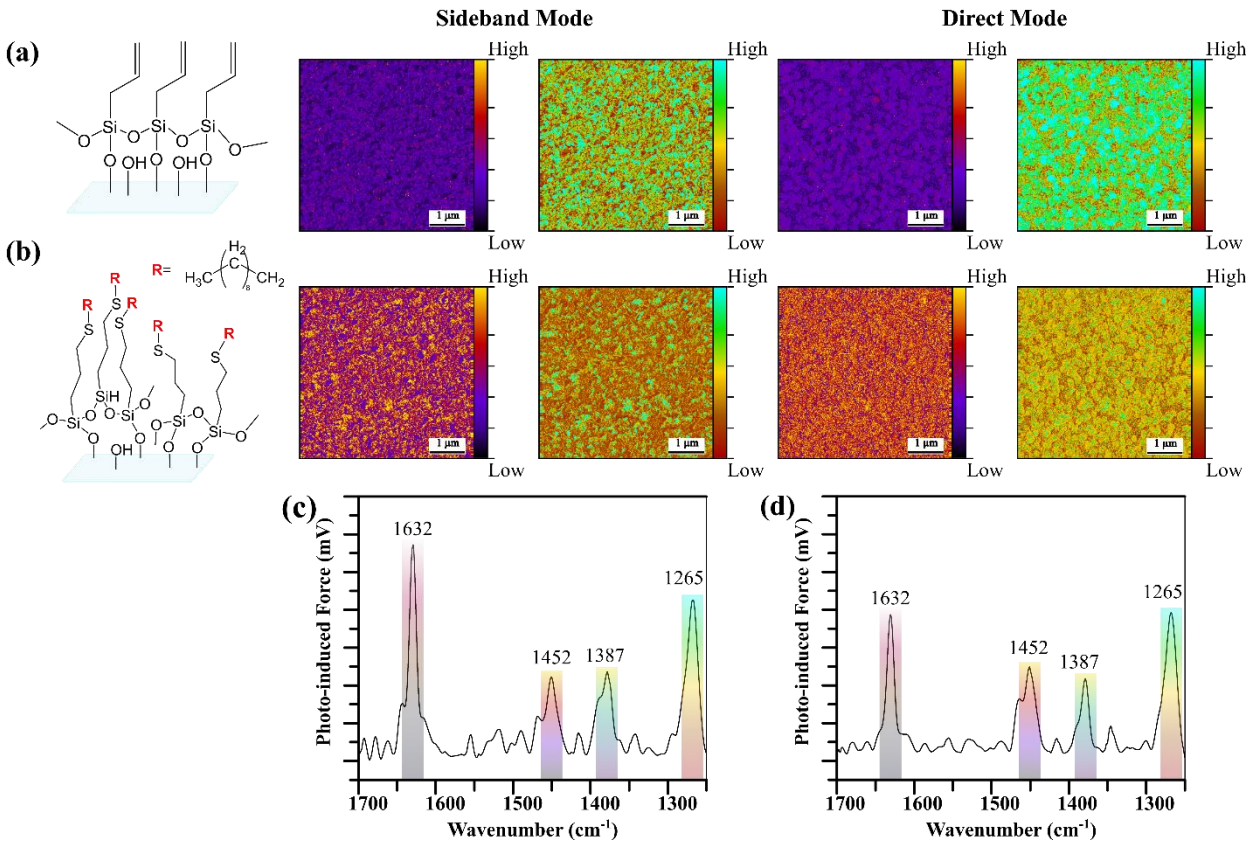

Figure S 4 PiFM chemical mapping and spectra images of glass surfaces modified with ATCS. (a) PiFM chemical mapping images before and (b) after functionalization, collected at 1452 cm^{-1} and 1265 cm^{-1} in sideband and direct modes. (c) PiFM spectra of VTCS-modified glass before and (d) after thiol-ene click reaction.

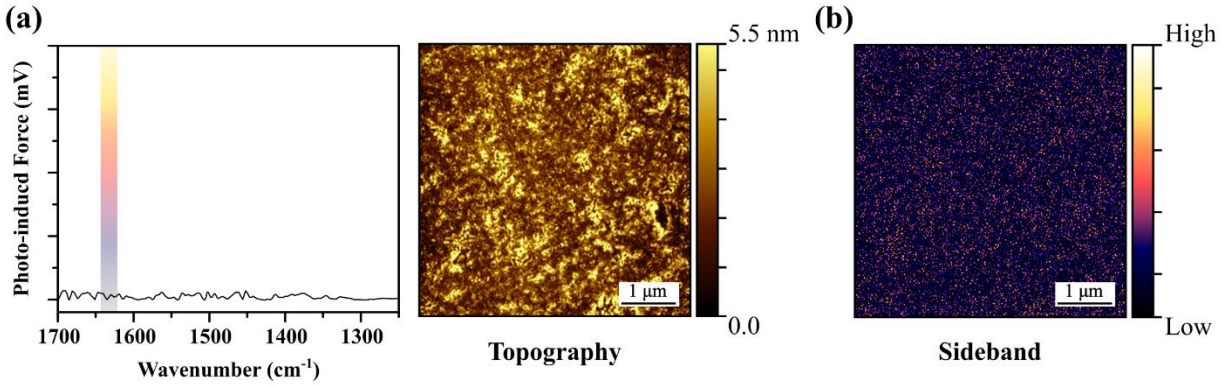

Figure S 5 PiFM negative control measurements of the bare soda-lime glass substrate. (a) The averaged PiFM mid-infrared spectrum of the unmodified substrate shows no detectable signal in the 1700-1250 cm^{-1} range. (b) The corresponding PiFM map at the C=C stretching band of VTCS displays a uniformly low-intensity distribution across the surface, consistent with the absence of signal on the bare substrate.

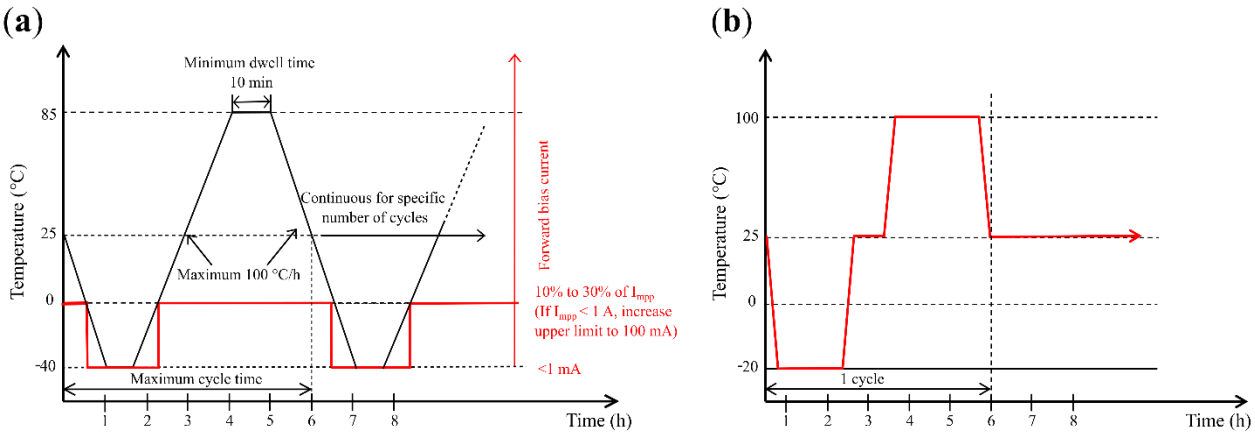

Figure S 6 Thermal cycling test from IEC-61215-1-4-2021, and (b) our customized thermal cycling test.

APPENDIX B
SCIENTIFIC CONTRIBUTIONS

Journal Articles:

1. Khitas, N., Cheng, C. C. H., & Nazemi, A. (2025). A comparative study between alkyl- and perfluoroalkyl silane coatings for glass. *Canadian Journal of Chemistry*, *103*(5), 174-183. https://doi.org/10.1139/cjc-2024-0173
2. Khitas, N., Jafari, M., Cheng, C. C. H., Siaj, M. & Nazemi, A. (2025). From vinyl to allyl: how a single-carbon difference alters glass surface architecture, reactivity and function. *RSC Applied Interfaces*, Advance Article. https://doi.org/10.1039/D5LF00162E

Conferences:

Khitas, N., Cheng, C. C. H., & Nazemi, A. "A Study on Glass Surface Modification Using Organosilanes for Enhanced Material Performance", Poster presented at the Canadian Chemistry Conference and Exhibition (CSC 2024), June 2024, Winnipeg, Canada. (Winner of the Surface Science Poster Award)

REFERENCES

Ahmad, D., Van Ven Boogaert, I., Miller, J., Presswell, R., & Jouhara, H. (2018). Hydrophilic and Hydrophobic Materials and Their Applications. *Energy Sources, Part A: Recovery, Utilization, and Environmental Effects*, *40*, 2686-2725. https://doi.org/10.1080/15567036.2018.1511642

Allsopp, B. L., Orman, R., Johnson, S. R., Baistow, I., Sanderson, G., Sundberg, P., Stålhandske, C., Grund, L., Andersson, A., Booth, J., Bingham, P. A., & Karlsson, S. (2020). Towards Improved Cover Glasses for Photovoltaic Devices. *Progress in Photovoltaics: Research and Applications*, *28*, 1187-1206. https://doi.org/10.1002/pip.3334

Amini, A., Tirgar, P., Bahmani, A., Jafari, M., Siaj, M., Barthelat, F., & Ehrlicher, A. (2024). Nacreous Glass Composites with Superior Performance Engineered Through Mechanical Vibration and Silanization. *Adv. Funct. Mater.*, *34*, 2405008. https://doi.org/10.1002/adfm.202405008

Amma, S.-i., Kim, S. H., & Pantano, C. G. (2016). Analysis of Water and Hydroxyl Species in Soda Lime Glass Surfaces Using Attenuated Total Reflection (ATR)-IR Spectroscopy. *J. Am. Ceram. Soc.*, *99*(1), 128-134. https://doi.org/https://doi.org/10.1111/jace.13856

Angst, D. L., & Simmons, G. W. (1991). Moisture Absorption Characteristics of Organosiloxane Self-Assembled Monolayers. *Langmuir*, *7*, 2236-2242. https://doi.org/10.1021/la00058a043

Arianpour, F., Farhadi, S., & Farzaneh, M. (2017). Effect of Heterogeneity on Hydro/Ice-phobic Properties of Alkylsilane/Fluoro-Alkylsilane-Based Coatings on Al Substrates. *Journal of Coatings Technology and Research*, *14*, 267-275. https://doi.org/10.1007/s11998-016-9901-6

Arianpour, F., Farzaneh, M., & Jafari, R. (2016). Hydrophobic and Ice-Phobic Properties of Self-Assembled Monolayers (SAMs) Coatings on AA6061. *Prog. Org. Coat.*, *93*, 41-45. https://doi.org/10.1016/j.porgcoat.2015.12.008

Ariga, K. (2012). *Organized Organic Ultrathin Films: Fundamentals and Applications*. John Wiley & Sons.

Artus, G. R. J., Jung, S., Zimmermann, J., Gautschi, H.-P., Marquardt, K., & Seeger, S. (2006a). Silicone Nanofilaments and Their Application as Superhydrophobic Coatings. *Advanced Materials*, *18*, 2758-2762. https://doi.org/10.1002/adma.200502030

Artus, G. R. J., Jung, S., Zimmermann, J., Gautschi, H.-P., Marquardt, K., & Seeger, S. (2006b). Silicone Nanofilaments and Their Application as Superhydrophobic Coatings. *Adv. Mater.*, *18*, 2758-2762. https://doi.org/10.1002/adma.200502030

Arzt, E., Quan, H., McMeeking, R. M., & Hensel, R. (2021). Functional Surface Microstructures Inspired by Nature–from Adhesion and Wetting Principles to Sustainable New Devices. *Progress in Materials Science*, *120*, 100823. https://doi.org/10.1016/j.pmatsci.2021.100823

Atthi, N., Dielen, M., Sripumkhai, W., Pattamang, P., Meananeatra, R., Saengdee, P., Thongsook, O., Ranron, N., Pankong, K., Uahchinkul, W., Supadech, J., Klunngien, N., Jeamsaksiri, W., Veldhuizen, P., & ter Meulen, J. M. (2021). Fabrication of High Aspect Ratio Micro-Structures with Superhydrophobic and Oleophobic Properties by Using Large-Area Roll-to-Plate Nanoimprint Lithography. *Nanomaterials*, *11*, 339. https://doi.org/10.3390/nano11020339

Azizova, L. R., Kulik, T. V., Palianytsia, B. B., & Lipkovska, N. A. (2015). Thermal and Hydrolytic Stability of Grafted Ester Groups of Carboxylic Acids on The Silica Surface. *Journal of Thermal Analysis and Calorimetry*, *122*, 517-523. https://doi.org/10.1007/s10973-015-4828-1

Babik, A., Mistrik, J., Zemek, J., & Cech, V. (2012). Self-Assembled Monolayers of Vinyltriethoxysilane and Vinyltrichlorosilane Deposited on Silicon Dioxide Surfaces. *J. Adhes. Sci. Technol.*, *26*, 2543-2554. https://doi.org/10.1163/156856111X623122

Bailey, D. L., & Pines, A. N. (1954). Reactions of Allylic Silicon Compounds. *Ind. Eng. Chem.*, *46*, 2363-2367. https://doi.org/10.1021/ie50539a042

Balordi, M., Cammi, A., Santucci de Magistris, G., & Chemelli, C. (2019). Role of Micrometric Roughness on Anti-Ice Properties and Durability of Hierarchical Super-Hydrophobic Aluminum Surfaces. *Surface and Coatings Technology*, *374*, 549-556. https://doi.org/10.1016/j.surfcoat.2019.06.001

Banerjee, S. (2008). Simple Derivation of Young, Wenzel and Cassie-Baxter Equations and its Interpretations. *[Preprint]. arXiv.* https://doi.org/10.48550/arXiv.0808.1460

Banga, R., Yarwood, J., Morgan, A. M., Evans, B., & Kells, J. (1995). FTIR and AFM Studies of The Kinetics and Self-Assembly of Alkyltrichlorosilanes and (Perfluoroalkyl) Trichlorosilanes Onto Glass and Silicon. *Langmuir*, *11*, 4393-4399. https://doi.org/10.1021/la00011a036

Barry, A. (2011). *Hydrophobicity, Hydrophilicity and Silane Surface Modification*.

Barthlott, W., & Ehler, N. (1977). *Raster-elektronenmikroskopie der Epidermis-oberflächen von Spermatophyten*. Akad. d. Wiss. ud Literatur.

Barthlott, W., & Neinhuis, C. (1997). Purity of the Sacred Lotus, or Escape From Contamination in Biological Surfaces. *Planta*, *202*, 1-8. https://doi.org/10.1007/s004250050096

Barthwal, S., Kim, Y. S., & Lim, S. H. (2013). Mechanically Robust Superamphiphobic Aluminum Surface with Nanopore-Embedded Microtexture. *Langmuir*, *29*, 11966-11974. https://doi.org/10.1021/la402600h

Barthwal, S., Uniyal, S., & Barthwal, S. (2024). Nature-Inspired Superhydrophobic Coating Materials: Drawing Inspiration from Nature for Enhanced Functionality. *Micromachines*, *15*, 391. https://doi.org/10.3390/mi15030391

Belhadjamor, M., El Mansori, M., Belghith, S., & Mezlini, S. (2018). Anti-fingerprint Properties of Engineering Surfaces: A Review. *Surface Engineering*, *34*, 85-120. https://doi.org/10.1080/02670844.2016.1258449

Ben-Naim, A. Y. (2012). *Hydrophobic Interactions*. Springer Science & Business Media.

Berendjchi, A., Khajavi, R., & Yazdanshenas, M. E. (2011). Fabrication of Superhydrophobic and Antibacterial Surface on Cotton Fabric by Doped Silica-Based Sols With Nanoparticles of Copper. *Nanoscale research letters*, *6*, 1-8.

Bernsmeier, D., Polte, J., Ortel, E., Krahl, T., Kemnitz, E., & Kraehnert, R. (2014). Antireflective Coatings with Adjustable Refractive Index and Porosity Synthesized by Micelle-Templated Deposition of MgF2 Sol Particles. *ACS applied materials & interfaces*, *6*, 19559-19565. https://doi.org/10.1021/am5052685

Bhushan, B. (2009). Biomimetics: Lessons from Nature–An Overview. *Philosophical Transactions of the Royal Society A: Mathematical, Physical and Engineering Sciences*, *367*, 1445-1486. https://doi.org/10.1098/rsta.2009.0011

Bhushan, B., & Chae Jung, Y. (2007). Wetting Study of Patterned Surfaces for Superhydrophobicity. *Ultramicroscopy*, *107*, 1033-1041. https://doi.org/10.1016/j.ultramic.2007.05.002

Bhushan, B., & Jung, Y. C. (2011). Natural and Biomimetic Artificial Surfaces for Superhydrophobicity, Self-Cleaning, Low Adhesion, and Drag Reduction. *Progress in Materials Science*, *56*, 1-108. https://doi.org/10.1016/j.pmatsci.2010.04.003

Bigelow, W. C., Pickett, D. L., & Zisman, W. A. (1946). Oleophobic Monolayers: I. Films Adsorbed from Solution in Non-Polar Liquids. *Journal of Colloid Science*, *1*, 513-538. https://doi.org/10.1016/0095-8522(46)90059-1

Biggs, C. I., Walker, M., & Gibson, M. I. (2016). "Grafting to" of RAFTed Responsive Polymers to Glass Substrates by Thiol–Ene and Critical Comparison to Thiol–Gold Coupling. *Biomacromolecules*, *17*, 2626-2633. https://doi.org/10.1021/acs.biomac.6b00662

Bittoun, E., & Marmur, A. (2012). The Role of Multiscale Roughness in the Lotus Effect: Is it Essential for Super-Hydrophobicity? *Langmuir*, *28*, 13933-13942. https://doi.org/10.1021/la3029512

Bohn, H. F., & Federle, W. (2004). Insect Aquaplaning: Nepenthes Pitcher Plants Capture Prey With The Peristome, A Fully Wettable Water-Lubricated Anisotropic Surface. *Proceedings of the National Academy of Sciences*, *101*, 14138-14143. https://doi.org/10.1073/pnas.0405885101

Boinovich, L. B., Modin, E. B., Sayfutdinova, A. R., Emelyanenko, K. A., Vasiliev, A. L., & Emelyanenko, A. M. (2017). Combination of Functional Nanoengineering and Nanosecond Laser Texturing for Design of Superhydrophobic Aluminum Alloy with Exceptional Mechanical and Chemical Properties. *ACS Nano*, *11*, 10113-10123. https://doi.org/10.1021/acsnano.7b04634

Bormashenko, E. (2015). Progress in Understanding Wetting Transitions on Rough Surfaces. *Advances in Colloid and Interface Science*, *222*, 92-103. https://doi.org/10.1016/j.cis.2014.02.009

Borras, A., & González-Elipe, A. R. (2010). Wetting Properties of Polycrystalline TiO_2 Surfaces: A Scaling Approach to the Roughness Factors. *Langmuir*, *26*, 15875-15882. https://doi.org/10.1021/la101975e

Bravo, J., Zhai, L., Wu, Z., Cohen, R. E., & Rubner, M. F. (2007). Transparent Superhydrophobic Films Based on Silica Nanoparticles. *Langmuir*, *23*, 7293-7298. https://doi.org/10.1021/la070159q

Brewster, M. Q. (1992). *Thermal Radiative Transfer and Properties*. John Wiley & Sons.

BRUKER. (2025). *Attenuated Total Reflectance (ATR)*. Retrieved May 01 from https://www.bruker.com/en/products-and-solutions/infrared-and-raman/ft-ir-routine-spectrometer/what-is-ft-ir-spectroscopy/atr-attenuated-total-reflectance.html

Brzoska, J. B., Azouz, I. B., & Rondelez, F. (1994). Silanization of Solid Substrates: A Step Toward Reproducibility. *Langmuir*, *10*, 4367-4373. https://doi.org/10.1021/la00023a072

Campos, M. A. C., Paulusse, J. M. J., & Zuilhof, H. (2010). Functional Monolayers on Oxide-Free Silicon Surfaces via Thiol–Ene Click Chemistry. *Chem. Commun.*, *46*, 5512-5514. https://doi.org/10.1039/C0CC01264E

Carson, G., & Granick, S. (1989a). Self-assembly of Octadecyltrichlorosilane Films on Mica. *Journal of Applied Polymer Science*, *37*, 2767-2772. https://doi.org/10.1002/app.1989.070370925

Carson, G., & Granick, S. (1989b). Self-assembly of Octadecyltrichlorosilane Films on Mica. *J. Appl. Polym. Sci.*, *37*, 2767-2772. https://doi.org/10.1002/app.1989.070370925

Caschera, D., Mezzi, A., Cerri, L., de Caro, T., Riccucci, C., Ingo, G. M., Padeletti, G., Biasiucci, M., Gigli, G., & Cortese, B. (2014). Effects of Plasma Treatments for Improving Extreme

Wettability Behavior of Cotton Fabrics. *Cellulose*, *21*, 741-756. https://doi.org/10.1007/s10570-013-0123-0
Cassie, A. B. D. (1948a). Contact angles. *Discuss. Faraday Soc.*, *3*, 11-16. https://doi.org/10.1039/DF9480300011
Cassie, A. B. D. (1948b). Contact angles. *Discussions of the Faraday society*, *3*, 11-16. https://doi.org/10.1039/DF9480300011
Cassie, A. B. D., & Baxter, S. (1944a). Wettability of porous surfaces. *Trans. Faraday Soc.*, *40*, 546-551. https://doi.org/10.1039/TF9444000546
Cassie, A. B. D., & Baxter, S. (1944b). Wettability of porous surfaces. *Transactions of the Faraday society*, *40*, 546-551. https://doi.org/10.1039/TF9444000546
Chambers, W. S., Hopkins, J. G., & Richards, S. M. (2021). A review of per-and polyfluorinated alkyl substance impairment of reproduction. *Frontiers in toxicology*, *3*, 732436.
Cheawchan, S., Uchida, S., Sogawa, H., Koyama, Y., & Takata, T. (2016). Thermotriggered Catalyst-Free Modification of a Glass Surface with an Orthogonal Agent Possessing Nitrile N-Oxide and Masked Ketene Functions. *Langmuir*, *32*(1), 309-315. https://doi.org/10.1021/acs.langmuir.5b03881
Checco, A., Rahman, A., & Black, C. T. (2014). Robust Superhydrophobicity in Large-Area Nanostructured Surfaces Defined by Block-Copolymer Self Assembly. *Advanced Materials*, *26*, 886-891. https://doi.org/10.1002/adma.201304006
Chen, J., Yuan, L., Shi, C., Wu, C., Long, Z., Qiao, H., Wang, K., & Fan, Q. H. (2021). Nature-Inspired Hierarchical Protrusion Structure Construction for Washable and Wear-Resistant Superhydrophobic Textiles with Self-Cleaning Ability. *ACS applied materials & interfaces*, *13*, 18142-18151. https://doi.org/10.1021/acsami.1c03539
Chen, L., Li, T., Hu, T., Li, Q., Cheng, J., & Liu, D. (2025). Fabrication and Morphological Characterization of Superhydrophobic PDMS Replicated with Laser-Processed Template. *Surfaces and Interfaces*, *58*, 105813. https://doi.org/10.1016/j.surfin.2025.105813
Chen, M. M., Kopittke, P. M., Zhao, F. J., & Wang, P. (2024). Applications and Opportunities of Click Chemistry in Plant Science. *Trends in Plant Science*, *29*, 167-178. https://doi.org/10.1016/j.tplants.2023.07.003
Chen, Y. C., Li, K., Zhang, S., Qin, L., Deng, S., Ge, L., Xu, L. P., Ma, L., Wang, S., & Zhang, X. (2020). Bioinspired Superwettable Microspine Chips with Directional Droplet Transportation for Biosensing. *ACS Nano*, *14*, 4654-4661. https://doi.org/10.1021/acsnano.0c00324
Cheng, D. F., Masheder, B., Urata, C., & Hozumi, A. (2013). Smooth Perfluorinated Surfaces with Different Chemical and Physical Natures: Their Unusual Dynamic Dewetting Behavior Toward Polar and Nonpolar Liquids. *Langmuir*, *29*, 11322-11329. https://doi.org/10.1021/la402398y
Chi, F., Zeng, Y., Liu, C., Pan, N., Ding, C., & Yi, F. (2020). Highly Stable Self-Cleaning Antireflection Coatings from Fluoropolymer Brush Grafted Silica Nanoparticles. *Applied Surface Science*, *507*, 144836. https://doi.org/10.1016/j.apsusc.2019.144836
Choi, S. J., & Huh, S. Y. (2010). Direct Structuring of a Biomimetic Anti-Reflective, Self-Cleaning Surface for Light Harvesting in Organic Solar Cells. *Macromol. Rapid Commun.*, *31*, 539-544. https://doi.org/10.1002/marc.200900658
Choi, W. K., Kim, H. I., Kang, S. J., Lee, Y. S., Han, J. H., & Kim, B. J. (2016). Mechanical Interfacial Adhesion of Carbon Fibers-Reinforced Polarized-Polypropylene Matrix Composites: Effects of Silane Coupling Agents. *Carbon letters*, *17*, 79-84. https://doi.org/10.5714/CL.2016.17.1.079

Cichomski, M., Borkowska, E., Prowizor, M., Batory, D., Jedrzejczak, A., & Dudek, M. (2020). The Effect of Physicochemical Properties of Perfluoroalkylsilanes Solutions on Microtribological Features of Created Self-Assembled Monolayers. *Materials*, *13*, 3357. https://www.mdpi.com/1996-1944/13/15/3357

Coffinier, Y., Piret, G., Das, M. R., & Boukherroub, R. (2013). Effect of Surface Roughness and Chemical Composition on The Wetting Properties of Silicon-Based Substrates. *Comptes Rendus Chimie*, *16*, 65-72. https://doi.org/10.1016/j.crci.2012.08.011

Daily Data Report for February to June 2022. Environment and Climate Change Canada. Retrieved August 15 2024 from https://climate.weather.gc.ca/climate_data/daily_data_e.html?StationID=51157&timeframe=2&StartYear=1840&EndYear=2024&Day=20&Year=2022&Month=2#

Daily Data Report for October to December 2021. Environment and Climate Change Canada. Retrieved August 15 2024 from https://climate.weather.gc.ca/climate_data/daily_data_e.html?StationID=51157&timeframe=2&StartYear=1840&EndYear=2024&Day=20&Year=2021&Month=10#

Dallinger, A., Steinwender, F., Gritzner, M., & Greco, F. (2023). Different Roles of Surface Chemistry and Roughness of Laser-Induced Graphene: Implications for Tunable Wettability. *ACS Applied Nano Materials*, *6*, 16201-16211. https://doi.org/10.1021/acsanm.3c02066

Dalvi, V. H., & Rossky, P. J. (2010). Molecular Origins of Fluorocarbon Hydrophobicity. *Proc. Natl. Acad. Sci. U. S. A.*, *107*, 13603-13607. https://doi.org/10.1073/pnas.0915169107

Darband, G. B., Aliofkhazraei, M., Khorsand, S., Sokhanvar, S., & Kaboli, A. (2020). Science and Engineering of Superhydrophobic Surfaces: Review of Corrosion Resistance, Chemical and Mechanical Stability. *Arabian Journal of Chemistry*, *13*, 1763-1802. https://doi.org/10.1016/j.arabjc.2018.01.013

Das, S., Kumar, S., Samal, S. K., Mohanty, S., & Nayak, S. K. (2018). A Review on Superhydrophobic Polymer Nanocoatings: Recent Development and Applications. *Industrial & Engineering Chemistry Research*, *57*, 2727-2745. https://doi.org/10.1021/acs.iecr.7b04887

David, Q., Aurélie, L., & José, B. (2003). Slippy and Sticky Microtextured Solids. *Nanotechnology*, *14*, 1109. https://doi.org/10.1088/0957-4484/14/10/307

Davies-Jones, J. A., & Davies, P. R. (2022). Photo Induced Force Microscopy: Chemical Spectroscopy Beyond The Diffraction Limit. *Mater. Chem. Front.*, *6*, 1552-1573. https://doi.org/10.1039/D2QM00040G

Diedenhofen, S. L., Vecchi, G., Algra, R. E., Hartsuiker, A., Muskens, O. L., Immink, G., Bakkers, E. P. A. M., Vos, W. L., & Rivas, J. G. (2009). Broad-band and Omnidirectional Antireflection Coatings Based on Semiconductor Nanorods. *Adv. Mater.*, *21*, 973-978. https://doi.org/10.1002/adma.200802767

Durig, J. R., & Hellams, K. L. (1968). Low-Frequency Vibrations of Some Organotrichlorosilanes. *Applied Spectroscopy*, *22*, 153-160. https://opg.optica.org/as/abstract.cfm?URI=as-22-3-153

El-Khozondar, H. J., El-Khozondar, R. J., Al Afif, R., & Pfeifer, C. (2021). Modified Solar Cells with Antireflection Coatings. *International Journal of Thermofluids*, *11*, 100103. https://doi.org/10.1016/j.ijft.2021.100103

Ensikat, H. J., Ditsche-Kuru, P., Neinhuis, C., & Barthlott, W. (2011). Superhydrophobicity in Perfection: The Outstanding Properties of The Lotus Leaf. *Beilstein Journal of Nanotechnology*, *2*, 152-161. https://doi.org/10.3762/bjnano.2.19

Erickson, P. W. (1970). Historical Background of the Interface—Studies and Theories. *J. Adhes.*, *2*, 131-146. https://doi.org/10.1080/0021846708544589

Esteves, A. C. C., Luo, Y., van de Put, M. W. P., Carcouët, C. C. M., & de With, G. (2014). Self-Replenishing Dual Structured Superhydrophobic Coatings Prepared by Drop-Casting of an All-In-One Dispersion. *Advanced Functional Materials*, *24*, 986-992. https://doi.org/10.1002/adfm.201301909

Fadeev, A. Y., & McCarthy, T. J. (1999). Trialkylsilane Monolayers Covalently Attached to Silicon Surfaces: Wettability Studies Indicating That Molecular Topography Contributes to Contact Angle Hysteresis. *Langmuir*, *15*, 3759-3766. https://doi.org/10.1021/la981486o

Fadeev, A. Y., & McCarthy, T. J. (2000). Self-Assembly Is Not the Only Reaction Possible between Alkyltrichlorosilanes and Surfaces: Monomolecular and Oligomeric Covalently Attached Layers of Dichloro- and Trichloroalkylsilanes on Silicon. *Langmuir*, *16*, 7268-7274. https://doi.org/10.1021/la000471z

Fantoni, N. Z., El-Sagheer, A. H., & Brown, T. (2021). A Hitchhiker's Guide to Click-Chemistry with Nucleic Acids. *Chemical Reviews*, *121*, 7122-7154. https://doi.org/10.1021/acs.chemrev.0c00928

Feng, L., Zhang, Y., Li, M., Zheng, Y., Shen, W., & Jiang, L. (2010). The Structural Color of Red Rose Petals and Their Duplicates. *Langmuir*, *26*, 14885-14888. https://doi.org/10.1021/la102406u

Feng, L., Zhang, Y., Xi, J., Zhu, Y., Wang, N., Xia, F., & Jiang, L. (2008). Petal Effect: A Superhydrophobic State with High Adhesive Force. *Langmuir*, *24*, 4114-4119. https://doi.org/10.1021/la703821h

Fürstner, R., Barthlott, W., Neinhuis, C., & Walzel, P. (2005). Wetting and Self-Cleaning Properties of Artificial Superhydrophobic Surfaces. *Langmuir*, *21*, 956-961. https://doi.org/10.1021/la0401011

Galy, T., Marszewski, M., King, S., Yan, Y., Tolbert, S. H., & Pilon, L. (2020). Comparing Methods for Measuring Thickness, Refractive Index, and Porosity of Mesoporous Thin Films. *Microporous and Mesoporous Materials*, *291*, 109677. https://doi.org/10.1016/j.micromeso.2019.109677

Gao, L., & McCarthy, T. J. (2006a). The "Lotus Effect" Explained: Two Reasons Why Two Length Scales of Topography Are Important. *Langmuir*, *22*, 2966-2967. https://doi.org/10.1021/la0532149

Gao, L., & McCarthy, T. J. (2006b). A Perfectly Hydrophobic Surface (θA/θR = 180°/180°). *Journal of the American Chemical Society*, *128*, 9052-9053. https://doi.org/10.1021/ja062943n

Gao, L., & McCarthy, T. J. (2006c). A Perfectly Hydrophobic Surface (θA/θR = 180°/180°). *J. Am. Chem. Soc.*, *128*, 9052-9053. https://doi.org/10.1021/ja062943n

Geng, Z., He, J., & Yao, L. (2015). Fabrication of Robust High-Transmittance Superamphiphobic Coatings Through Dip-Coating Followed by Spray-Coating. *RSC Advances*, *5*, 89262-89268. https://doi.org/10.1039/C5RA16708F

Geng, Z., Shin, J. J., Xi, Y., & Hawker, C. J. (2021). Click Chemistry Strategies for the Accelerated Synthesis of Functional Macromolecules. *Journal of Polymer Science*, *59*, 963-1042. https://doi.org/10.1002/pol.20210126

Genzer, J., & Efimenko, K. (2000). Creating Long-Lived Superhydrophobic Polymer Surfaces Through Mechanically Assembled Monolayers. *Science*, *290*, 2130-2133. https://doi.org/10.1126/science.290.5499.2130

Ghosal, K., Bhattacharyya, S. K., Mishra, V., & Zuilhof, H. (2024). Click Chemistry for Biofunctional Polymers: From Observing to Steering Cell Behavior. *Chemical Reviews*, *124*, 13216-13300. https://doi.org/10.1021/acs.chemrev.4c00251

Gidi, Y., Bayram, S., Ablenas, C. J., Blum, A. S., & Cosa, G. (2018). Efficient One-Step PEG-Silane Passivation of Glass Surfaces for Single-Molecule Fluorescence Studies. *ACS applied materials & interfaces*, *10*, 39505-39511. https://doi.org/10.1021/acsami.8b15796

Glasheen, J. W., & Mcmahon, T. A. (1996). Size-Dependence of Water-Running Ability in Basilisk Lizards (Basiliscus Basiliscus). *Journal of Experimental Biology*, *199*, 2611-2618. https://doi.org/10.1242/jeb.199.12.2611

Gogolides, E., Ellinas, K., & Tserepi, A. (2015). Hierarchical Micro and Nano Structured, Hydrophilic, Superhydrophobic and Superoleophobic Surfaces Incorporated in Microfluidics, Microarrays and Lab on Chip Microsystems. *Microelectronic Engineering*, *132*, 135-155.

Good, R. J. (1992). Contact Angle, Wetting, and Adhesion: A Critical Review. *Journal of Adhesion Science and Technology*, *6*, 1269-1302. https://doi.org/10.1163/156856192X00629

Grigoras, S., & Lane, T. H. (1988). Molecular Mechanics Parameters for Organosilicon Compounds Calculated from ab Initio Computations. *J. Comput. Chem.*, *9*, 25-39. https://doi.org/10.1002/jcc.540090105

Guirgis, G. A., Nashed, Y. E., Gounev, T. K., & Durig, J. R. (1998). Conformational Stability, Structural Parameters, Vibrational Frequencies, and Raman and Infrared Intensities of Allylsilane. *Struct. Chem.*, *9*, 265-277. https://doi.org/10.1023/A:1022478913441

Guo-hua, X., & Higashitani, K. (2000). Formation of OTS Self-Assembled Monolayer on Glass Surface Investigated By aFM. *J. Zhejiang Univ., Sci., A*, *1*, 162-170. https://doi.org/10.1631/BF02839234

Guo, R., Wang, Y., Lu, H., Wang, S., Wang, B., & Zhang, Q. (2024). Micron-Smooth, Robust Hydrophobic Coating for Photovoltaic Panel Surfaces in Arid and Dusty Areas. *Coatings*, *14*, 239. https://doi.org/10.3390/coatings14020239

Guo, Z., & Liu, W. (2007). Biomimic From the Superhydrophobic Plant Leaves in Nature: Binary Structure and Unitary Structure. *Plant Sci.*, *172*, 1103-1112. https://doi.org/10.1016/j.plantsci.2007.03.005

Gupta, R. K., Kumar, A., Yadav, V., Arora, S., Singh, D. P., Joshi, S. K., Chawla, A. K., & Biswas, A. (2016). Challenges and Opportunities in Fabrication of Transparent Superhydrophobic Surfaces. *Current Nanoscience*, *12*, 429-447. https://doi.org/10.2174/1573413712666151216221401

Haensch, C., Hoeppener, S., & Schubert, U. S. (2010). Chemical Modification of Self-Assembled Silane Based Monolayers by Surface Reactions. *Chemical Society Reviews*, *39*, 2323-2334. https://doi.org/10.1039/B920491A

Hamdi, M., & Poulis, J. A. (2021). Effect of UV/ozone Treatment on the Wettability and Adhesion of Polymeric Systems. *The Journal of Adhesion*, *97*, 651-671. https://doi.org/10.1080/00218464.2019.1693372

Han, G., Nguyen, T. B., Park, S. C., Jung, Y. C., Lee, J., & Lim, H. (2020). Moth-Eye Mimicking Solid Slippery Glass Surface with Icephobicity, Transparency, and Self-Healing. *ACS Nano*. https://doi.org/10.1021/acsnano.0c03463

Han, Z., Wang, Z., Li, B., Feng, X., Jiao, Z., Zhang, J., Zhao, J., Niu, S., & Ren, L. (2019). Flexible Self-Cleaning Broadband Antireflective Film Inspired by the Transparent Cicada Wings. *ACS applied materials & interfaces*, *11*, 17019-17027. https://doi.org/10.1021/acsami.9b01948

Haritha, A. H., Faturíková, K., Duran, A., Galusek, D., Castro, Y., & Velázquez, J. J. (2024). High Performance Double Layer Hydrophobic Antireflective Coatings on Glass Prepared by Sol–Gel Method. *Open Ceramics*, *18*, 100607. https://doi.org/10.1016/j.oceram.2024.100607

Harrop, R. (1978). Hydrophilic Protective Coatings on Glass. *Surf. Technol.*, *6*, 385-393. https://doi.org/10.1016/0376-4583(78)90084-5

Hassanizadeh, S. M. (2024). The Origin of Surface Tension. *InterPore Journal*, *1*(1), ipj260424-260423. https://doi.org/10.69631/ipj.v1i1nr21

Henriksson, A., Friedbacher, G., & Hoffmann, H. (2011). Surface Modification of Silicon Nanowires via Copper-Free Click Chemistry. *Langmuir*, *27*, 7345-7348. https://doi.org/10.1021/la200951x

Heywood, H. (1937). Numerical Definitions of Particle Size and Shape. *J. Soc. Chem. Ind.*, *56*, 149-154. https://doi.org/10.1002/jctb.5000560702

Hideo, N., Ryuichi, I., Yosuke, H., & Hiroyuki, S. (1998). Effects of Surface Roughness on Wettability. *Acta Materialia*, *46*, 2313-2318. https://doi.org/10.1016/S1359-6454(98)80012-8

Hoyle, C. E., & Bowman, C. N. (2010). Thiol–Ene Click Chemistry. *Angewandte Chemie International Edition*, *49*, 1540-1573. https://doi.org/10.1002/anie.200903924

Hoyle, C. E., Lee, T. Y., & Roper, T. (2004). Thiol–enes: Chemistry of The Past with Promise for The Future. *Journal of Polymer Science Part A: Polymer Chemistry*, *42*, 5301-5338. https://doi.org/10.1002/pola.20366

Hu, D. L., & Bush, J. W. M. (2005). Meniscus-Climbing Insects. *Nature*, *437*, 733-736. https://doi.org/10.1038/nature03995

Hu, X., Wang, T., Li, F., & Mao, X. (2023). Surface Modifications of Biomaterials in Different Applied Fields. *RSC Advances*, *13*, 20495-20511. https://doi.org/10.1039/d3ra02248j

Hu, X., Zhao, X., He, B., Zhao, Z., Zheng, Z., Zhang, P., Shi, X., Kwok, R. T. K., Lam, J. W. Y., Qin, A., & Tang, B. Z. (2018). A Simple Approach to Bioconjugation at Diverse Levels: Metal-Free Click Reactions of Activated Alkynes with Native Groups of Biotargets without Prefunctionalization. *Research*, *2018*. https://doi.org/10.1155/2018/3152870

Huang, H., Wang, W., & Wang, L. (2019). Theoretical Assessment of Wettability on Silane Coatings: from Hydrophilic to Hydrophobic. *Physical Chemistry Chemical Physics*, *21*, 8257-8263. https://doi.org/10.1039/C9CP01232J

Huang, J., Cai, P., Li, M., Wu, Q., Li, Q., & Wang, S. (2020). Preparation Of CNF/PDMS Superhydrophobic Coatings with Good Abrasion Resistance Using A One-Step Spray Method. *Materials*, *13*, 5380. https://doi.org/10.3390/ma13235380

Huang, J., Liu, X., Qiu, X., Xie, L., Yan, B., Wang, X., Huang, Q., & Zeng, H. (2017a). Octadecyltrichlorosilane Deposition on Mica Surfaces: Insights into the Interface Interaction Mechanism. *J. Phys. Chem. B*, *121*, 3151-3161. https://doi.org/10.1021/acs.jpcb.7b00828

Huang, J., Liu, X., Qiu, X., Xie, L., Yan, B., Wang, X., Huang, Q., & Zeng, H. (2017b). Octadecyltrichlorosilane Deposition on Mica Surfaces: Insights into the Interface Interaction Mechanism. *The Journal of Physical Chemistry B*, *121*, 3151-3161. https://doi.org/10.1021/acs.jpcb.7b00828

Huang, W.-H., & Lin, C.-S. (2014). Robust superhydrophobic transparent coatings fabricated by a low-temperature sol–gel process. *Applied Surface Science*, *305*, 702-709.

Huang, W., Huang, J., Guo, Z., & Liu, W. (2022). Icephobic/anti-icing properties of superhydrophobic surfaces. *Advances in Colloid and Interface Science*, *304*, 102658. https://doi.org/10.1016/j.cis.2022.102658

Huang, X., & Yu, R. (2021). Robust Superhydrophobic and Repellent Coatings Based on Micro/Nano SiO_2 and Fluorinated Epoxy. *Coatings*, *11*, 663. https://www.mdpi.com/2079-6412/11/6/663

Huhtamäki, T., Tian, X., Korhonen, J. T., & Ras, R. H. A. (2018). Surface-Wetting Characterization Using Contact-Angle Measurements. *Nature Protocols*, *13*, 1521-1538. https://doi.org/10.1038/s41596-018-0003-z

Imanishi, A., Yamane, S., & Nakato, Y. (2008). Si(111) Surface Modified with α,β-Unsaturated Carboxyl Groups Studied by MIR-FTIR. *Langmuir*, *24*, 10755-10761. https://doi.org/10.1021/la801586d

Indumathy, B., Sathiyanathan, P., Prasad, G., Reza, M. S., Prabu, A. A., & Kim, H. I. (2023). A Comprehensive Review on Processing, Development and Applications of Organofunctional Silanes and Silane-Based Hyperbranched Polymers. *Polymers*, *15*, 2517. https://doi.org/10.3390/polym15112517

Itoh, N. (2019). Transparent Superhydrophobic Film Created through Biomimetics of Lotus Leaf and Moth Eye Structures. In *Industrial Biomimetics* (pp. 195-212). Jenny Stanford Publishing.

Jafari, M., Salek, S., Goubert, G., Byers, J. C., & Siaj, M. (2024). Photo-Induced Force Microscopy-Based Spectroscopy and Chemical Mapping of Grafted Electrochemically Reduced Aryl Diazonium Salts. *J. Phys. Chem. C*, *128*, 21720-21729. https://doi.org/10.1021/acs.jpcc.4c04226

Jafari, R., Asadollahi, S., & Farzaneh, M. (2013). Applications of Plasma Technology in Development of Superhydrophobic Surfaces. *Plasma Chemistry and Plasma Processing*, *33*, 177-200. https://doi.org/10.1007/s11090-012-9413-9

Jagdheesh, R., Pathiraj, B., Karatay, E., Römer, G. R. B. E., & Huis in't Veld, A. J. (2011). Laser-Induced Nanoscale Superhydrophobic Structures on Metal Surfaces. *Langmuir*, *27*, 8464-8469. https://doi.org/10.1021/la2011088

Jeong, H. J., Kim, D. K., Lee, S. B., Kwon, S. H., & Kadono, K. (2001). Preparation of Water-Repellent Glass by Sol–Gel Process Using Perfluoroalkylsilane and Tetraethoxysilane. *J. Colloid Interface Sci.*, *235*, 130-134. https://doi.org/10.1006/jcis.2000.7313

Jiang, Y., Lian, J., Jiang, Z., Li, Y., & Wen, C. (2020). Thermodynamic Analysis on Wetting States and Wetting State Transitions of Rough Surfaces. *Advances in Colloid and Interface Science*, *278*, 102136. https://doi.org/10.1016/j.cis.2020.102136

Jin, H., Tian, X., Ikkala, O., & Ras, R. H. A. (2013). Preservation of Superhydrophobic and Superoleophobic Properties upon Wear Damage. *ACS applied materials & interfaces*, *5*, 485-488. https://doi.org/10.1021/am302541f

Jin, M., Wang, J., Yao, X., Liao, M., Zhao, Y., & Jiang, L. (2011a). Underwater Oil Capture by a Three-Dimensional Network Architectured Organosilane Surface [RGC 21 - Publication in refereed journal]. *Adv. Mater.*, *23*, 2861-2864. https://doi.org/10.1002/adma.201101048

Jin, M., Wang, J., Yao, X., Liao, M., Zhao, Y., & Jiang, L. (2011b). Underwater Oil Capture by a Three-Dimensional Network Architectured Organosilane Surface [RGC 21 - Publication in refereed journal]. *Advanced Materials*, *23*, 2861-2864. https://doi.org/10.1002/adma.201101048

Joly, L., & Biben, T. (2009). Wetting and Friction on Superoleophobic Surfaces. *Soft Matter*, *5*, 2549-2557. https://doi.org/10.1039/B821214G

Jothi Prakash, C. G., & Prasanth, R. (2021). Approaches to Design a Surface with Tunable Wettability: A Review on Surface Properties. *Journal of materials science*, *56*, 108-135. https://doi.org/10.1007/s10853-020-05116-1

Jumrus, N., Chaisen, T., Sriboonruang, A., Panthawan, A., Kumpika, T., Kantarak, E., Singjai, P., & Thongsuwan, W. (2020a). A Facile Methodology to Make the Glass Surface Superhydrophobic. *Materials Letters*, *264*, 127347. https://doi.org/10.1016/j.matlet.2020.127347

Jumrus, N., Chaisen, T., Sriboonruang, A., Panthawan, A., Kumpika, T., Kantarak, E., Singjai, P., & Thongsuwan, W. (2020b). A Facile Methodology to Make the Glass Surface Superhydrophobic. *Mater. Lett.*, *264*, 127347. https://doi.org/10.1016/j.matlet.2020.127347

Kaczmarek, M., Przybylska, A., Szymańska, A., Dutkiewicz, A., & Maciejewski, H. (2023a). Thiol-ene Click Reaction as an Effective Tool for the Synthesis of PEG-Functionalized Alkoxysilanes-Precursors of Anti-Fog Coatings. *Scientific Reports*, *13*, 21025. https://doi.org/10.1038/s41598-023-48192-4

Kaczmarek, M., Przybylska, A., Szymańska, A., Dutkiewicz, A., & Maciejewski, H. (2023b). Thiol-ene Click Reaction as an Effective Tool for the Synthesis of PEG-Functionalized Alkoxysilanes-Precursors of Anti-Fog Coatings. *Sci. Rep.*, *13*, 21025. https://doi.org/10.1038/s41598-023-48192-4

Karunakaran, R. G., Lu, C. H., Zhang, Z., & Yang, S. P. (2011). Highly Transparent Superhydrophobic Surfaces from the Coassembly of Nanoparticles (⩽ 100 nm). *Langmuir*, *27*, 4594-4602. https://doi.org/10.1021/la104067c

Katasho, Y., Liang, Y., Murata, S., Fukunaka, Y., Matsuoka, T., & Takahashi, S. (2015). Mechanisms for Enhanced Hydrophobicity by Atomic-Scale Roughness. *Scientific Reports*, *5*(1), 13790. https://doi.org/10.1038/srep13790

Kessel, C. R., & Granick, S. (1991). Formation and Characterization of a Highly Ordered and Well-Anchored Alkylsilane Monolayer on Mica by Self-Assembly. *Langmuir*, *7*, 532-538. https://doi.org/10.1021/la00051a020

Khitas, N., Cheng, C. C. H., & Nazemi, A. (2025a). A Comparative Study Between Alkyl- and Perfluoroalkyl Silane Coatings for Glass. *Canadian Journal of Chemistry*, *103*, 174-183. https://doi.org/10.1139/cjc-2024-0173

Khitas, N., Cheng, C. C. H., & Nazemi, A. (2025b). A Comparative Study Between Alkyl- and Perfluoroalkyl Silane Coatings for Glass. *Can. J. Chem.*, *103*, 174-183. https://doi.org/10.1139/cjc-2024-0173

Khoo, H. S., & Tseng, F. G. (2008). Engineering the 3D Architecture and Hydrophobicity of Methyltrichlorosilane Nanostructures. *Nanotechnology*, *19*, 345603. https://doi.org/10.1088/0957-4484/19/34/345603

Kim, H. C., Wilds, J. B., Kreller, C. R., Volksen, W., Brock, P. J., Lee, V. Y., Magbitang, T., Hedrick, J. L., Hawker, C. J., & Miller, R. D. (2002). Fabrication of Multilayered Nanoporous Poly(methyl silsesquioxane). *Advanced Materials*, *14*, 1637-1639. https://doi.org/10.1002/1521-4095(20021118)14:22<1637::AID-ADMA1637>3.0.CO;2-C

Kim, J. (2010). Probing Organic Self-Assembled Monolayers (SAMs) on Silicon by FTIR with Single Reflectance ATR. *Applied Surface Science*, *256*, 6805-6813. https://doi.org/10.1016/j.apsusc.2010.04.093

Kim, Y. J., Lee, K. H., Sano, H., Han, J., Ichii, T., Murase, K., & Sugimura, H. (2008). Surface Chemical Conversion of Organosilane Self-Assembled Monolayers with Active Oxygen Species Generated by Vacuum Ultraviolet Irradiation of Atmospheric Oxygen Molecules. *Jpn. J. Appl. Phys.*, *47*, 307. https://doi.org/10.1143/JJAP.47.307

Kluger, R. (2010). Click Chemistry for Biotechnology and Materials Science. *Journal of the American Chemical Society*, *132*, 6611-6612. https://doi.org/10.1021/ja102850q

Knepper, T. P., & Lange, F. T. (2011). *Polyfluorinated Chemicals and Transformation Products* (Vol. 17). Springer Science & Business Media. https://doi.org/10.1007/978-3-642-21872-9

Kolb, H. C., Finn, M. G., & Sharpless, K. B. (2001). Click Chemistry: Diverse Chemical Function from a Few Good Reactions. *Angewandte Chemie International Edition*, *40*, 2004-2021. https://doi.org/10.1002/1521-3773(20010601)40:11<2004::AID-ANIE2004>3.0.CO;2-5

Kondo, T., Yamada, R., & Uosaki, K. (2013). Self-Assembled Monolayer (SAM). In *Organized Organic Ultrathin Films* (pp. 7-42). https://doi.org/10.1002/9783527654666.ch2

Kruszelnicki, M., Polowczyk, I., & Kowalczuk, P. B. (2022). Control of Glass Surface Wettability via Esterification with n-Alkyl Alcohols [journal article]. *Physicochemical Problems of Mineral Processing*, *58*, 145147. https://doi.org/10.37190/ppmp/145147

Kubiak, K. J., Wilson, M. C. T., Mathia, T. G., & Carval, P. (2011). Wettability Versus Roughness of Engineering Surfaces. *Wear*, *271*, 523-528. https://doi.org/10.1016/j.wear.2010.03.029

Kujawa, J., Cerneaux, S., Kujawski, W., Bryjak, M., & Kujawski, J. (2016). How To Functionalize Ceramics by Perfluoroalkylsilanes for Membrane Separation Process? Properties and Application of Hydrophobized Ceramic Membranes. *ACS applied materials & interfaces*, *8*, 7564-7577. https://doi.org/10.1021/acsami.6b00140

Lafuma, A., & Quéré, D. (2003). Superhydrophobic States. *Nature Materials*, *2*, 457-460. https://doi.org/10.1038/nmat924

Law, K.-Y. (2014). Definitions for Hydrophilicity, Hydrophobicity, and Superhydrophobicity: Getting the Basics Right. *The Journal of Physical Chemistry Letters*, *5*(4), 686-688. https://doi.org/10.1021/jz402762h

Law, K. Y. (2022). Contact Angle Hysteresis on Smooth/Flat and Rough Surfaces. Interpretation, Mechanism, and Origin. *Accounts of Materials Research*, *3*, 1-7. https://doi.org/10.1021/accountsmr.1c00051

Lee, H., Lee, B. P., & Messersmith, P. B. (2007). A Reversible Wet/Dry Adhesive Inspired by Mussels and Geckos. *Nature*, *448*, 338-341. https://doi.org/10.1038/nature05968

Lee, K. S., & Ram, R. J. (2009). Plastic–PDMS Bonding for High Pressure Hydrolytically Stable Active Microfluidics. *Lab Chip*, *9*, 1618-1624. https://doi.org/10.1039/B820924C

Li, B., Zhang, J., Wu, L., & Wang, A. (2013). Durable Superhydrophobic Surfaces Prepared by Spray Coating of Polymerized Organosilane/Attapulgite Nanocomposites. *ChemPlusChem*, *78*, 1503-1509. https://doi.org/10.1002/cplu.201300222

Li, J., & Horton, J. H. (2002a). A Scanning Probe Study of Some Short Chain Self-Assembled Alkylsilane Films. *J. Mater. Chem.*, *12*, 1268-1273. https://doi.org/10.1039/B110353A

Li, J., & Horton, J. H. (2002b). A Scanning Probe Study of Some Short Chain Self-Assembled Alkylsilane Films. *Journal of Materials Chemistry*, *12*, 1268-1273. https://doi.org/10.1039/B110353A

Li, J., Li, L., Du, X., Feng, W., Welle, A., Trapp, O., Grunze, M., Hirtz, M., & Levkin, P. A. (2015a). Reactive Superhydrophobic Surface and Its Photoinduced Disulfide-ene and Thiol-ene (Bio)functionalization. *Nano Letters*, *15*, 675-681. https://doi.org/10.1021/nl5041836

Li, J., Li, L., Du, X., Feng, W., Welle, A., Trapp, O., Grunze, M., Hirtz, M., & Levkin, P. A. (2015b). Reactive Superhydrophobic Surface and Its Photoinduced Disulfide-ene and Thiol-ene (Bio)functionalization. *Nano Lett.*, *15*, 675-681. https://doi.org/10.1021/nl5041836

Li, N., Zhang, Y., Zhi, H., Tang, J., Shao, Y., Yang, L., Sun, T., Liu, H., & Xue, G. (2022). Micro/nano-cactus structured aluminium with superhydrophobicity and plasmon-enhanced photothermal trap for icephobicity. *Chemical Engineering Journal*, *429*, 132183.

Li, S., Huang, J., Chen, G., & Lai, Y. (2017). A Review on Special Wettability Textiles: Theoretical Models, Fabrication Technologies and Multifunctional Applications. *Journal of Materials Chemistry A*, *5*, 31-55. https://doi.org/10.1039/C6TA07984A

Li, X. M., Reinhoudt, D., & Crego-Calama, M. (2007). What Do We Need for A Superhydrophobic Surface? A Review on the Recent Progress in the Preparation of Superhydrophobic Surfaces [10.1039/B602486F]. *Chemical Society Reviews*, *36*(8), 1350-1368. https://doi.org/10.1039/B602486F

Li, Y., Li, L., & Sun, J. (2010). Bioinspired Self‐Healing Superhydrophobic Coatings. *Angewandte Chemie*, *122*, 6265-6269. https://doi.org/10.1002/ange.201001258

Li, Y., Yang, K., Xia, B., Yang, B., Yan, L., He, M. Y., Yan, H., & Jiang, B. (2017). Preparation of Mechanically Stable Triple-Layer Interference Broadband Antireflective Coatings with Self-Cleaning Property by Sol–Gel Technique. *RSC Advances*, *7*, 14660-14668. https://doi.org/10.1039/C7RA00844A

Li, Y. S., Vecchio, N. E., Wang, Y., & McNutt, C. (2007). Vibrational Spectra of Metals Treated with Allyltrimethoxysilane Sol–Gel and Self-Assembled Monolayer of Allytrichlorosilane. *Spectrochim. Acta, Part A*, *67*, 598-603. https://doi.org/10.1016/j.saa.2006.07.043

Li, Z., Song, C., Li, Q., Xiang, X., Yang, H., Wang, X., & Gao, J. (2019). Hybrid Nanostructured Antireflection Coating by Self-Assembled Nanosphere Lithography. *Coatings*, *9*, 453. https://www.mdpi.com/2079-6412/9/7/453

Liang, L., Wen, T., Xin, J., Su, C., Song, K., Zhao, W., Liu, H., & Su, G. (2023). Fluoropolymer: A Review on Its Emulsion Preparation and Wettability to Solid-Liquid Interface. *Molecules*, *28*, 905. https://doi.org/10.3390/molecules28020905

Liapis, A. C., Rahman, A., & Black, C. T. (2017). Self-assembled nanotextures impart broadband transparency to glass windows and solar cell encapsulants. *Applied Physics Letters*, *111*(18). https://doi.org/10.1063/1.5000965

Lin, L.-Y., Kim, H.-J., & Kim, D.-E. (2008). Wetting characteristics of ZnO smooth film and nanowire structure with and without OTS coating. *Applied Surface Science*, *254*(22), 7370-7376. https://doi.org/10.1016/j.apsusc.2008.05.337

Liu, H., Szunerits, S., Xu, W., & Boukherroub, R. (2009). Preparation of Superhydrophobic Coatings on Zinc as Effective Corrosion Barriers. *ACS applied materials & interfaces*, *1*(6), 1150-1153. https://doi.org/10.1021/am900100q

Liu, K., Ma, Z., Mai, K., Wang, X., Li, B., & Chu, J. (2024). Fabrication of Flexible and Re-entrant Liquid-Superrepellent Surface Using Proximity and PNIPAM-Assisted Soft Lithography. *ACS applied materials & interfaces*, *16*, 50012-50026. https://doi.org/10.1021/acsami.4c12185

Liu, M., Wang, S., & Jiang, L. (2013). Bioinspired Multiscale Surfaces with Special Wettability. *MRS Bulletin*, *38*, 375-382. https://doi.org/10.1557/mrs.2013.100

Liu, Y., & Li, G. (2012). A New Method for Producing "Lotus Effect" on a Biomimetic Shark Skin. *J. Colloid Interface Sci.*, *388*, 235-242. https://doi.org/10.1016/j.jcis.2012.08.033

Liu, Y., Yamazaki, S., Yamabe, S., & Nakato, Y. (2005). A Mild and Efficient Si (111) Surface Modification via Hydrosilylation of Activated Alkynes. *Journal of Materials Chemistry*, *15*, 4906-4913. https://doi.org/10.1039/B511535C

Lo, T. N. H., Lee, J., Hwang, H. S., & Park, I. (2021). Nanoscale Coatings Derived from Fluoroalkyl and PDMS Alkoxysilanes on Rough Aluminum Surfaces for Improved Durability and Anti-Icing Properties. *ACS Applied Nano Materials*, *4*(7), 7493-7501. https://doi.org/10.1021/acsanm.1c01526

Lowe, A. B. (2010). Thiol-Ene "Click" Reactions and Recent Applications in Polymer and Materials Synthesis. *Polymer Chemistry*, *1*, 17-36. https://doi.org/10.1039/B9PY00216B

Lowe, A. B. (2014). Thiol–Ene "Click" Reactions and Recent Applications in Polymer and Materials Synthesis: a First Update. *Polymer Chemistry*, *5*, 4820-4870. https://doi.org/10.1039/C4PY00339J

Lowe, A. B., Hoyle, C. E., & Bowman, C. N. (2010). Thiol-Yne Click Chemistry: A Powerful And Versatile Methodology for Materials Synthesis [10.1039/B917102A]. *Journal of Materials Chemistry*, *20*, 4745-4750. https://doi.org/10.1039/B917102A

Luo, W., Xu, J., Li, G., Niu, G., Ng, K. W., Wang, F., & Li, M. (2022). Fabrication of Robust, Anti-reflective, Transparent Superhydrophobic Coatings with a Micropatterned Multilayer Structure. *Langmuir*, *38*, 7129-7136. https://doi.org/10.1021/acs.langmuir.2c00264

Lyu, J., Wu, B., Wu, N., Peng, C., Yang, J., Meng, Y., & Xing, S. (2021). Green Preparation of Transparent Superhydrophobic Coatings with Persistent Dynamic Impact Resistance for Outdoor Applications. *Chemical Engineering Journal*, *404*, 126456. https://doi.org/10.1016/j.cej.2020.126456

Malavasi, I., Bernagozzi, I., Antonini, C., & Marengo, M. (2015a). Assessing Durability of Superhydrophobic Surfaces. *Surf. Innovations*, *3*, 49-60. https://doi.org/10.1680/si.14.00001

Malavasi, I., Bernagozzi, I., Antonini, C., & Marengo, M. (2015b). Assessing Durability of Superhydrophobic Surfaces. *Surface Innovations*, *3*, 49-60. https://doi.org/10.1680/si.14.00001

Marquez-Velasco, J., Vlachopoulou, M.-E., Tserepi, A., & Gogolides, E. (2010). Stable Superhydrophobic Surfaces Induced by Dual-Scale Topography on Su-8. *Microelectronic Engineering*, *87*(5), 782-785. https://doi.org/10.1016/j.mee.2009.11.113

Materne, T. F. E., Buyl, F. d., & Witucki, G. L. (2012). *Organosilane Technology in Coating Applications : Review and Perspectives*. https://www.semanticscholar.org/paper/Organosilane-Technology-in-Coating-Applications-%3A-Materne-Buyl/c15e4edbb3a210ef580ca0c23b69ab97f4b2b8fb

Mathew, M., & Sandhyarani, N. (2014). Detection of Glucose Using Immobilized Bienzyme on Cyclic Bisureas–Gold Nanoparticle Conjugate. *Analytical Biochemistry*, *459*, 31-38. https://doi.org/10.1016/j.ab.2014.05.003

Matin, A., Baig, U., Akhtar, S., Merah, N., Gondal, M. A., Bake, A. H., & Ibrahim, A. (2019a). UV-Resistant and Transparent Hydrophobic Surfaces with Different Wetting States by a Facile Dip-Coating Method. *Progress in Organic Coatings*, *136*, 105192. https://doi.org/10.1016/j.porgcoat.2019.06.038

Matin, A., Baig, U., Akhtar, S., Merah, N., Gondal, M. A., Bake, A. H., & Ibrahim, A. (2019b). UV-Resistant and Transparent Hydrophobic Surfaces with Different Wetting States by a Facile Dip-Coating Method. *Prog. Org. Coat.*, *136*, 105192. https://doi.org/10.1016/j.porgcoat.2019.06.038

Mazumder, P., Jiang, Y., Baker, D., Carrilero, A., Tulli, D., Infante, D., Hunt, A. T., & Pruneri, V. (2014). Superomniphobic, Transparent, and Antireflection Surfaces Based on Hierarchical Nanostructures. *Nano Letters*, *14*(8), 4677-4681. https://doi.org/10.1021/nl501767j

McCamy, J. W., Ganjoo, A., & Hung, C. H. (2018). Modification of the Glass Surface during Manufacturing. In *78th Conference on Glass Problems* (pp. 263-270). https://doi.org/10.1002/9781119519713.ch22

McGovern, M. E., Kallury, K. M. R., & Thompson, M. (1994). Role of Solvent on The Silanization of Glass with Octadecyltrichlorosilane. *Langmuir*, *10*, 3607-3614. https://doi.org/10.1021/la00022a038

McHale, G., Shirtcliffe, N. J., & Newton, M. I. (2004). Contact-Angle Hysteresis on Super-Hydrophobic Surfaces. *Langmuir*, *20*, 10146-10149. https://doi.org/10.1021/la0486584

Menawat, A., Joseph, H., & Siriwardane, R. (1984). Control of Surface Energy of Glass by Surface Reactions: Contact Angle and Stability. *J. Colloid Interface Sci.*, *101*, 110-119. https://doi.org/10.1016/0021-9797(84)90012-2

Mezger, M., Reichert, H., Schöder, S., Okasinski, J., Schröder, H., Dosch, H., Palms, D., Ralston, J., & Honkimäki, V. (2006). High-Resolution in Situ X-Ray Study of the Hydrophobic Gap at the Water–Octadecyl-Trichlorosilane Interface. *Proceedings of the National Academy of Sciences*, *103*(49), 18401-18404. https://doi.org/doi:10.1073/pnas.0608827103

Michael, N., & Bhushan, B. (2007). Hierarchical Roughness Makes Superhydrophobic States Stable. *Microelectronic Engineering*, *84*, 382-386. https://doi.org/10.1016/j.mee.2006.10.054

Mikoliunaite, L., Rodriguez, R. D., Sheremet, E., Kolchuzhin, V., Mehner, J., Ramanavicius, A., & Zahn, D. R. T. (2015). The substrate Matters in The Raman Spectroscopy Analysis of Cells. *Scientific Reports*, *5*, 13150. https://doi.org/10.1038/srep13150

Milionis, A., Loth, E., & Bayer, I. S. (2016). Recent Advances in The Mechanical Durability of Superhydrophobic Materials. *Advances in Colloid and Interface Science*, *229*, 57-79. https://doi.org/10.1016/j.cis.2015.12.007

Miwa, M., Nakajima, A., Fujishima, A., Hashimoto, K., & Watanabe, T. (2000). Effects of the Surface Roughness on Sliding Angles of Water Droplets on Superhydrophobic Surfaces. *Langmuir*, *16*, 5754-5760. https://doi.org/10.1021/la991660o

Moses, J. E., & Moorhouse, A. D. (2007). The Growing Applications of Click Chemistry [10.1039/B613014N]. *Chemical Society Reviews*, *36*, 1249-1262. https://doi.org/10.1039/B613014N

Moskalik, M. Y., & Shainyan, B. A. (2024). Unsaturated Organosilanes: Synthesis, Transformations and Applications. *Russ. Chem. Rev.*, *93*, 1-34. https://doi.org/10.59761/RCR5140

Motamedi, M., Warkiani, M. E., & Taylor, R. A. (2018a). Transparent Surfaces Inspired by Nature. *Advanced Optical Materials*, *6*, 1800091. https://doi.org/10.1002/adom.201800091

Motamedi, M., Warkiani, M. E., & Taylor, R. A. (2018b). Transparent Surfaces Inspired by Nature. *Adv. Opt. Mater.*, *6*, 1800091. https://doi.org/10.1002/adom.201800091

Musgraves, J. D., Hu, J., & Calvez, L. (2019). *Springer handbook of glass*. Springer Nature.

Nadkarni, G. D., & Garoff, S. (1994). Reproducibility of Contact Line Motion on Surfaces Exhibiting Contact Angle Hysteresis. *Langmuir*, *10*, 1618-1623. https://doi.org/10.1021/la00017a049

Nakajima, A. (2004a). Design of a Transparent Hydrophobic Coating. *J. Ceram. Soc. Jpn.*, *112*, 533-540. https://doi.org/10.2109/jcersj.112.533

Nakajima, A. (2004b). Design of a Transparent Hydrophobic Coating. *Journal of the Ceramic Society of Japan*, *112*, 533-540. https://doi.org/10.2109/jcersj.112.533

Nakajima, A., Fujishima, A., Hashimoto, K., & Watanabe, T. (1999). Preparation of Transparent Superhydrophobic Boehmite and Silica Films by Sublimation of Aluminum Acetylacetonate. *Adv. Mater.*, *11*, 1365-1368. https://doi.org/10.1002/(SICI)1521-4095(199911)11:16<1365::AID-ADMA1365>3.0.CO;2-F

Nakajima, A., Hashimoto, K., Watanabe, T., Takai, K., Yamauchi, G., & Fujishima, A. (2000). Transparent Superhydrophobic Thin Films with Self-Cleaning Properties. *Langmuir*, *16*, 7044-7047. https://doi.org/10.1021/la000155k

Nambafu, G. S., Kim, N., & Kim, J. (2022). Hydrophobic Coatings Prepared Using Various Dipodal Silane-Functionalized Polymer Precursors. *Applied Surface Science Advances*, *7*, 100207. https://doi.org/10.1016/j.apsadv.2021.100207

Nanda, D., Varshney, P., Satapathy, M., Mohapatra, S. S., & Kumar, A. (2017a). Self-Assembled Monolayer of Functionalized Silica Microparticles for Self-Cleaning Applications. *Colloids Surf., A*, *529*, 231-238. https://doi.org/10.1016/j.colsurfa.2017.06.007

Nanda, D., Varshney, P., Satapathy, M., Mohapatra, S. S., & Kumar, A. (2017b). Self-Assembled Monolayer of Functionalized Silica Microparticles for Self-Cleaning Applications. *Colloids and Surfaces A: Physicochemical and Engineering Aspects*, *529*, 231-238. https://doi.org/10.1016/j.colsurfa.2017.06.007

Navascues, G. (1979). Liquid Surfaces: Theory of Surface Tension. *Reports on Progress in Physics*, *42*(7), 1131. https://doi.org/10.1088/0034-4885/42/7/002

Nayshevsky, I., Xu, Q. F., Barahman, G., & Lyons, A. M. (2020). Fluoropolymer Coatings for Solar Cover Glass: Anti-Soiling Mechanisms in the Presence of Dew. *Solar Energy Materials and Solar Cells*, *206*, 110281.

Neděla, O., Slepička, P., & Švorčík, V. (2017). Surface Modification of Polymer Substrates for Biomedical Applications. *Materials (Basel)*, *10*. https://doi.org/10.3390/ma10101115

Neinhuis, C., & Barthlott, W. (1997a). Characterization and Distribution of Water-repellent, Self-cleaning Plant Surfaces. *Annals of Botany*, *79*, 667-677. https://doi.org/10.1006/anbo.1997.0400

Neinhuis, C., & Barthlott, W. (1997b). Characterization and Distribution of Water-repellent, Self-cleaning Plant Surfaces. *Ann. Bot.*, *79*, 667-677. https://doi.org/10.1006/anbo.1997.0400

Noll, W. (2012). *Chemistry and technology of silicones*. Elsevier.

Novotný, M., & Bartle, K. D. (1970). Surface Modification of Glass Capillaries for Gas Chromatography by Silylation. *Chromatographia*, *3*, 272-274. https://doi.org/10.1007/BF02263693

Nuzzo, R. G., Dubois, L. H., & Allara, D. L. (1990). Fundamental Studies of Microscopic Wetting on Organic Surfaces. 1. Formation and Structural Characterization of A Self-Consistent Series of Polyfunctional Organic Monolayers. *Journal of the American Chemical Society*, *112*, 558-569. https://doi.org/10.1021/ja00158a012

Oh, S., Cho, J. W., Lee, J., Han, J., Kim, S. K., & Nam, Y. (2022). A Scalable Haze-Free Antireflective Hierarchical Surface with Self-Cleaning Capability. *Advanced Science*, *9*, 2202781. https://doi.org/10.1002/advs.202202781

Ollivier, H. (1907). Recherches sur la Capillarité. *Journal of Theoretical and Applied Physics*, *6*, 757-782. https://doi.org/10.1051/jphystap:019070060075700

Otten, A., & Herminghaus, S. (2004). How Plants Keep Dry: A Physicist's Point of View. *Langmuir*, *20*, 2405-2408. https://doi.org/10.1021/la034961d

Padhan, A. K., Singh, V., Ray, S., & Voolapalli, R. K. (2025). High-Performance Multi-Functional Solar Panel Coatings: Recent Advances, Challenges, Strategies and Industrial Aspects. *RSC Applied Polymers*, *3*(2), 317-335. https://doi.org/10.1039/D4LP00295D

Pallandre, A., de Lambert, B., Attia, R., Jonas, A. M., & Viovy, J. L. (2006). Surface Treatment and Characterization: Perspectives to Electrophoresis and Lab-on-Chips. *ELECTROPHORESIS*, *27*, 584-610. https://doi.org/10.1002/elps.200500761

Pan, S., Kota, A., Mabry, J. M., & Tuteja, A. (2013). Superomniphobic Surfaces for Effective Chemical Shielding. *Journal of the American Chemical Society*, *135*, 578-581. https://doi.org/10.1021/ja310517s

Papadopoulos, P., Mammen, L., Deng, X., Vollmer, D., & Butt, H. J. (2013). How Superhydrophobicity Breaks Down. *Proc. Natl. Acad. Sci. U. S. A.*, *110*, 3254-3258. https://doi.org/10.1073/pnas.1218673110

Patankar, N. A. (2003). On the Modeling of Hydrophobic Contact Angles on Rough Surfaces. *Langmuir*, *19*, 1249-1253. https://doi.org/10.1021/la026612+

Patankar, N. A. (2004). Mimicking the Lotus Effect: Influence of Double Roughness Structures and Slender Pillars. *Langmuir*, *20*, 8209-8213. https://doi.org/10.1021/la048629t

Peng, S., Yang, X., Tian, D., & Deng, W. (2014). Chemically Stable and Mechanically Durable Superamphiphobic Aluminum Surface with a Micro/Nanoscale Binary Structure. *ACS applied materials & interfaces*, *6*, 15188-15197. https://doi.org/10.1021/am503441x

Pesek, J. J., & Matyska, M. T. (1997a). Methods for the Modification and Characterization of Oxide Surfaces. *Interface Science*, *5*, 103-117. https://doi.org/10.1023/A:1008648923962

Pesek, J. J., & Matyska, M. T. (1997b). Methods for the Modification and Characterization of Oxide Surfaces. *Interface Sci.*, *5*, 103-117. https://doi.org/10.1023/A:1008648923962

Pieter Rein ten, W. (2002). Hydrophobic Interactions: An Overview. *Journal of Physics: Condensed Matter*, *14*(40), 9445. https://doi.org/10.1088/0953-8984/14/40/328

Prakash, S., Long, T. M., Selby, J. C., Moore, J. S., & Shannon, M. A. (2007). "Click" Modification of Silica Surfaces and Glass Microfluidic Channels. *Analytical Chemistry*, *79*, 1661-1667. https://doi.org/10.1021/ac061824n

Prashar, D. (2012). Self Assembled Monolayers -A Review.

Pujari, S. P., Scheres, L., Marcelis, A. T. M., & Zuilhof, H. (2014a). Covalent Surface Modification of Oxide Surfaces. *Angew. Chem., Int. Ed.*, *53*, 6322-6356. https://doi.org/10.1002/anie.201306709

Pujari, S. P., Scheres, L., Marcelis, A. T. M., & Zuilhof, H. (2014b). Covalent Surface Modification of Oxide Surfaces. *Angewandte Chemie International Edition*, *53*, 6322-6356. https://doi.org/10.1002/anie.201306709

Quéré, D. (2005). Non-sticking drops. *Reports on Progress in Physics*, *68*, 2495. https://doi.org/10.1088/0034-4885/68/11/R01

Rahmawan, Y., Xu, L., & Yang, S. (2013). Self-Assembly of Nanostructures Towards Transparent, Superhydrophobic Surfaces. *J. Mater. Chem. A*, *1*, 2955-2969. https://doi.org/10.1039/C2TA00288D

Raja, R. S. S., Selvakumar, P., & Babu, P. D. (2020). A novel fabrication of superhydrophobic surfaces on aluminium substrate by picosecond pulsed laser. *Journal of Mechanical Science and Technology*, *34*, 1667-1674.

Ramapanicker, R., & Chauhan, P. (2016). Click Chemistry: Mechanistic and Synthetic Perspectives. In *Click Reactions in Organic Synthesis* (pp. 1-24). https://doi.org/10.1002/9783527694174.ch1

Raut, H. K. (2014). *Studies on Nanostructured Antireflective Coatings* National University of Singapore]. Singapore.

Raut, H. K., Ganesh, V. A., Nair, A. S., & Ramakrishna, S. (2011). Anti-Reflective Coatings: A Critical, In-Depth Review [10.1039/C1EE01297E]. *Energy & Environmental Science*, *4*, 3779-3804. https://doi.org/10.1039/C1EE01297E

Raza, M. A., Kooij, E. S., Van Silfhout, A., Zandvliet, H. J. W., & Poelsema, B. (2012). A Colloidal Route to Fabricate Hierarchical Sticky and non-Sticky Substrates. *Journal of colloid and interface science*, *385*(1), 73-80. https://doi.org/10.1016/j.jcis.2012.07.021

Raza, M. A., Zandvliet, H. J. W., Poelsema, B., & Kooij, E. S. (2015). Hydrophobic Surfaces With Tunable Dynamic Wetting Properties via Colloidal Assembly of Silica Microspheres And Gold Nanoparticles. *Journal of Sol-Gel Science and Technology*, *74*(2), 357-367. https://doi.org/10.1007/s10971-014-3476-4

Ren, T., Geng, Z., He, J., Zhang, X., & He, J. (2017). A Versatile Route to Polymer-Reinforced, Broadband Antireflective and Superhydrophobic Thin Films Without High-Temperature Treatment. *Journal of colloid and interface science*, *486*, 1-7. https://doi.org/10.1016/j.jcis.2016.09.054

Ren, W. (2014). Wetting Transition on Patterned Surfaces: Transition States and Energy Barriers. *Langmuir*, *30*, 2879-2885. https://doi.org/10.1021/la404518q

Resetco, C., Hendriks, B., Badi, N., & Du Prez, F. (2017). Thiol–Ene Chemistry for Polymer Coatings and Surface Modification – Building In Sustainability And Performance. *Materials Horizons*, *4*, 1041-1053. https://doi.org/10.1039/C7MH00488E

Rodič, P., Kapun, B., Panjan, M., & Milošev, I. (2020). Easy and Fast Fabrication of Self-Cleaning and Anti-Icing Perfluoroalkyl Silane Film on Aluminium. *Coatings*, *10*, 234. https://doi.org/10.3390/coatings10030234

Rollings, D. A. E., Tsoi, S., Sit, J. C., & Veinot, J. G. C. (2007). Formation and Aqueous Surface Wettability of Polysiloxane Nanofibers Prepared via Surface Initiated, Vapor-Phase Polymerization of Organotrichlorosilanes. *Langmuir*, *23*, 5275-5278. https://doi.org/10.1021/la063604a

Rollings, D. A. E., & Veinot, J. G. C. (2008). Polysiloxane Nanofibers via Surface Initiated Polymerization of Vapor Phase Reagents: A Mechanism of Formation and Variable Wettability of Fiber-Bearing Substrates. *Langmuir*, *24*, 13653-13662. https://doi.org/10.1021/la801595m

Roscioni, O. M., Muccioli, L., Mityashin, A., Cornil, J., & Zannoni, C. (2016). Structural Characterization of Alkylsilane and Fluoroalkylsilane Self-Assembled Monolayers on SiO2 by Molecular Dynamics Simulations. *The Journal of Physical Chemistry C*, *120*, 14652-14662. https://doi.org/10.1021/acs.jpcc.6b03226

Saadatbakhsh, M., Asl, S. J., Kiani, M. J., & Nouri, N. M. (2020). Slip Length Measurement of Pdms/Hydrophobic Silica Superhydrophobic Coating For Drag Reduction Application. *Surface and Coatings Technology*, *404*, 126428. https://doi.org/10.1016/j.surfcoat.2020.126428

Sagiv, J. (1980a). Organized Monolayers By Adsorption. Formation And Structure Of Oleophobic Mixed Monolayers On Solid Surfaces. *Journal of the American Chemical Society*, *102*, 92-98. https://doi.org/10.1021/ja00521a016

Sagiv, J. (1980b). Organized Monolayers By Adsorption. Formation And Structure Of Oleophobic Mixed Monolayers On Solid Surfaces. *J. Am. Chem. Soc.*, *102*, 92-98. https://doi.org/10.1021/ja00521a016

Sahraei, N., Dauzou, F., Kashi, S., & Cheng, C. C. H. (2020, 15 June-21 Aug. 2020). Angular Efficiency of Solar Panels: How Nanotextured Anti-Reflection Surfaces Improve Annual Energy Output. 2020 47th IEEE Photovoltaic Specialists Conference (PVSC),

Sakhuja, M., Son, J., Le, H. V., Baojuan, X., Verma, L. K., Zeng, H. C., Yang, H., Danner, A. J., & Bhatia, C. S. (2011, 27-29 Dec. 2011). Nanopatterned and Self-Cleaning Glass Substrates For Solar Cell Packaging. The 2nd International Conference on Control, Instrumentation and Automation,

Sandhyarani, N. (2019). Chapter 3 - Surface Modification Methods for Electrochemical Biosensors. In A. A. Ensafi (Ed.), *Electrochemical Biosensors* (pp. 45-75). Elsevier. https://doi.org/10.1016/B978-0-12-816491-4.00003-6

Schwartz, D. K. (2001). Mechanisms and Kinetics of Self-Assembled Monolayer Formation. *Annu Rev Phys Chem*, *52*, 107-137. https://doi.org/10.1146/annurev.physchem.52.1.107

Schwartz, D. K., Steinberg, S., Israelachvili, J., & Zasadzinski, J. A. N. (1992). Growth of a Self-Assembled Monolayer by Fractal Aggregation. *Phys. Rev. Lett.*, *69*, 3354-3357. https://doi.org/10.1103/PhysRevLett.69.3354

Scott, R. E., & Frisch, K. C. (1951). Unsaturated Chlorosilanes. *J. Am. Chem. Soc.*, *73*, 2599-2600. https://doi.org/10.1021/ja01150a051

Seeharaj, P., Pasupong, P., Detsri, E., & Damrongsak, P. (2018). Superhydrophobilization of SiO 2 surface with two alkylsilanes for an application in oil/water separation. *Journal of materials science*, *53*, 4828-4839.

Seo, M. K., & Park, S. J. (2009). Surface Characteristics of Carbon Fibers Modified by Direct Oxyfluorination. *Journal of colloid and interface science*, *330*, 237-242. https://doi.org/10.1016/j.jcis.2008.10.005

Sethi, S. K., & and Manik, G. (2018). Recent Progress in Super Hydrophobic/Hydrophilic Self-Cleaning Surfaces for Various Industrial Applications: A Review. *Polymer-Plastics Technology and Engineering*, *57*(18), 1932-1952. https://doi.org/10.1080/03602559.2018.1447128

Shang, Q., & Zhou, Y. (2016). Fabrication of Transparent Superhydrophobic Porous Silica Coating for Self-Cleaning and Anti-Fogging. *Ceramics International*, *42*, 8706-8712. https://doi.org/10.1016/j.ceramint.2016.02.105

Shanmugam, N., Pugazhendhi, R., Madurai Elavarasan, R., Kasiviswanathan, P., & Das, N. (2020). Anti-Reflective Coating Materials: A Holistic Review from PV Perspective. *Energies*, *13*, 2631. https://doi.org/10.3390/en13102631

Shen, S., Guirgis, G. A., & Durig, J. R. (2001). Spectra and Structure of Silicon-Containing Compounds. XXVIII1 Infrared and Raman Spectra, Vibrational Assignment, and Ab Initio Calculations of Vibrational Spectrum and Structural Parameters of Vinyltrichlorosilane. *Struct. Chem.*, *12*, 33-43. https://doi.org/10.1023/A:1009258017813

Shome, A., Das, A., Borbora, A., Dhar, M., & Manna, U. (2022). Role of Chemistry in Bio-Inspired Liquid Wettability. *Chemical Society Reviews*, *51*, 5452-5497. https://doi.org/10.1039/D2CS00255H

Shull, E. R., Thursack, R. A., & Birdsall, C. M. (1956). Vibrational Spectra of Organosilicon Compounds. I. Vinyltrichlorosilane. *J. Chem. Phys.*, *24*, 147-150. https://doi.org/10.1063/1.1700817

Siedlecki, C. A., Eppell, S. J., & Marchant, R. E. (1994). Interactions of Human Von Willebrand Factor With a Hydrophobic Self‐Assembled Monolayer Studied by Atomic Force Microscopy. *Journal of biomedical materials research*, *28*(9), 971-980.

Sigmund, W. M., & Hsu, S. H. (2015). Cassie-Baxter Model. In E. Drioli & L. Giorno (Eds.), *Encyclopedia of Membranes* (pp. 1-2). Springer Berlin Heidelberg. https://doi.org/10.1007/978-3-642-40872-4_1381-4

Silberzan, P., Leger, L., Ausserre, D., & Benattar, J. (1991). Silanation of Silica Surfaces. A New Method of Constructing Pure or Mixed Monolayers. *Langmuir*, *7*, 1647-1651. https://doi.org/10.1021/la00056a017

Silvestrini, M., & Brito, C. (2017). Wettability of Reentrant Surfaces: A Global Energy Approach. *Langmuir*, *33*, 12535-12545. https://doi.org/10.1021/acs.langmuir.7b03230

Smith, A. L. (1960). Infrared Spectra-Structure Correlations for Organosilicon Compounds. *Spectrochim. Acta*, *16*, 87-105. https://doi.org/10.1016/0371-1951(60)80074-4

Soderquist, J. A., & Brown, H. C. (1980). Hydroboration. 56. Convenient and Regiospecific Route to Functionalized Organosilanes Through The Hydroboration of Alkenylsilanes. *The Journal of Organic Chemistry*, *45*, 3571-3578. https://doi.org/10.1021/jo01306a006

Song, K., Lee, J., Choi, S. O., & Kim, J. (2019). Interaction of Surface Energy Components between Solid and Liquid on Wettability, and Its Application to Textile Anti-Wetting Finish. *Polymers*, *11*, 498. https://doi.org/10.3390/polym11030498

Song, Y., Nair, R. P., Zou, M., & Wang, Y. (2009). Superhydrophobic surfaces produced by applying a self-assembled monolayer to silicon micro/nano-textured surfaces. *Nano Research*, *2*(2), 143-150. https://doi.org/10.1007/s12274-009-9012-0

Spinelli, P., Verschuuren, M. A., & Polman, A. (2012). Broadband Omnidirectional Antireflection Coating Based on Subwavelength Surface Mie Resonators. *Nature communications*, *3*, 692. https://doi.org/10.1038/ncomms1691

Srinivasan, S., Chhatre, S. S., Mabry, J. M., Cohen, R. E., & McKinley, G. H. (2011). Solution Spraying Of Poly (Methyl Methacrylate) Blends to Fabricate Microtextured, Superoleophobic Surfaces. *Polymer*, *52*, 3209-3218. https://doi.org/10.1016/j.polymer.2011.05.008

Sriram, S., Singh, R. K., & Kumar, A. (2020). Silica and Silane Based Polymer Composite Coating on Glass Slide by Dip-Coating Method. *Surf. Interfaces*, *19*, 100472. https://doi.org/10.1016/j.surfin.2020.100472

Standard Practice for Operating Salt Spray (Fog) Apparatus. (2016). (ASTM B117-16).

Stefanie, B., Bas de, H., Markus, L., & Martin, S. (2004). Selective Chemical Surface Modification of Fluidic Microsystems and Characterization Studies. *Journal of Micromechanics and Microengineering*, *14*, 497. https://doi.org/10.1088/0960-1317/14/4/009

Stevens, M. J. (1999). Thoughts on the Structure of Alkylsilane Monolayers. *Langmuir*, *15*, 2773-2778. https://doi.org/10.1021/la981064e

Stojanovic, A., Artus, G. R. J., & Seeger, S. (2010). Micropatterning of Superhydrophobic Silicone Nanofilaments by A Near-Ultraviolet Nd:YAG Laser. *Nano Res.*, *3*, 889-894. https://doi.org/10.1007/s12274-010-0062-0

Su, B., Tian, Y., & Jiang, L. (2016a). Bioinspired Interfaces with Superwettability: From Materials to Chemistry. *J. Am. Chem. Soc.*, *138*, 1727-1748. https://doi.org/10.1021/jacs.5b12728

Su, B., Tian, Y., & Jiang, L. (2016b). Bioinspired Interfaces with Superwettability: From Materials to Chemistry. *Journal of the American Chemical Society*, *138*, 1727-1748. https://doi.org/10.1021/jacs.5b12728

Su, Y., Wang, S., Yao, D., Fu, Y., Zang, H., Xu, H., & Polynkin, P. (2019). Stand-off Fabrication of Irregularly Shaped, Multi-Functional Hydrophobic and Antireflective Metal Surfaces Using Femtosecond Laser Filaments in Air. *Applied Surface Science*, *494*, 1007-1012. https://doi.org/10.1016/j.apsusc.2019.07.261

Sun, G., Fang, Y., Cong, Q., & Ren, L. (2009). Anisotropism of the Non-Smooth Surface of Butterfly Wing. *Journal of Bionic Engineering*, *6*(1), 71-76. https://doi.org/10.1016/S1672-6529(08)60094-3

Sun, M., Luo, C., Xu, L., Ji, H., Ouyang, Q., Yu, D., & Chen, Y. C. (2005). Artificial Lotus Leaf by Nanocasting. *Langmuir*, *21*, 8978-8981. https://doi.org/10.1021/la050316q

Sun, M., Watson, G. S., Zheng, Y., Watson, J. A., & Liang, A. (2009). Wetting Properties on Nanostructured Surfaces of Cicada Wings. *J. Exp. Biol.*, *212*, 3148-3155. https://doi.org/10.1242/jeb.033373

Sun, T., Feng, L., Gao, X., & Jiang, L. (2005). Bioinspired Surfaces with Special Wettability. *Accounts of Chemical Research*, *38*, 644-652. https://doi.org/10.1021/ar040224c

Suzuki, K., Malfatti, L., Takahashi, M., Carboni, D., Messina, F., Tokudome, Y., Takemoto, M., & Innocenzi, P. (2017). Design of Carbon Dots Photoluminescence through Organo-Functional Silane Grafting for Solid-State Emitting Devices. *Sci. Rep.*, *7*, 5469. https://doi.org/10.1038/s41598-017-05540-5

Sypabekova, M., Kleiss, J., Hagemann, A., Schuemann, S., Wills, R., Zechmann, B., & Kim, S. K. (2025). Improvement of The Optical Cavity-Based Biosensor's Limit of Detection Using Optimal 3-Aminopropyltriethoxysilane Process. *Scientific Reports*, *15*, 7739. https://doi.org/10.1038/s41598-025-92151-0

Szczepanski, C. R., Guittard, F., & Darmanin, T. (2017). Recent Advances in The Study and Design of Parahydrophobic Surfaces: From Natural Examples To Synthetic Approaches. *Advances in Colloid and Interface Science*, *241*, 37-61. https://doi.org/10.1016/j.cis.2017.01.002

Terrestrial Photovoltaic (PV) Modules – Design Qualification and Type Approval – Part 2: Test Procedures. (2021). [International Standard](IEC 61215-2).

Tian, X., Verho, T., & Ras, R. H. A. (2016). Moving Superhydrophobic Surfaces Toward Real-World Applications. *Science*, *352*, 142-143. https://doi.org/10.1126/science.aaf207

Tillman, N., Ulman, A., Schildkraut, J. S., & Penner, T. L. (1988). Incorporation of Phenoxy Groups in Self-Assembled Monolayers of Trichlorosilane Derivatives. Effects on Film Thickness, Wettability, And Molecular Orientation. *Journal of the American Chemical Society*, *110*(18), 6136-6144. https://doi.org/10.1021/ja00226a031

Tripp, C. P., & Hair, M. L. (1992). Reaction of Alkylchlorosilanes with Silica at The Solid/Gas and Solid/Liquid Interface. *Langmuir*, *8*, 1961-1967. https://doi.org/10.1021/la00044a014

Tucker-Schwartz, A. K., Farrell, R. A., & Garrell, R. L. (2011a). Thiol–ene Click Reaction as a General Route to Functional Trialkoxysilanes for Surface Coating Applications. *Journal of the American Chemical Society*, *133*, 11026-11029. https://doi.org/10.1021/ja202292q

Tucker-Schwartz, A. K., Farrell, R. A., & Garrell, R. L. (2011b). Thiol–ene Click Reaction as a General Route to Functional Trialkoxysilanes for Surface Coating Applications. *J. Am. Chem. Soc.*, *133*, 11026-11029. https://doi.org/10.1021/ja202292q

Uelzen, T., & Müller, J. (2003). Wettability Enhancement by Rough Surfaces Generated by Thin Film Technology. *Thin Solid Films*, *434*, 311-315. https://doi.org/10.1016/S0040-6090(03)00484-X

Ulman, A. (1996). Formation and Structure of Self-Assembled Monolayers. *Chemical Reviews*, *96*, 1533-1554. https://doi.org/10.1021/cr9502357

Veerbeek, J., Steen, R., Vijselaar, W., Rurup, W. F., Korom, S., Rozzi, A., Corradini, R., Segerink, L., & Huskens, J. (2018). Selective Functionalization with PNA of Silicon Nanowires on Silicon Oxide Substrates. *Langmuir*, *34*, 11395-11404. https://doi.org/10.1021/acs.langmuir.8b02401

Verho, T., Bower, C., Andrew, P., Franssila, S., Ikkala, O., & Ras, R. H. A. (2011). Mechanically Durable Superhydrophobic Surfaces. *Advanced Materials*, *23*, 673-678. https://doi.org/10.1002/adma.201003129

Vista, M. *Scientific Principles of PiFM and PiF-IR*. Retrieved March 26, 2025 from https://molecularvista.com/technology/pifm-and-pif-ir/scientific-principles/

Wagner, T., Neinhuis, C., & Barthlott, W. (1996). Wettability and Contaminability of Insect Wings as a Function of Their Surface Sculptures. *Acta Zool.*, *77*, 213-225. https://doi.org/10.1111/j.1463-6395.1996.tb01265.x

Wang, B., Ruud, C. J., Price, J. S., Kim, H., & Giebink, N. C. (2019). Graded-Index Fluoropolymer Antireflection Coatings for Invisible Plastic Optics. *Nano Letters*, *19*, 787-792. https://doi.org/10.1021/acs.nanolett.8b03886

Wang, F., Yu, S., Ou, J., & Li, W. (2015). Anti-Icing Performance of Transparent And Superhydrophobic Surface Under Wind Action. *Journal of Sol-Gel Science and Technology*, *75*, 625-634. https://doi.org/10.1007/s10971-015-3733-1

Wang, J., Gan, J., Zhang, C., Hong, W., & Jiang, F. (2023). Natural and biomimetic superhydrophobic surface: Review of the manufacturing techniques. 3rd International Conference on Materials Chemistry and Environmental Engineering,

Wang, K. K., Yan, H., Zhao, C. X., Xu, G., Qi, Y., Wu, Y., & Hu, N. X. (2010). Direct Method of Tracing the Wetting States on Nanocomposite Surfaces. *Langmuir*, *26*, 7686-7689. https://doi.org/10.1021/la101259h

Wang, L., Schubert, U. S., & Hoeppener, S. (2021). Surface Chemical Reactions on Self-Assembled Silane Based Monolayers. *Chemical Society Reviews*, *50*, 6507-6540. https://doi.org/10.1039/D0CS01220C

Wang, L., Shu, L., Hu, Q., Jiang, X., Yang, H., Wang, H., & Rao, L. (2024). Mechanism of Self-Recovery of Hydrophobicity After Surface Damage of Lotus Leaf. *Plant Methods*, *20*, 47. https://doi.org/10.1186/s13007-024-01174-7

Wang, Q., Xu, S., Xing, X., & Wang, N. (2022). Progress in Fabrication and Applications of Micro/Nanostructured Superhydrophobic Surfaces. *Surface Innovations*, *10*, 89-110. https://doi.org/10.1680/jsuin.21.00031

Wang, S. D., & Shu, Y. Y. (2013). Superhydrophobic Antireflective Coating with High Transmittance. *Journal of Coatings Technology and Research*, *10*, 527-535. https://doi.org/10.1007/s11998-012-9468-9

Wang, X., Fu, C., Zhang, C., Qiu, Z., & Wang, B. (2022). A Comprehensive Review of Wetting Transition Mechanism on the Surfaces of Microstructures from Theory and Testing Methods. *Materials*, *15*, 4747. https://doi.org/10.3390/ma15144747

Wang, X., Liu, X., Zhou, F., & Liu, W. (2011). Self-healing Superamphiphobicity [10.1039/C0CC04066E]. *Chemical Communications*, *47*, 2324-2326. https://doi.org/10.1039/C0CC04066E

Wang, Y., He, M. Y., & Chen, R. Y. (2015). Fabrication of Mechanically Robust Antireflective Films Using Silica Nanoparticles With Enhanced Surface Hydroxyl Groups [10.1039/C4TA04840G]. *Journal of Materials Chemistry A*, *3*, 1609-1618. https://doi.org/10.1039/C4TA04840G

Wang, Y., & Lieberman, M. (2003). Growth of Ultrasmooth Octadecyltrichlorosilane Self-Assembled Monolayers on SiO2. *Langmuir*, *19*, 1159-1167. https://doi.org/10.1021/la020697x

Wasserman, S. R., Tao, Y. T., & Whitesides, G. M. (1989). Structure and Reactivity of Alkylsiloxane Monolayers Formed by Reaction of Alkyltrichlorosilanes on Silicon Substrates. *Langmuir*, *5*, 1074-1087. https://doi.org/10.1021/la00088a035

Watson, G. S., Green, D. W., Schwarzkopf, L., Li, X., Cribb, B. W., Myhra, S., & Watson, J. A. (2015). A Gecko Skin Micro/Nano Structure – A Low Adhesion, Superhydrophobic, Anti-Wetting, Self-Cleaning, Biocompatible, Antibacterial Surface. *Acta Biomater.*, *21*, 109-122. https://doi.org/10.1016/j.actbio.2015.03.007

Watson, S., Nie, M., Wang, L., & Stokes, K. (2015). Challenges and Developments of Self-Assembled Monolayers and Polymer Brushes as A Green Lubrication Solution for Tribological Applications. *RSC Advances*, *5*, 89698-89730. https://doi.org/10.1039/C5RA17468F

Webb, H. K., Hasan, J., Truong, V. K., Crawford, R. J., & Ivanova, E. P. (2011). Nature inspired structured surfaces for biomedical applications. *Curr Med Chem*, *18*, 3367-3375. https://doi.org/10.2174/092986711796504673

Wen, Q., & Guo, Z. (2016). Recent Advances in the Fabrication of Superhydrophobic Surfaces. *Chemistry Letters*, *45*(10), 1134-1149. https://doi.org/10.1246/cl.160621

Weng, D., Xu, F., Li, X., Li, Y., & Sun, J. (2018). Bioinspired Photothermal Conversion Coatings with Self-Healing Superhydrophobicity for Efficient Solar Steam Generation. *Journal of Materials Chemistry A*, *6*, 24441-24451. https://doi.org/10.1039/C8TA08706G

Wenzel, R. N. (1936). Resistance of Solid Surfaces to Wetting by Water. *Industrial & engineering chemistry*, *28*, 988-994. https://doi.org/10.1021/ie50320a024

Wilson, S. J., & Hutley, M. C. (1982). The Optical Properties of 'Moth Eye' Antireflection Surfaces. *Optica Acta: International Journal of Optics*, *29*, 993-1009. https://doi.org/10.1080/713820946

Wong, J. X. H., Asanuma, H., & Yu, H. Z. (2012). Simple and Reproducible Method of Preparing Transparent Superhydrophobic Glass. *Thin Solid Films*, *522*, 159-163. https://doi.org/10.1016/j.tsf.2012.08.033

Wong, J. X. H., & Yu, H. Z. (2013a). Preparation of Transparent Superhydrophobic Glass Slides: Demonstration of Surface Chemistry Characteristics. *J. Chem. Educ.*, *90*, 1203-1206. https://doi.org/10.1021/ed300809m

Wong, J. X. H., & Yu, H. Z. (2013b). Preparation of Transparent Superhydrophobic Glass Slides: Demonstration of Surface Chemistry Characteristics. *Journal of Chemical Education*, *90*, 1203-1206. https://doi.org/10.1021/ed300809m

Wong, T. S., Sun, T., Feng, L., & Aizenberg, J. (2013). Interfacial Materials with Special Wettability. *MRS Bulletin*, *38*, 366-371. https://doi.org/10.1557/mrs.2013.99

Wong, W. S. Y., Liu, G., Nasiri, N., Hao, C., Wang, Z., & Tricoli, A. (2017). Omnidirectional Self-Assembly of Transparent Superoleophobic Nanotextures. *ACS Nano*, *11*, 587-596. https://doi.org/10.1021/acsnano.6b06715

Worch, J. C., Stubbs, C. J., Price, M. J., & Dove, A. P. (2021). Click Nucleophilic Conjugate Additions to Activated Alkynes: Exploring Thiol-yne, Amino-yne, and Hydroxyl-yne Reactions from (Bio)Organic to Polymer Chemistry. *Chemical Reviews*, *121*, 6744-6776. https://doi.org/10.1021/acs.chemrev.0c01076

Wu, C.-W., Shen, Y.-K., Chuang, S.-Y., & Wei, C. (2007). Anti-adhesive effects of diverse self-assembled monolayers in nanoimprint lithography. *Sensors and Actuators A: Physical*, *139*(1-2), 145-151.

Wu, J., Xia, J., Lei, W., & Wang, B. P. (2013). Advanced Understanding of Stickiness on Superhydrophobic Surfaces. *Scientific Reports*, *3*, 3268. https://doi.org/10.1038/srep03268

Wu, S., Du, Y., Alsaid, Y., Wu, D., Hua, M., Yan, Y., Yao, B., Ma, Y., Zhu, X., & He, X. (2020). Superhydrophobic Photothermal Icephobic Surfaces Based on Candle Soot. *Proceedings of the National Academy of Sciences*, *117*, 11240-11246. https://doi.org/10.1073/pnas.2001972117

Wu, W., Guijt, R. M., Silina, Y. E., Koch, M., & Manz, A. (2016). Plant Leaves as Templates for Soft Lithography [10.1039/C5RA25890A]. *RSC Advances*, *6*, 22469-22475. https://doi.org/10.1039/C5RA25890A

Wu, X., Xiao, M., Zhang, J., Tan, G., Pan, Y., Lai, Y., & Chen, Z. (2023). An Underwater Stable Superhydrophobic Surface for Robust Ultra-Long-Lasting Biofouling Resistance. *Chemical Engineering Journal*, *462*, 142091. https://doi.org/10.1016/j.cej.2023.142091

Wu, X., Yang, F., Gan, J., Kong, Z., & Wu, Y. (2021). A Superhydrophobic, Antibacterial, and Durable Surface of Poplar Wood. *Nanomaterials*, *11*, 1885. https://doi.org/10.3390/nano11081885

Wu, Y., Du, J., Liu, G., Ma, D., Jia, F., Klemeš, J. J., & Wang, J. (2022). A Review of Self-Cleaning Technology to Reduce Dust and Ice Accumulation in Photovoltaic Power Generation Using Superhydrophobic Coating. *Renewable Energy*, *185*, 1034-1061. https://doi.org/10.1016/j.renene.2021.12.123

Xi, W., Scott, T. F., Kloxin, C. J., & Bowman, C. N. (2014). Click Chemistry in Materials Science. *Advanced Functional Materials*, *24*, 2572-2590. https://doi.org/10.1002/adfm.201302847

Xiang, S., & Liu, W. (2021). Self-Healing Superhydrophobic Surfaces: Healing Principles and Applications. *Advanced Materials Interfaces*, *8*, 2100247. https://doi.org/10.1002/admi.202100247

Xu, L., Geng, Z., He, J., & Zhou, G. (2014). Mechanically Robust, Thermally Stable, Broadband Antireflective, and Superhydrophobic Thin Films on Glass Substrates. *ACS applied materials & interfaces*, *6*, 9029-9035. https://doi.org/10.1021/am5016777

Xu, S., Wang, Q., & Wang, N. (2020). Chemical Fabrication Strategies for Achieving Bioinspired Superhydrophobic Surfaces with Micro and Nanostructures: A Review. *Advanced Engineering Materials*, *23*. https://doi.org/10.1002/adem.202001083

Xu, W., Liu, H., Lu, S., Xi, J., & Wang, Y. (2008). Fabrication of Superhydrophobic Surfaces with Hierarchical Structure Through A Solution-Immersion Process on Copper And Galvanized Iron Substrates. *Langmuir*, *24*, 10895-10900. https://doi.org/10.1021/la800613d

Xuan, C., Xiaoran, S., Zhaoji, S., Jiaen, Z., Zhong, Q., Huimin, X., & Hui, W. (2021). Analysis of the Spatio-Temporal Changes in Acid Rain and Their Causes in China (1998–2018). *J. Resour. Ecol.*, *12*, 593-599, 597. https://doi.org/10.5814/j.issn.1674-764x.2021.05.002

Xue, C.-H., Jia, S.-T., Zhang, J., & Ma, J.-Z. (2010). Large-Area Fabrication of Superhydrophobic Surfaces for Practical Applications: An Overview. *Science and Technology of Advanced Materials*, *11*(3), 033002. https://doi.org/10.1088/1468-6996/11/3/033002

Yan, X., Huang, Z., Sett, S., Oh, J., Cha, H., Li, L., Feng, L., Wu, Y., Zhao, C. X., Orejon, D., Chen, F., & Miljkovic, N. (2019). Atmosphere-Mediated Superhydrophobicity of Rationally Designed Micro/Nanostructured Surfaces. *ACS Nano*, *13*, 4160-4173. https://doi.org/10.1021/acsnano.8b09106

Yang, Y., He, H., Li, Y., & Qiu, J. (2019). Using Nanoimprint Lithography to Create Robust, Buoyant, Superhydrophobic PVB/SiO2 Coatings on wood Surfaces Inspired by Red roses petal. *Scientific Reports*, *9*(1), 9961. https://doi.org/10.1038/s41598-019-46337-y

Ye, H., Zhang, X., Zhang, Y., Ye, L., Xiao, B., Lv, H., & Jiang, B. (2011). Preparation of Antireflective Coatings with High Transmittance and Enhanced Abrasion-Resistance by A

Base/Acid Two-Step Catalyzed Sol–Gel Process. *Solar Energy Materials and Solar Cells*, *95*, 2347-2351. https://doi.org/10.1016/j.solmat.2011.04.004

Yilbas, B. S., Salhi, B., Yousaf, M. R., Al-Sulaiman, F., Ali, H., & Al-Aqeeli, N. (2016). Surface Characteristics of Silicon Nanowires/Nanowalls Subjected to Octadecyltrichlorosilane Deposition and N-Octadecane Coating. *Scientific Reports*, *6*(1), 38678. https://doi.org/10.1038/srep38678

Yong, J., Chen, F., Yang, Q., Huo, J., & Hou, X. (2017). Superoleophobic Surfaces. *Chemical Society Reviews*, *46*, 4168-4217. https://doi.org/10.1039/C6CS00751A

Yong, J., Yang, Q., Chen, F., Zhang, D., Du, G., Bian, H., Si, J., & Hou, X. (2014). Bioinspired Superhydrophobic Surfaces with Directional Adhesion. *RSC Advances*, *4*, 8138-8143. https://doi.org/10.1039/C3RA46929H

Young, T. (1805). III. An Essay on the Cohesion Of Fluids. *Philosophical Transactions of the Royal Society of London*, *95*, 65-87. https://doi.org/10.1098/rstl.1805.0005

Youngblood, J. P., & Sottos, N. R. (2008). Bioinspired Materials for Self-Cleaning and Self-Healing. *MRS Bull.*, *33*, 732-741. https://doi.org/10.1557/mrs2008.158

Yu, E., Kim, S.-C., Lee, H. J., Oh, K. H., & Moon, M.-W. (2015). Extreme wettability of nanostructured glass fabricated by non-lithographic, anisotropic etching. *Scientific Reports*, *5*(1), 9362. https://doi.org/10.1038/srep09362

Yu, M., Liu, M., Hou, Y., Fu, S., Zhang, L., Li, M., & Wang, D. (2020). Covalently Grafted Liquids for Transparent and Omniphobic Surfaces via Thiol-Ene Click Chemistry. *Journal of materials science*, *55*, 12811-12825. https://doi.org/10.1007/s10853-020-04929-4

Yu, S., Guo, Z., & Liu, W. (2015). Biomimetic Transparent and Superhydrophobic Coatings: From Nature And Beyond Nature [10.1039/C4CC06868H]. *Chem. Commun.*, *51*, 1775-1794. https://doi.org/10.1039/C4CC06868H

Zahner, D., Abagat, J., Svec, F., Fréchet, J. M. J., & Levkin, P. A. (2011). A Facile Approach to Superhydrophilic–Superhydrophobic Patterns in Porous Polymer Films. *Adv. Mater.*, *23*, 3030-3034. https://doi.org/10.1002/adma.201101203

Zarubin, D. (1999). Infrared spectra of hydrogen bonded hydroxyl groups in silicate glasses. A re‐interpretation. *Phys. Chem. Glasses*, *40*(4), 184-192.

Zeng, T. W., & Zhan, J. R. (2024). Improvement of Mechanical Properties of Silica Nanoparticle Antireflection Films via Including A Tetraethoxysilane-Based Sol. *Optical Materials*, *149*, 114981. https://doi.org/10.1016/j.optmat.2024.114981

Zhai, L., Berg, M. C., Cebeci, F. Ç., Kim, Y. S., Milwid, J. M., Rubner, M. F., & Cohen, R. E. (2006). Patterned Superhydrophobic Surfaces: Toward a Synthetic Mimic of the Namib Desert Beetle. *Nano Letters*, *6*, 1213-1217. https://doi.org/10.1021/nl060644q

Zhang, D., Ji, J., Yan, C., Zhang, J., An, Z., & Shen, Y. (2024). Research Advances in Bio-Inspired Superhydrophobic Surface: Bridging Nature To Practical Applications. *Ind. Eng. Chem.*, *140*, 20-46. https://doi.org/10.1016/j.jiec.2024.05.051

Zhang, J., Li, L., Li, B., & Seeger, S. (2014a). Solvent-Controlled Growth Of Silicone Nanofilaments. *RSC Advances*, *4*, 33424-33430. https://doi.org/10.1039/C4RA04475D

Zhang, J., Li, L., Li, B., & Seeger, S. (2014b). Solvent-Controlled Growth Of Silicone Nanofilaments. *RSC Adv.*, *4*, 33424-33430. https://doi.org/10.1039/C4RA04475D

Zhang, J., & Seeger, S. (2011). Superoleophobic Coatings with Ultralow Sliding Angles Based on Silicone Nanofilaments. *Angewandte Chemie International Edition*, *50*, 6652-6656. https://doi.org/10.1002/anie.201101008

Zhang, J., & Seeger, S. (2013). Silica/Silicone Nanofilament Hybrid Coatings with Almost Perfect Superhydrophobicity. *ChemPhysChem*, *14*, 1646-1651. https://doi.org/10.1002/cphc.201200995

Zhang, J., Wang, A., & Seeger, S. (2014). Nepenthes Pitcher Inspired Anti-Wetting Silicone Nanofilaments Coatings: Preparation, Unique Anti-Wetting and Self-Cleaning Behaviors. *Advanced Functional Materials*, *24*, 1074-1080. https://doi.org/10.1002/adfm.201301481

Zhang, L., Zhou, A. G., Sun, B. R., Chen, K. S., & Yu, H.-Z. (2021). Functional and Versatile Superhydrophobic Coatings via Stoichiometric Silanization. *Nature communications*, *12*(1), 982. https://doi.org/10.1038/s41467-021-21219-y

Zhang, P., Chen, H., Zhang, L., Zhang, Y., Zhang, D., & Jiang, L. (2016). Stable Slippery Liquid-Infused Anti-Wetting Surface at High Temperatures. *Journal of Materials Chemistry A*, *4*(31), 12212-12220. https://doi.org/10.1039/C6TA03857C

Zhang, W., Li, S., Wei, D., Zheng, Z., Han, Z., & Liu, Y. (2024). Fluorine-free, Robust and Self-Healing Superhydrophobic Surfaces with Anticorrosion and Antibacterial Performances. *Journal of Materials Science & Technology*, *186*, 231-243. https://doi.org/10.1016/j.jmst.2023.10.059

Zhang, W., Wang, D., Sun, Z., Song, J., & Deng, X. (2021). Robust superhydrophobicity: mechanisms and strategies [10.1039/D0CS00751J]. *Chemical Society Reviews*, *50*, 4031-4061. https://doi.org/10.1039/D0CS00751J

Zhang, X., Liu, S., Salim, A., & Seeger, S. (2019). Hierarchical Structured Multifunctional Self-Cleaning Material with Durable Superhydrophobicity and Photocatalytic Functionalities. *Small*, *15*, 1901822. https://doi.org/10.1002/smll.201901822

Zhang, X., Shi, F., Niu, J., Jiang, Y., & Wang, Z. (2008). Superhydrophobic Surfaces: from Structural Control to Functional Application. *Journal of Materials Chemistry*, *18*(6), 621-633. https://doi.org/10.1039/B711226B

Zhang, Y., Chu, C. W., Ma, W., & Takahara, A. (2020). Functionalization of Metal Surface via Thiol-Ene Click Chemistry: Synthesis, Adsorption Behavior, and Postfunctionalization of a Catechol- and Allyl-Containing Copolymer. *ACS Omega*, *5*, 7488-7496. https://doi.org/10.1021/acsomega.0c00259

Zhang, Y. L., Xia, H., Kim, E., & Sun, H. B. (2012). Recent Developments in Superhydrophobic Surfaces with Unique Structural and Functional Properties. *Soft Matter*, *8*, 11217-11231. https://doi.org/10.1039/C2SM26517F

Zhao, X., Li, J., Li, Q., Qiao, L., Zhang, L., Liu, Z., & Yang, C. (2018). Fabrication of a Scratch & Heat Resistant Superhydrophobic Sio 2 Surface with Self-Cleaning and Semi-Transparent Performance. *RSC Advances*, *8*(44), 25008-25013. https://doi.org/10.1039/C8RA04383C

Zhou, W., Tao, M., Chen, L., & Yang, H. (2007). Microstructured Surface Design for Omnidirectional Antireflection Coatings on Solar Cells. *Journal of Applied Physics*, *102*. https://doi.org/10.1063/1.2817470

Zhu, H., Huang, Y., Lou, X., & Xia, F. (2021). Bioinspired Superwetting Surfaces for Biosensing. *VIEW*, *2*, 20200053. https://doi.org/10.1002/VIW.20200053

Zhu, J., & Liao, K. (2020). Preparation of Superhydrophobic Surface with Tunable Adhesion on Glass Substrate. *Materials Research Express*, *7*(7), 076409. https://doi.org/10.1039/C8RA04383C

Zhu, J., & Wu, J. (2020). One-Step Fabrication of an Anti-Corrosion Superhydrophobic Surface on Stainless Steel. *Materials Research Express*, *7*(7), 076404. https://doi.org/10.1088/2053-1591/aba218

Zhu, S., Xie, K., Lin, Q., Cao, R., & Qiu, F. (2023). Experimental Determination of Surface Energy for High-Energy Surface: A Review. *Advances in Colloid and Interface Science*, *315*, 102905. https://doi.org/10.1016/j.cis.2023.102905

Zimmermann, J., Artus, G. R. J., & Seeger, S. (2007). Long term studies on the chemical stability of a superhydrophobic silicone nanofilament coating. *Applied Surface Science*, *253*, 5972-5979. https://doi.org/10.1016/j.apsusc.2006.12.118

Zimmermann, J., J., A. G. R., & Seeger, S. (2008). Superhydrophobic Silicone Nanofilament Coatings. *J. Adhes. Sci. Technol.*, *22*, 251-263. https://doi.org/10.1163/156856108X305165

Zimmermann, J., Reifler, F. A., Schrade, U., Artus, G. R. J., & Seeger, S. (2007). Long term Environmental Durability of A Superhydrophobic Silicone Nanofilament Coating. *Colloids and Surfaces A: Physicochemical and Engineering Aspects*, *302*, 234-240. https://doi.org/10.1016/j.colsurfa.2007.02.033

Zimmermann, J. H. (2008). *Silicone Nanofilaments as Functional Coatings: Properties, Applications and Modifications* University of Zurich].